THE WAKSMAN FOUNDATION OF JAPAN INC.

Honorary President

Prince Takahito Mikasa

Honorary Counselor

Shozo Yokogawa, Counselor, Yokogawa Electric Corp.

Board of Directors

Chairman : Ichiro Kitasato, Chairman of the Board, Meiji Seika Kaisha, Ltd.

Shogo Sasaki, Prof. Emeritus, Keio Univ.

Kazuhisa Saito, Prof. Emeritus, Keio Univ.

Teruhiko Beppu, Prof. Emeritus, Tokyo Univ.

Takao Saruta, vice President, Keio Univ.

Takeshi Ishikawa, Secretary General, Keio Univ.

Shigeo Koyasu, Prof., Keio Univ. Sch. Med.

Kazumine Kobari, Prof. Emeritus, Ryukyu Univ.

Shogo Kuwahara, Prof. Emeritus, Toho Univ.

Rinji Kawana, Prof. Emeritus, Iwate Med. Univ.

Tadakatsu Shimamura, Prof., Showa Univ. Sch. Med.

Managing Director : Takeji Nishikawa, Prof., Keio Univ. Sch. Med.

Comptroller : Kannosuke Nakamura, Counselor, Kyowa Hakko Kogyo, Co., Ltd.

Yoshiharu Wakiyama, Senior Advisor, Kaken Pharmaceutical, Co., Ltd.

Councilors

Kimio Uyeno, Honorary Chairman, Chugai Pharmaceutical, Co., Ltd.

Susumu Sato, Chairman, Sato Pharmaceutical, Co., Ltd.

Yuji Naito, Director and Senior Advisor, Eisai Pharmaceutical, Co., Ltd.

Ryoichi Mori, Prof. Emeritus, Kyushu Univ.

Masaki Kitajima, Dean, Keio Univ. Sch. Med.

Yuichiro Anzai, President, Keio Univ.

Keizo Takemi, Member, The House of Councilors

Kiyoshi Morita, President, Daiichi Pharmaceutical, Co., Ltd.

Tetsuo Takato, Chairman of the Board and Representative Director, Sankyo, Co., Ltd.

Akira Uehara, President, Taisho Pharmaceutical, Co., Ltd.

Koichi Yamanishi, Dean, Osaka Univ. Sch. Med.

Masamichi Fujii, Prof. Emeritus, St. Marianna Univ.

Osamu Sato, Prof. Emeritus, Tokai Univ.

Sachiko Goto, Prof. Emeritus, Toho Univ.

Yoshihiro Miwa, President, Kowa Company, Ltd.

2004

Edited and Published by

THE WAKSMAN FOUNDATION OF JAPAN INC.

30-8 Daikyo-cho, Shinjuku-ku,
Tokyo 160-0015, Japan
http : //www.waksman.or.jp/
E-mail ad-off@waksman.or.jp

Printed by

FUKOKU PRINTING CO., LTD.

Tokyo, Japan

PREFACE (2000)

Since the Waksman Foundation published its first cinqueannual report in 1962, annual report followed regularly until 1986 without changing its style, i.e. yellow cover in B5 size. The royalties of patent of streptomycin expired in 1970 and the Foundation was forced to change the way of running. Fortunately, it manages to continue its activity by supporting the research activities of Japanese investigators and by encouraging them to take part in an international meeting and also by hosting scientific meetings with professional societies. The total number of support counts 628 research projects and costs approximately 4,500,000 U.S. dollars. The Foundation is administered by the Board of Directors consisting of 5-9 representatives of professional societies and Prince Takahito Mikasa as the honorary President.

At our recent business meeting it was decided unanimously to publish the reports of the researchers who recieved research grant from the Foundation for the past 15 years to commemorate the year 2000. To meet with the current style of a scientific journal the Foundation has adopted an international size and totally renewed the cover as you are aware of. From the new millennium on it is expected that the report from the awardees of the research grants will be distributed regularly each year.

Shozo Yokogawa
Chairman, Board of Directors,
The Waksman Foundation of Japan, Inc.

Preface to the First Report (1962)

It is indeed a privilege to take this opportunity to write a few words of introduction to the first report of the Waksman Foundation of Japan Inc., covering five years of its activities and comprising the results of the work of the first two years of research carried out by various scholars in Japan in the fields of microbiology and medical science, supported by this Foundation.

In 1952, I accepted the invitation from Keio University and the Kitasato Institute, to deliver the centennial lecture in honor of the great Japanese bacteriologist, Shibasaburo Kitasato. Before departing for Japan, I proposed to the trustees of the Rutgers Research and Educational Foundation which owned the patents on streptomycin, to share the royalties under the patent in Japan, for the support of research in microbiology and allied fields in that country. The trustees heartily approved my recommendation that I make such announcement to that effect.

Soon upon my arrival in Japan (December 17, 1952), I invited a group of eminent microbiologists, biochemists, and clinical investigators to meet with me in order to discuss the plan. Everyone present was very enthusiastic about the proposal. It was decided that a proper committee be selected to work out the plan of a Foundation under which the royalties were to be received and distributed for the support of Japanese investigators working in different universities in Japan and elsewhere, in the fields of microbiology and medical research. The committee recommended that a Board of Directors be selected and the proposed Foundation be named THE WAKSMAN FOUNDATION OF JAPAN INCORPORATION.

The Rutgers Research and Educational Foundation approved at once the above recommendations and issued a statement, signed by Dr. Lewis Webster Jones, President of the Foundation, to the effect that

"The Rutgers Research and Educational Foundation desires to emphasize that its principal concern is the advancement of scientific knowledge in the public interest and that it confidently expects that the Waksman Foundation for Microbiology and Medical Research in Japan will be similarly motivated, thereby serving the peoples of both countries."

This announcement was received with enthusiasm both by the scientific world and the popular press in Japan and in the United States. It took several years before the Waksman Foundation of Japan Inc. was properly organized, and before applications were received and approved. In 1958, I had the privilege of participating in the first official meetings of the Board of Directors of the Japanese Foundation and to greet personally the first group of scholars to whom grants had been made.

In summarizing these brief remarks in connection with the first cinqueannual report of the Waksman Foundation of Japan Inc., I would like to enphasize that this example of collaboration between universities and scientists of the United States and Japan may serve to encourage collaboration between scientific workers throughout the world towards a better understanding between men and women and towards a happier and healthier human race, so that all the nations on this earth can live in peace and that man may finally "break

his swords and build out of them plowshares" for the betterment of mankind as a whole.

Selman A. Waksman
Professor Emeritus
Rutgers-State University N. J., U. S. A.

The "Waksman Foundation of Japan Inc." was established in 1957 with the spirit of humanity by Dr. S.A. Waksman, Professor of Microbiology, Rutgers University, U.S.A. The Foundation's operations are possible only because Dr. S.A. Waksman and the Rutgers Research and Educational Foundation donated patent royalties he received from the production in Japan of the discovery, Streptomycin.

Because of these royalties, each year many Japanese scholars and research workers in the fields of Microbiology and medical science are encouraged and find it possible to continue their work. Especially, in accordance with Dr. Waksman's suggestion, the funds are distributed to scholars in local and economically hampered schools and laboratories and to those developing research workers who are endeavoring to expand in their fields. This thought of Dr. Waksman's is most appreciated, as it matches our Oriental phylosophy, and results in the search for a jewel among ordinary stones, which is the highest work of the science-leader.

Some five years have now passed since the start of this Foundation, and many persons have received aid through this period.

The reports which are presented herein cover the first and second group of research workers who received financial assistance from the Foundation.

Toshio Katow, M. D.
Executive Director

Contents

—— Report of Researches in 2003 ——

Studies on Goadsporin : Mechanism of Its Action on the Induction of Secondary Metabolism and Sporulation in Streptomycetes, and Its Application

Hiroyasu Onaka

Biotechnology Research Center, Toyama Prefectural University, Kosugi-machi, Toyama 939-0398, Japan

Introduction

A number of antibiotics and other bioactive molecules with a variety of chemical structures have been found from actinomycetes as their secondary metabolites. Owing to this diversity of the secondary metabolites, extensive screening of bioactive compounds from actinomycetes has been conducted aiming at the pharmaceutical usage. In the screening of bioactive compounds from soil-derived actinomycetes, it is widely recognized that the growth condition influences the productivity of secondary metabolite production because actinomycetes regulate the secondary metabolism and morphogenesis in response to the environmental condition. In industrial fermentation, physical and chemical conditions such as temperature, aeration and medium composition are restrictively controlled to gain the maximum productivity for the aimed product.

In recent years, molecular microbiological studies are disclosing the common regulation systems for secondary metabolism and cell differentiation in streptomycetes (1,2). For example, in *Streptomyces griseus*, *S. virginiae*, and *S. coelicolor* A3(2), low molecular-weight substances containing a butylolactone serve as chemical signal molecules or microbial hormones for secondary metabolism and/or cellular differentiation (3, 4). In addition, eukaryotic protein kinases (5) and sigma cascades (6) are shown to exist as a common component in the regulatory pathway.

S. lividans is known to possess a complete set of the biosynthetic gene for actinorhodin, red pigment, although it does not produce the pigment under conventional growth conditions. Interestingly, it is reported that *afsR* gene which was cloned from *S. coelicolor* A3(2) stimulates the actinorhodin production in *S. lividans* (7). This result shows that *S. lividans* has a potency to produce actinorhodin under a specific condition while the production is repressed under usual conditions.

There are several reports on the small molecules, which induce the secondary metabolism and/or cell differentiation in streptomycetes. A-factor, the most well known butyrolactone, induces streptomycin production, streptomycin resistance, yellow pigment production and aerial mycelium formation of *S. griseus* at the concentration of less than 1 nM (8−10). Recently, homologues of A-factor receptor gene were cloned from *S. coelicolor* A3(2) and shown to be involved in pigment production and cell differentiation (11). These findings suggest that small molecules containing a butyrolactone moiety are widely distributed in streptomycetes as a microbial hormone. Their hormone-like activity is observed only to the hormone-producing strain itself but not to the non-producing streptomycetes, indicating the high specificity in the recognition of the butyrolactones.

To date there is no reports on the substance which induces the secondary metabolism and morphogenesis in a wide variety of different *Streptomyces* species although a common regulatory system is expected to exist in streptomycetes. Recently, we found such

inducer, goadsporin from soil-derived actinomycetes. In this paper, we describe the screening method for goadsporin, its characterization and its biosynthesis.

Materials and Methods

Media and strains.

Production culture for actinomycetes was carried out in A-3M medium consisting of glucose 0.5 %, glycerol 2 %, soluble starch 2 %, pharmamedia 1.5 %, Yeast extract (Difco Laboratory, MI) 0.3% and Diaion HP-20 1 % (pH 7.0). Seed culture for actinomycetes was carried out in V-22 medium consisting of soluble starch 1 %, glucose 0.5 %, NZ-case 0.3 %, Yeast extract (Difco) 0.2 %, Bacto Tryptone 0.5 %, K_2HPO_4 0.1 %, $MgSO_4 \cdot 7H_2O$ 0.05 % and $CaCO_3$ 0.3 % (pH 7.0). Bennett's agar and Nutrient Broth agar medium were used for paper disc diffusion assay. Bennett's agar consisted of Yeast extract (Difco) 0.1 %, Meat extract (Wako Pure Chemicals) 0.1 %, NZ amine 0.2 %, and glucose 1.0 % (pH 7.2). Nutrient Broth agar was purchased from Difco Lab.

Bacterial strains and plasmids used in this study are shown in Table 1. ATCC strains were obtained from American Type Culture Collection, Rockville, MD. IFO strains were obtained from Institution of Fermentation, Osaka, Japan. An NRRL strain was

Table 1. Bacterial strains and plasmids used in this study

Designation	Relevant characteristics	Source of reference
Streptomyces sp. TP-A0584	goadsporin producer	this study
S. lividans TK23	goadsporin responder	D. A. Hopwood
S. spinicoumarensis ATCC29813		ATCC
S. violaceoruber IFO15146		IFO
S. griseolus NRRL3739		NRRL
S. hygroscopicus TP-A0342		this study
Microbispora sp. TP-A0184		18
Streptomyces scabies JCM7914		JCM
Bacillus subtilis ATCC6633	Gram (+)	ATCC
Escherichia coli NIHJ JC-2	Gram (−)	
Staphylococcus aureus 209P JC-1	Gram (+)	
Pseudomonas aeruginosa TP-B0270	Gram (−)	this study
Proteus mirabilis ATCC21100	Gram (−)	ATCC
Sacchromyces cerevisiae TP-F0176	yeast cell	this study
Candida albicans TP-F0594	yeast cell	this study
Cryptococcus neoformans ATCC90112	yeast cell	ATCC
Torulopsis glabrata IFO0622	yeast cell	IFO
Aspergillus fumigatus IFO8866	filamentous fungi	IFO
Escherichia coli DH5a	for gene cloning	13
Escherichia coli XL-1 Blue MR	for cosmid library construction	13
Escherichia coli S17-1	conjugational host	14
plasmids		
pTOYAMAcos	bi-functional cosmid	12
pTYM19	bi-functional vector	12
pGSB14k	The genes between *godA* and *godR* was cloned into pTYM19	this study
pGSB16k	The genes between *godA* and *orf3* was cloned into pTYM19	this study
pGSB20k	The genes between *godA* and *orf5* was cloned into pTYM19	this study
pGSBC1	goadsporin biosynthetic genes cloned into pTOYAMAcos	this study

obtained from Northern Utilization Research and Development Division, U.S. Department of Agriculture, Peoria, Illinois.

General recombinant DNA techniques.

Restriction enzymes, T4 DNA ligase, and *Taq* polymerase were purchased from New England Biolabs. PCR was carried out with PTC-200 DNA Engine (MJ Research, MA, USA). Automatic DNA sequencing was carried out with BigDye terminator cycle sequencing ready reaction kit (Applied Biosystems) and analyzed on an ABI PRISM 310 DNA sequencer (Applied Biosystems). DNA manipulations in *E. coli* were performed as described by Sambrook and Russell (13), and those in *Streptomyces* were done as described by Kieser et al. (14).

Sample preparation for paper disc diffusion assay.

Actinomycetes strains isolated from the soil samples collected in Kosugi-machi, Toyama prefecture, Japan were used for the screening. The isolated strains were inoculated into 500 ml K-1 flasks containing 100 ml of V-22 medium. After incubation at 30ºC for 4 days on a rotary shaker at 200 rpm, five milliliters aliquots of this seed culture were transferred into 500 ml K-1 flasks each containing 100 ml of A-3M medium. The fermentation was carried out at 30ºC for 7 days on the same rotary shaker. The culture broth was extracted with 100 ml of *n*-butanol and the extract was subjected to the screening assay.

Assay procedure for secondary metabolism and sporulation promoter.

Nutrient broth soft agar containing 10^8 spores of *S. lividans* TK23 was overlaid on Bennett's agar plate. *n*-Butanol extracts described above were absorbed in paper discs (diameter: 10 mm), dried up, placed on the plates and incubated at 30ºC. Pigment production and cell differentiation around the paper disc was observed every 24 h. Spore suspension was prepared according to the procedure reported by Kieser et al (14).

Purification of goadsporin.

Paper disc diffusion assay described above was used to detect the active fractions and the amount and purity of goadsporin was estimated by HPLC analysis described below. Goadsporin was purified by the following procedures.

(i) Fermentation. *Streptomyces* sp. TP-A0584 was inoculated into 500 ml K-1 flasks containing 100 ml of V-22 medium. After incubation at 30ºC for 2 days on a rotary shaker at 200 rpm, five milliliter aliquots of the seed culture were transferred into a hundred 500 ml K-1 flasks each containing 100 ml of A-3M medium. The fermentation was carried out at 30 ºC for 4 days.

(ii) Diaion HP-20 column chromatography. The cultured broth (10 liters) was centrifuged at 5000 × *g* for 10 min. The supernatant was discarded and the precipitated mycelial cake was extracted with 5 liters of 80 % aqueous acetone solution three times. After the evaporation to remove acetone, the resultant aqueous solution was applied onto a column of Diaion HP-20 resin (9.5 i.d. × 29 cm; Mitsubishi Chemical Co., Japan) equilibrated with distilled water. The column was washed with 2.5 liters of distilled water and eluted with 5 liters each of 20, 40, 60 and 80 % aqueous acetone. Inducing activity on pigment and spore formation was found in the fraction eluted with 60 % aqueous acetone. This fraction was concentrated *in vacuo* and the resultant 2.2 liters of aqueous layer was extracted with 1.1 liters of ethyl acetate twice and concentrated *in vacuo* to give 2.2 g of crude extract.

(iii) Silica gel column chromatography. The crude extract was dissolved in 10 ml of methanol and applied to a column of silica gel 60 (4 i.d. × 22 cm, Merck, NJ) equilibrated with chloroform. The column was eluted with a gradient of chloroform-methanol (30:1~ 2:1, 1.5 liters) . The fractions containing the active component were eluted in chloroform-methanol (5:1), pooled and evaporated *in vacuo* to give crude goadsporin (782 mg).

(iv) LH-20 gel filtration chromatography. The crude goadsporin was dissolved in 10 ml of chloroform-methanol (1:1) and applied to a column of Sephadex LH-20 (2.1 i.d. × 86 cm, Amersham

Pharmacia Biotech, UK) equilibrated with chloroform-methanol (1:1). The column was eluted with chloroform-methanol (1:1). The fractions containing goadsporin were pooled and evaporated *in vacuo* to give semi-pure goadsporin (576 mg).

(v) Reverse phase silica gel column chromatography. The residue (semi-pure goadsporin) dissolved in 10 ml of methanol was applied to ODS-AM reverse phase silica gel column (4.6 i.d. × 20 cm, YMC, Japan) equilibrated with acetonitrile-0.15 % KH_2PO_4 (pH 3.5) (2:8). The column was eluted with acetonitrile-0.15 % KH_2PO_4 (pH 3.5) (1:1). The fractions containing active material were pooled, evaporated *in vacuo*. The resultant aqueous layer was extracted with ethyl acetate. The organic layer was dried over anhydrous Na_2SO_4 and concentrated *in vacuo* to give pure goadsporin (316 mg).

HPLC analysis.

HPLC analysis was performed with HP1090 (Hewlett Packard, CA) system using C18 Rainin microsorb column (3 m, 4.6 i.d. × 100 mm, Rainin Instrument Co., MA). Acetonitrile-0.15 % KH_2PO_4 was used for an elution buffer. The sample was eluted at a flow rate of 1.2 ml/min with a gradient of acetonitrile-0.15 % KH_2PO_4 (pH 3.5), and goadsporin was detected at 254 nm.

Antimicrobial assay.

The minimum inhibitory concentrations against bacteria and yeasts were determined by the 2-fold serial dilution method in heart infusion broth or Yeast morphology broth (Difco Lab.).

Results and Discussion

Screening of the inducer of secondary metabolism and morphogenesis.

Fermentation broth of 405 actinomycetes strains isolated from soil samples were subjected to the induction test of the pigment production in *S. lividans* TK23. The spore suspension of *S. lividans* TK23 was mixed with Nutrient Broth soft agar and ca. 10^8 spores were plated on a Bennett's agar plate. Actinomycetes were cultured in A-3M medium and the culture broth was extracted with *n*-butanol. The extracts were assayed for induction of pigment formation and sporulation of *S. lividans* TK23, and *Streptomyces* sp. TP-A0584 was found to produce a substance which promotes the formation of diffusible red pigment and aerial hyphae and the sporulation in *S. lividans* TK23.

Fermentation and purification of goadsporin.

Fermentation for production of goadsporin was carried out for 6 days and the cultured cells were collected by centrifugation. The cells were extracted with the equal volume of 80 % aqueous acetone and the extract was applied to a series of column chromatography: HP-20 adsorption resin, silica gel, LH-20 gel filtration and reversed phase silica gel, as described in Materials and Methods. 316 mg of pure active compound was obtained from 10 liters of culture broth. The purity was confirmed by HPLC and NMR analysis. This compound was named goadsporin after its ability to stimulate (goad) the sporulation.

Goadsporin is a chemically and biologically novel compound.

Structure of goadsporin (Fig. 1) was determined

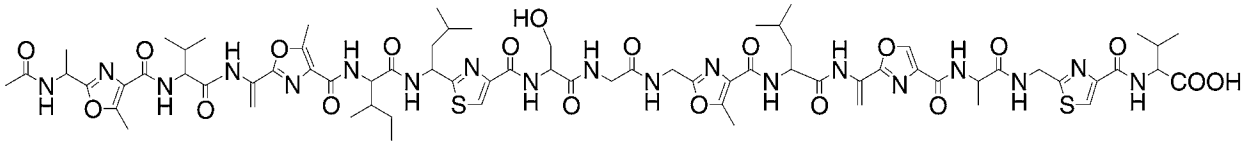

Fig. 1. Structure of goadsporin.

by the analysis of NMR and mass spectra. Determination of structure of goadsporin has been reported in another paper (16). The molecular formula of goadsporin is $C_{72}H_{97}N_{19}O_{20}S_2$ (M.w. 1611.66). Goadsporin is a linear oligopeptide containing nineteen amino acids, six of which are cyclized to form four oxazole and two thiazole rings. Most of the amino acids in goadsporin are hydrophobic. The N-terminal is acetylated while the C-terminal is a free carboxylic acid. Database search of this structure using C.A. file resulted in finding of no coincidence with the structures of known classes of natural products. Database search found no analogous compounds ever reported, suggesting that goadsporin is a unigue compound specifically active against streptomycetes. In fact, goadsporin did not show any antibiotics and cytotoxic activity, protein kinase C phospholylation inhibition and apoptosis induction to mammalian cells (data not shown). Thus, the molecular target of goadsporin is supposed to be a specific one in streptomycetes but not a common one in all organisms such as DNA, protein kinases or ribosomes.

Goadsporin promotes the morphogenesis in a wide variety of streptomycetes.

As shown in Fig. 2, ring-shaped zones of the sporulation and the pigment production by various streptomycetes cultures were observed around the goadsporin containing paper disc placed on Bennett's agar medium. This Figure shows the concentration dependency of goadsporin in the precocious induction of sporulation and the red pigment formation. The spore formation in the gray zone was confirmed by electron microscope observation (data not shown).

Induction of secondary metabolism and sporulation with goadsporin was examined on 42 streptomycetes strains randomly selected from the stock strains in our laboratory. Among the 42 strains, 10 μg goadsporin/paper disc induced sporulation in 32 strains (76%) around the disc (Fig. 2), and promoted pigment production in 20 strains (48 %). Growth inhibition was observed at the high concentration of goadsporin in 32 strains (76 %). It is obvious that the sporulation was induced in some range of goadsporin

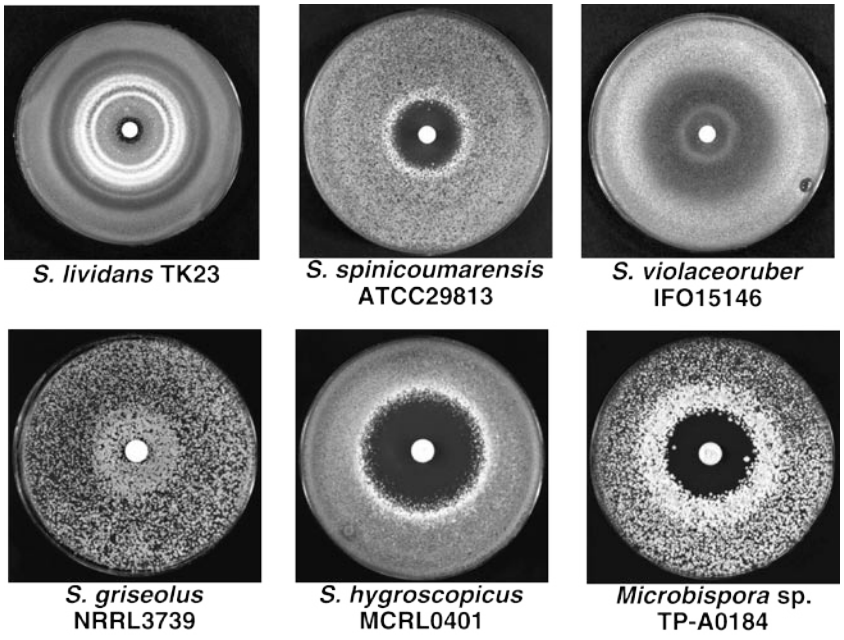

Fig. 2. Effects of goadsporin on the morphogenesis and pigment production of various streptomycetes on solid medium. Photographs show cultures of various streptomycetes on Bennett's agar medium on which 6 nmol (ca. 10 μg) of goadsporin-absorbed paper disc was placed.

concentration because the spore formation was observed as a ring-shaped zone around the paper disc. In addition, growth inhibition was caused by goadsporin at high concentration in streptomycetes which can respond to goadsporin to sporulate. So, we expected that some antibiotics may induce the sporulation like goadsporin. 200 μg of streptomycin, kanamycin, thiostrepton, bacitracin and gramicidin D were absorbed in a paper disc and assayed their activity on induction of sporulation. However, none of them showed goadsporin-like activity on *S. lividans* TK23. In the life cycle of streptomycetes, formation of the aerial hyphae and subsequent sporulation take place after the sufficient growth of substrate mycelium. If the high concentration of goadsporin is present in the early stage of the growth, it may promote the aerial hyphae formation before the enough development of substrate mycelium, resulting in the growth inhibition. A recent study revealed that the spore pigment derives from polyketide (17), most common secondary metabolites in streptomycetes. In this study, we have shown that goadsporin promotes both the sporulation and secondary metabolism in several streptomycetes, suggesting the presence of common regulation components for sporulation and secondary metabolism and the possible involvement of goadsporin with them.

Antibiotic activity of goadsporin.

The antibiotic activity of goadsporin was examined (Table 2). It showed growth inhibition against *Streptomyces*, but no activity against the other microorganisms even at 100 μg/ml. *Streptomyces scabies*, the causative agent of potato scab, distributes widely in potato growing areas and causes considerable economic loss in the world. It is expected that goadsporin can be utilized as an agrochemical against potato scab.

Goadsporin does not have any biological activity against its producing strain.

Interestingly, goadsporin added to the medium did not induce the precocious spore and pigment formation in the goadsporin producing strain, *Streptomyces* sp. TP-A0584 (data not shown). All of the so far reported signal molecules in streptomycetes induce their sporulation or secondary metabolism. Goadsporin is a different type molecule, because it dose not activate sporulation or secondary metabolism of goadsporin producing strain. Considering the fact that the goadsporin producing strain accumulates goadsporin within the cell, it is possible that goadsporin does not permeate the cell membrane of

Table 2. *In vitro* antibacterial activities of goadsporin

Organism	Relevant characteristics	MIC (γ: μg/ml)
Streptomyces lividans TK23	Gram (+)	6.4
Streptomyces coelicolor A3(2)	Gram (+)	3.2
Streptomyces scabies JCM7913	Gram (+)	0.2
Bacillus subtilis ATCC6633	Gram (+)	>100
Escherichia coli NIHJ JC-2	Gram (−)	>100
Staphylococcus aureus 209P JC-1	Gram (+)	>100
Pseudomonas aeruginosa TP-B0270	Gram (−)	>100
Proteus mirabilis ATCC21100	Gram (−)	>100
Sacchromyces cerevisiae TP-F0176	yeast cell	>100
Candida albicans TP-F0594	yeast cell	>100
Cryptococcus neoformans ATCC90112	yeast cell	>100
Torulopsis glabrata IFO0622	yeast cell	>100
Aspergillus fumigatus IFO8866	filamentous fungi	>100

the producing strain. Some of tested streptomycetes did not respond to goadsporin stimulation, and this may be due to the same reason. One possible explanation for goadsporin function in nature is that *Streptomyces* sp. TP-A0584 controls the other goadsporin-nonproducer *Streptomyces* species with goadsporin by the growth inhibition or the sporulation acceleration to take advantage of its own survival.

Cloning of the goadsporin biosynthetic gene cluster.

We predicted that goadsporin is biosynthesized ribosomally, because purified goadsporin contained 19 amino acids and all of them are L-form. Dehydroalanin and oxazole ring might be derived from serine, methyloxazole from threonine, and thiazole from cystein. Therefore the amino acid sequence of goadsporin precursor would be ATVSTILCSGGTLSSAGCV. Then based on the amino acid sequence, oligonucleotide was synthesized. Southern hybridization was performed with this oligonucleotide as the probe against the *Streptomyces* sp. TP-A0584 chromosomal DNA digested with various restriction endonucleases. Among positive signals with different sizes depending on the restriction enzymes used, we chose 1.3-kb signal in the *Bam*HI digest and cloned the corresponding DNA sequence into pUC19. Nucleotide sequencing of the 1.3-kb *Bam*HI fragment revealed that 49-amino-acid length open reading frame contained the above-described amino acid sequence. We named this gene *god*A, one of the god cluster. To clone an entire set of goadsporin biosynthetic gene cluster, a cosmid library of genomic DNA of strain TP-A0584, which was constructed with *Sau*3AI partially digested genomic DNA and a bi-functional cosmid, pTOYAMAcos, was screened by colony hybridization with the 1.3-kb *Bam*HI fragment as a probe. Three positive clones were obtained and designated pGSBC1, pGSBC2, and pGSBC3, respectively.

Heterologous expression of goadsporin in S. lividans.

Three clones were transformed into *S. lividans* TK23, that is a surrogate host for heterologous expression. pTOYAMAcos cosmid vector is integrated into the specific chromosome *attC* site in actinomycetes (12). Only a pGSBC1 integrated strain produced goadsporin. Nucleotide sequencing of the pGSBC1 fragment revealed that *godA* is located on the end of the fragment and 14 ORFs are located on the downstream of *godA* spanning 20-kb. Subcloning experiments revealed that essential region for goadsporin biosynthesis is between *godA* and *orf5* spanning 20-kb as shown in Fig. 3. In conclusion, the ten genes, *godA*, *godB*, *godC*, *godD*, *godE*, *godF*,

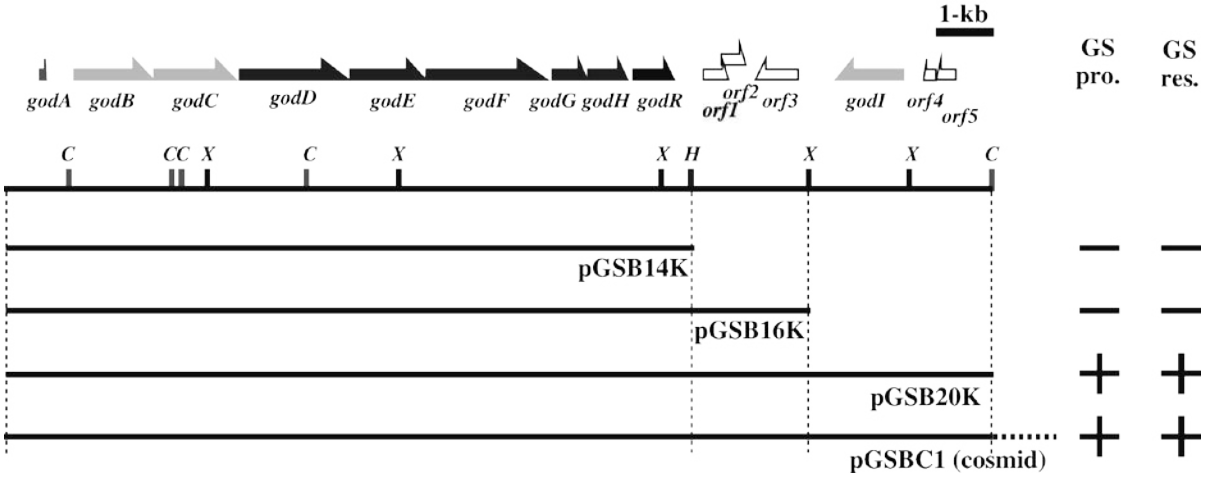

Fig. 3. Restriction and gene organization map of the plasmid cloned DNA fragment from *Streptomyces* sp. TP-A0584. C, ClaI; X, XhoI; H, HindIII; GS pro., goadsporin production; GS res., goadsporin resistance.

godG, *godH*, *godI*, and *godR* are responsible for goadsporin biosynthesis.

Characterization of the goadsporin biosynthetic gene cluster.

Computer-aided analysis of the DNA sequence of the cloning region led to identification of the genes listed in Table 3.

The structural gene for goadsporin, *godA* encodes the 49-amino acid propeptide of goadsporin. GodA is a 49 amino acid protein.

godB encoded a protein of 550 amino acids. BLAST search reveals that GodB is similar to LktB, Leukotoxin secretion ATP-binding protein in *Actinobacillus actinomycetemcomitans*. Both show 22 % identity over the entire sequences. Hydropathy plots predict the formation of six membrane-spanning helices in membrane domain (from 1 to 300 amino acid position). ATP-binding motif (GSSGSGKS) are conserved in the amino acid position between 375 and 382 residue.

GodC is a 577-amino-acid protein that shows sequence similarity to ABC transporter family as well as GodB. ATP-binding motif, GPSGAGKT is conserved at the position 362 to 369 amino acid residue from N-terminal. GodC shows sequence similarity to GodB over the entire sequence (20.0 % identity). Both protein might be responsible for translocation of goadsporin and/or goadsporin

Table 3. Deduced genes and their proposed functions in the *god* cluster

gene	amino acids	homologous gene	% identity of products	origin (biosynthetic gene cluster)	accession No.
godA	49	goadsporin structure gene			
godB	550	*lktB*:Leukotoxin secretion ATP-binding protein	22.7	*Actinobacillus actinomycetemcomitans*	P23702
godC	557	*lktB*	18.7	*A. actinomycetemcomitans*	P23702
godD	735	*gra-orf12* involved in granaticin biosynthesis	44.4	*Streptomyces violaceoruber*	T46517
godE	522	nitroreductase (putative)	32.0	*Trichodesmium erythraeum*	ZP00072007
godF	867	function unknown			
godG	229	function unknown			
godH	222	acetyltransferase (putative)	40.9	*Mycobacterium tuberculosis*	NP215317
godR	238	*brpA*:regulator protein of bialaphos biosynthesis	22.7	*Streptomyces hygroscopicus*	Q01108
orf1	160	transposase (putative)	93.8	*Streptomyces avermitilis*	NP828729
orf2	147	transposase (putative)	89.8	*S. avermitilis*	NP828730
orf3	304	transposase (putative)	76.3	*Streptomyces coelicolor* A3(2)	NP631141
godI	518	*ffh*:signal recognition particle protein	44.6	*Escherichia coli*	P07019
orf5	73	transposase (putative)	*43.8	*S. avermitilis*	NP821430
orf6	128	transposase (putative)	*42.5	*S. avermitilis*	NP821430

*:The homologous region is partial.

modifying enzymes to the membrane.

GodD is a 735-amino-acid protein that shows over the entire sequence similarity to *gra-orf12*, which is involved in granaticin biosynthetic gene cluster (44.4 % identity, 60 % similarity). Granaticin is a benzoisochromaquinone type antibiotics produced by *Streptomyces violaceoruber*, however the function of *gra-orf12* in the granaticin biosynthesis is unknown.

godE encoded a protein of 522 amino acid residues. A Blast search indicated 25 % identity to the *mcbC* at the amino acid position between 280 and 454 residue. McbC forms the multimeric microcin synthetase complex (composed of the McbB, -C, and -D proteins), and cyclizes four cysteine and four serine to thiazoles and oxazoles in the propeptide of microcin B17, respectively.

godF and *godG* encoded proteins of 867 and 229 amino acid residues, respectively. A Blast search shows no similar proteins in GenBank database.

godH encodes a putative 222 amino-acid protein that shows sequence similarity to Rv0802c, the putative acetyltransferase (40.9 % identity). In goadsporin biosynthesis, GodH protein is supposed to catalyze acetylation of N-terminal of goadsporin.

godR encodes a 238 amino acid protein with sequence similarity to *brpA* (22.7 % identity) from the bialaphos biosynthetic gene cluster in *Streptomyces hygroscopicus*. In particular, helix turn helix DNA binding motif is strongly conserved at the position 208 to 227 amino acid residues from N-terminal (75 % similarity).

godI shows a sequence similarity to *ffh*, signal recognition particle protein in *Escherichia coli* (44.6 % identity, 74.9 % similarity). Signal recognition particle (SRP) is one of ribosomal proteins and catalyzes targeting of nascent secretory and membrane proteins to the protein translocation apparatus of the cell. SRP homologs have been identified in all living cells analyzed to date. Hypothetical *ffh* homologs in *Streptomyces avermetilis* and *S. coelicolor* are also highly conserved in *godI* (76.6% and 75.9% identity). To the best of my knowledge, it is the first case that SRP system is involved in secondary metabolite biosynthesis.

Proposed overall biosynthetic pathway of goadsporin.

A proposed biosynthetic pathway of the goadsporin is shown in Fig. 4. The 49 residue *godA* polypeptide is a substrate, and processed by putative goadsporin synthetase, *godD*, *E*, *F*, *G* products. They introduce six heterocycles and converts GodA to proGoadsporin. Proteolysis of proGoadsporin is performed by GodB which contains a conserved peptidase domain. Finally GodH, which encodes the putative acetyltransferase, catalyses the N-acetylation of N-terminal to end goadsporin biosynthesis. GodI may be responsible for the resistance of goadsporin and/or translocation of goadsporin and its biosynthesis apparatus.

Conclusion

Goadsporin which was isolated from *Streptomyces* sp. TP-A0584 is a 19-amino-acid polypeptide containing four oxazole and two thiazole rings within its backbone (15). Except for goadsporin, linear polypeptides containing thiazole and oxazole rings have not been isolated from actinomycetes. Goadsporin promotes secondary metabolism and morphogenesis in actinomycetes. For example, it promotes the formation of red pigment and sporulation at a concentration of 1 μM and induces growth inhibition at more than 1 μM in *Streptomyces lividans*. Such an activity was observed to a wide variety of actinomycetes, but no activity to the other organisms (15). The biosynthesis of goadsporin would be started by the translation of *godA* structural gene, and then the serine residue is modified to oxazole or dehydro-alanine, threonine to methyloxazole, and cystein to thiazole. *godD*, *godE*, *godF*, and *godG* products would be involved in such a post translational modification. Finally, the peptide sequence of N terminal region would be digested and acetylated by functions of *godC* and *godH* procusts to afford mature goadsporin.

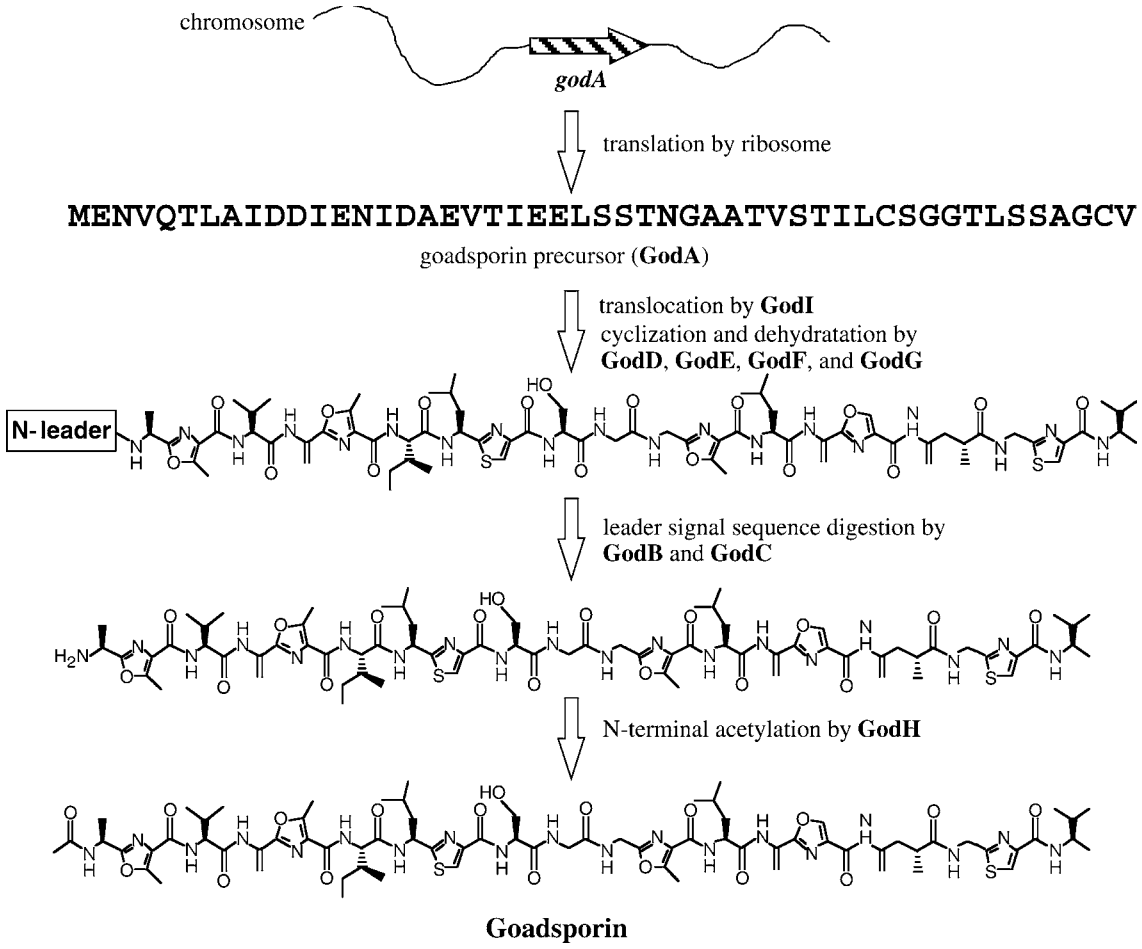

Fig. 4. Proposed overall biosynthetic pathway of goadsporin.

References

(1) Bibb M: The regulation of antibiotic production in *Streptomyces coelicolor* A3(2). *Microbiology* **142**:1335−1344, 1996

(2) Chater, K. F: Taking a genetic scalpel to the *Strepomyces* colony. *Microbiology* **144**:1465−1478, 1998

(3) Horinouchi, S, and T. Beppu: Autoregulatory factors and communication in actinomycetes. *Annu. Rev. Microbiol.* **46**:377−98, 1992.

(4) Yamada Y: Butyrolactone autoregulators, inducers of secondary metabolites, in *Streptomyces*. *Actinomycetology* **9**:57−65. 1995

(5) Matsumoto A, SK. Hong, H. Ishizuka, S. Horinouchi, and T. Beppu : Phosphorylation of the AfsR protein involved in secondary metabolism in *Streptomyces* species by a eukaryotic-type protein kinase. *Gene* **146**:47−56, 1994

(6) Chater KF, CJ. Bruton, KA. Plaskitt, MJ. Buttner, C. Mendez, and JD. Helmann: The developmental fate of *S. coelicolor* hyphae depends upon a gene product homologous with the motility sigma factor of *B. subtilis*. *Cell* **59**:133−43, 1989

(7) Horinouchi S, and T. Beppu : Production in large quantities of actinorhodin and undecylprodigiosin induced by *afsB* in *Streptomyces lividans*. *Agric. Biol. Chem.* **48**:2131−2133, 1984

(8) Horinouchi S, and T. Beppu : A-factor as a microbial hormone that controls cellular differentiation and secondary metabolism in *Streptomyces griseus*. *Mol. Microbiol.* **12**:859−

864, 1994

(9) Khokhlov, A. S, I. I. Tovarova, L. N. Borisova, S. A. Pliner, L. A. Schevchenko, E. Y. Kornitskaya, N. S. Ivkina, and I. A. Rapoport : A-factor responsible for the biosynthesis of streptomycin by a mutant strain of *Actinomyces streptomycini*. *Dokl*. *Akad*. *Nauk SSSR* **177**:232−235, 1967

(10) Onaka, H, N. Ando, T. Nihira, Y. Yamada, T. Beppu, and S. Horinouchi : Cloning and characterization of the A-factor receptor gene from *Streptomyces griseus*. *J. Bacteriol*. **177**: 6083−6092, 1995

(11) Onaka, H, T. Nakagawa, and S. Horinouchi : Involvement of two A-factor receptor homologues in *Streptomyces coelicolor* A3(2) in the regulation of secondary metabolism and morphogenesis. *Mol*. *Microbiol*. **28**: 743−753, 1998

(12) Onaka, H, S. Taniguchi, Y. Igarashi, and T. Furumai : pTOYAMAcos, pTYM18, and pTYM19, actinomycete-*Escherichia coli* integrating vectors for heterologous gene expression. *J. Antibiot*. **56**: 950−956, 2003

(13) Sambrook, J, and D. W. Russell: *Molecular cloning*, a laboratory manual, third edition. Cold Spring Harbor Laboratory Press, NY, USA., 2001

(14) Kieser, T, M. J. Bibb, M. J. Buttner, K. F. Chater, and D. A. Hopwood: *Practical Streptomyces genetics*. (The John Innes Foundation, Norwich, UK), 2000

(15) Onaka, H, H. Tabata, Y. Igarashi, Y. Sato, and T. Furumai: Goadsporin, a chemical substance which promotes secondary metabolism and morphogenesis in streptomycetes. I. Purification and characterization. *J. Antibiot*. **54**: 1036−1044, 2001

(16) Igarashi Y, Y. Kan, K. Fujii, T. Fujita, K. Harada, H. Naoki, H. Tabata, H. Onaka, and T. Furumai: Goadsporin, chemical substance which promotes secondary metabolism and morphogenesis in streptomycetes. II. structure determination. *J. Antibiot*. **54**: 1045−1053, 2001

(17) Davis N.K, and K.F. Chater : Spore colour in *Streptomyces coelicolor* A3(2) involves the developmentally regulated synthesis of a compound biosynthetically related to polyketide antibiotics. *Mol*. *Microbiol*. **4** : 1679−91, 1991

(18) Igarashi, Y, K. Takagi, T. Kajiura, and T. Furumai : Glycosylquestiomycin, a novel antibiotic from *Microbispora* sp. TP-A0184: fermentation, isolation, structure determination, synthesis and biological activities. *J. Antibiot*. **51**: 915−920, 1998

A Novel 120kDa Wall-Anchored Protein Produced by Oral *Streptococcus mutans*

Yutaka Sato

Department of Biochemistry, Tokyo Dental College, 2-2 Masago 1-chome, Mihama-ku, Chiba City 261-8502, Japan

Introduction

Streptococcus mutans is regarded as the primary etiologic agent of human dental caries and resides in the oral biofilm called dental plaque attached to tooth surfaces. To adhere to tooth surfaces through dental plaque, *S. mutans* produces several extracellular proteins or enzymes, which have been extensively studied at the molecular level during the past two decades. Several genes encoding these molecules were identified, characterized, and classified (7).

We have examined cell wall proteins from several strains of this organism following lysis of the cell wall with a peptidoglycan N-acetylmuramylhydrolase as previously described (38), and in some strains of this organism, found several major protein bands by Coomassie brilliant blue (CBB) staining of an electrophoresed SDS-polyacrylamide gel. However, several of these proteins were unexpectedly found to be intracellular proteins, e.g., 60 kDa heat-shock protein GroEL (a 60 kDa band), enolase (a 50 kDa band), and glyceraldehyde-3-phosphate dehydrogenase (a 40 kDa band), following analyses by N-terminal amino acid sequencing.

As typical examples of these protein bands, wall samples from strains Z1 and UA159 are shown in Fig. 1. Recently, the intracellular proteins were reported to be extracellularly detected, even though they do not have the typical signal sequence and were suggested to be involved in pathogenesis of bacteria (25). Besides the three protein bands indicated with asterisks in Fig. 1, a 120 kDa protein band was detected by CBB staining of the same gel in Z1 strain. Since this protein was so far unidentified, we focused on this 120 kDa protein.

Recently, we found a correlation between constitutive expression of this 120 kDa protein and a phenomenon that we designated cold-agglutination (defined as reversible agglutination after incubation at <25°C for two hours), suggesting that the 120 kDa protein interacts with molecules in its environment. In addition, we found that cold-agglutination was not observed in sortase mutants of a 120 kDa protein-positive strain. Therefore, this protein was expected to be a true wall protein member designated wall-anchored protein (13, 14, 17). Wall-anchored proteins are a group of extracellular proteins that are exported but tethered to the peptidoglycan mediated by the extracellular sortase (23). Wall-anchored proteins are commonly expressed in Gram-positive bacteria and are characterized by a common structure. These molecules contain an N-terminal signal peptide and a common LPXTG sequence motif to be recognized by the sortase which is followed by a C-terminal hydrophobic domain and charged tail (23). Five genes encoding wall-anchored protein have been characterized in *S. mutans* up to now, i.e., *pac, fruA, dexA, gbpC,* and *wapA* (6, 10, 12, 24, 35).

The genome project of this organism has been recently completed (1) and reported to add one more gene for a new wall-anchored protein. However, the 120 kDa protein was not likely encoded by any of the six previously described wall-anchored protein genes and we were not able to identify any candidate gene encoding this protein by the genome database search

of *S. mutans* strain UA159 (http://www.genome.ou.edu/smutans.html).

In the present report, we describe utilization of a random mutagenesis strategy using the *Himar1* minitransposon recently developed by Akerly and Lampe (2) to isolate cold-agglutination-negative mutants, which should be defective in this protein, and also describe successful identification of the gene encoding the 120 kDa protein and its characterization.

Materials and Methods

Bacterial strains.

S. mutans strain used for random mutagenesis was Z1, which is one of the previously isolated strains in Tokyo Dental College. Its mutant 05A02 in which the *cnm* gene (see the section "Isolation of eold eggalutination-negative mutants.") was interrupted by minitransposon insertion was isolated by an *in vitro* random mutagenesis described below. The strain Z1 showed colony morphology specific for *S. mutans* on the Mitis-Salivarius-Bacitracin agar plate and exhhibited *S. mutans* specific biotype reported by Shklair (41). Nucleotide sequence of the 16 S rRNA gene from the strain Z1 indicated that this strain belongs to *S. mutans* species (5). The PCR method recently developed to distinguish serotypes of *S.mutans* (40) determined the strain Z1 to be serotype f. Other *S. mutans* strains used were shown in Fig. 6. Streptococci were maintained and cultured in Todd-Hewitt (TH) broth/agar plates and kanamycin (Km) was added at 500 μg/ml in the media where indicated. *Escherichia coli* strain TOP10 obtained from a commercial supplier (Invitrogen, Carlsbad, CA) was used as a host for plasmid pBAD/His and its derivatives, and strain DH5a was routinely used for standard procedures of DNA manipulation (34).

Isolation of the 120 kDa wall protein.

The streptococcal cells were harvested, washed, and suspended in 10 mM potassium phosphate buffer (KPB). The cells were disrupted by ultrasonication, and fractionation of wall proteins was carried out as described previously (38) with the following slight modifications for large sized preparation. The cells at late exponential growth were collected from 100 ml of the respective TH broth cultures of strains Z1 and UA159 and transferred into sealed styrene-acrylonitrile co-polymer tubes. The tubes were subjected to 40 cycles of 30 sec ultrasonication with 60 sec cooling intervals to obtain disrupted wall particles. The washed wall particles were suspended in 200 μl of KPB containing 0.1 mM $MgCl_2$ and digested for 2 h by the addition of 60 μl of 1 mg/ml N-acetylmuramidase SG™ (2,000 u/mg protein, Seikagaku Corporation, Tokyo, Japan). The resultant 240 μl wall sample was mixed with 80 μl of the SDS sample buffer and frozen until electrophoresis on the gel system of Laemmli (SDS-PAGE). Sixty μl of the sample were applied to each well, separated on 10 % SDS-PAGE, and transferred to a polyvinylidene difluoride (PVDF) membrane (Immobilon-P™, Millipore Corporation, Bedford, MA) that had been pre-soaked in methanol. SDS-PAGE was carried out at 1 mA/cm^2 for 60 min in equilibrating buffer. Protein bands were visualized by staining with 0.1 %(w/v) Coomassie brilliant blue R-250 in 50 %(v/v) methanol, 10 %(v/v) acetic acid. The protein band corresponding to the 120 kDa protein was excised from the PVDF membrane blot and its amino acid residues were sequenced (Shimadzu Corporation, Kyoto, Japan).

DNA manipulations.

Isolation of plasmid DNA and cloning procedures were carried out by standard procedures (34).

Random mutagenesis by in vitro transposition.

1) Isolation and purification of transposase. The expression plasmid pMALC9 encoding the *Himar1* transposase was generously provided by D. J. Lampe (Duquesne University, Pittsburg) (15), and propagated in *E. coli* strain DH5a. The amplified plasmid was then introduced into *E. coli* strain TB1. Induction, isolation, and purification of the *Himar1* transposase were performed according to the protocol recently described (2). Briefly, 800 μl of an overnight culture of *E. coli*

TB1 harboring pMALC9 was inoculated into 80 ml of LB medium supplemented with 100 μg/ml ampicillin and incubated with shaking at 37°C for 3 h (OD_{600}=0.47). To induce protein production, 240 μl of 0.1 M isopropyl-β-thiogalactopyranoside (IPTG) was added and the culture was grown for additional 2 h. Cells were collected, washed, and disrupted by a single pass through a French Press at 150 MPa. Insoluble material in the cell lysate was spun down and the supernatant was subjected to purification using amylose resin (New England Biolabs, Beverly, MA), since active *Himar1* transposase coded by pMALC9 is an MBP (maltose-binding protein)-transposase fusion protein. Thirty μl aliquots of purified transposase were stored at −80 ºC until use.

2) Minitransposon plasmid. Plasmid pJFP2 was generously provided by T. Kitten (Virginia Commonwealth University, Richmond,VA) and was amplified in *E. coli.* Concentration of the plasmid was adjusted to approximately 100 femto moles/μl. This plasmid contains the *Himar1* minitransposon with a gene encoding kanamycin resistance when inserted into streptococcal chromosomal DNA.

3) *In vitro transposition mutagenesis with the HimarI minitransposon. In vitro* transposition was carried out according to the protocols described recently (2) (T. Kitten, personal communication) with slight modifications. The transposition reaction mixture containing 10 μl of *S. mutans* strain Z1 chromosomal DNA (1.35 μg), 1 μl of pJFP2 (100 femto moles), 4 μl of 50 % glycerol, 1 μl of purified transposase (1/10 diluted), and 4 μl of 5 × reaction buffer (125 mM Hepes pH 7.9, 1.25 mg/ml acetylated BSA, 10mM DTT (dithiothreitol), 500 mM NaCl, 25 mM $MgCl_2$) was incubated at 30 ºC for 1.5 h to allow transposition of the elements from pJFP to Z1 chromosomal DNA. The reaction was terminated by heating at 70 ºC for 10 min and precipitated with ethanol. The precipitated material was dissolved in 20 μl of the reaction buffer containing T4 DNA polymerase (1.75 units, Takara, Kyoto, Japan) with dNTP, and incubated at room temperature for 20 min. The reaction was then terminated by heating at 70ºC for 10 min. Following cooling to 16ºC, the reaction mixture was mixed with 4μl of 10 × T4 ligase reaction buffer, 4μl of 10 mM ATP, 11 μl of sterile water and 1μl of T4 DNA ligase (4 units, Toyobo, Osaka, Japan), and incubated overnight at 16 ºC. Then, 10μl of the mixture was used for transformation of *S. mutans* Z1, and the remaining 30μl was stored at 4ºC and used within a week. Transformation of *S. mutans* was accomplished by procedures routinely carried out in this laboratory (28).

Screening for the mutants that lack cold-agglutination.

All of the transformants detected on TH/Km or MS/Km agar plates following transformation of strain Z1 with the transposon mutagenized DNA were inoculated into 100μl of TH/Km broth dispensed into 96 well round bottom microplates (Code 3875-096, Asahi Techno Glass Corporation, Funabashi city, Japan). The microplates were sealed with adhesive seal-sheets (MS-30010, Sumitomo Bakelite Co. Ltd., Tokyo, Japan) to prevent evaporation of media and incubated overnight at 37ºC without shaking. Cells were suspended by shaking with a micromixer (R = 2.0 mm, Taitec EM-36, Koshigaya city, Japan) for 20 sec at approximately 1700 rpm, and the microplates were then stored at 4ºC for 2 h. After equilibration to room temperature, the microplates were again subjected to shaking with the micromixer for one min at approximately 800 rpm. Then, the cell suspensions in the wells were examined for agglutination on a specially devised light box , and non-agglutinated clones were selected (35).

Chromosome walking.

In order to isolate chromosomal fragments flanking the minitransposon targeted dinucleotide (TA), the fragments were amplified by PCR with the Universal GenomeWalker Kit (Clontech, Palo Alto, CA) using specific primers recommended by the supplier. The primers used are listed in Table 1. Chromosomal fragments flanking the minitransposon were initially amplified with a specific primer (2tp1 or 2tp2) corresponding to either end of the minitransposon and an adopter primer (AP1 or AP2) as recommended by the supplier. Amplified fragments

Table 1. Primers used in this study

ACAAGTACGCATGATGCCAT	(srt5')
CCAACTGATACGCTCTGGTG	(srt3')
GTAATACGACTCACTATAGGGC	(AP1)
ACTATAGGGCACGCGTGGT	(AP2)
TACTAGCGACGCCATCTATGTGTCAGA	(1., 2tp1)
GGGTATCGCTCTTGAAGGGAACTATGT	(2., 2tp2)
CCTGCTGGAACTGATGTCGT	(3., DSHpa1R)
AAGCTATGAAAAACATTGGCA	(4., DVPvII1R)
TCAGCTGATCCGGCTAGT	(5., DSHpa1F)
CTTAGAAGGTCTTCTTTTTTATTATTCGT	(6., DVPvII2F)
CCTTAACTTTAGTAGTTGTTTCTTCAGCT	(7., DSHpa2R)
GTAGCTAATGTTAATGCCGCC	(8., DSHpa2F)
CTGTAGTAGTGGTTGTTCTTCCGT	(9., DSHpa3R)
AAACAACTACTAAAGTTAAGGAACCAGA	(10., DSHpa3F)
TCAGCTATGATATTTACGGTAAACTAGA	(11., 120KD_Rv)
ATCTGCAGTGATGTCAGCAGTAACATTTCA	(12., 120kDFwFu)

Primer names are indicated in the parentheses, and numbers preceded the names correspond to those indicating the location in Fig. 3. Primers AP1 and AP2 were supplied with the Universal GenomeWalker Kit (Clontech, Palo Alto, CA).

were purified and sequenced using the same primers. Based on the obtained nucleotide sequence information, subsequent primers were designed and appropriate fragments were amplified for sequencing using chromosomal DNA from parental strain Z1 and mutant 05A02 as templates. The location of these primers used are indicated in Fig.3.

Nucleotide sequencing and sequence analysis.

The amplified fragments were purified with QIAquick PCR Purification Kit (Qiagen K.K., Tokyo, Japan), and the corresponding regions were directly sequenced with a BigDye Terminator Cycle Sequencing FS Ready Reaction Kit using primers listed in Table 1 and the ABI PRISM Genetic Analyzer 310 (Applied Biosystems, Foster City, CA) as described previously (37). Sequence analysis was carried out with the DNASIS-Mac program (Hitachi Software Engineering, Yokohama, Japan). The *S. mutans* genome Database at the University of Oklahoma's Advanced Center for Genome Technology (http://www.genome.ou.edu/smutans.html) and the International DNA databases (EMBL, GenBank and DDBJ) were searched for similar amino acid sequences by using BLAST programs.

Southern hybridization analysis.

The restriction enzyme (*Hin*dIII etc.)-digested chromosomal DNA fragments from strain Z1, reference strains including strain UA159, and natural isolates were analyzed by use of the ECL direct nucleic acid labeling and detection system (Amersham Co. LTD., Tokyo, Japan) as described previously (35).

Cloning and expression of a collagen-binding domain of Cnm protein.

A gene fragment corresponding to the predicted collagen-binding domain of Cnm protein was amplified by PCR with primers, 120kDFwFu and DSHpa3R (Table 1) and ligated inframe to the 5' histidine-tag region of an expression vector pBAD/HisA (Invitrogen, Carlsbad, CA). Following transformation of *Escherichia coli* strain TOP10 with

the ligated vector, the resulting clones were analyzed as described previously (34). One of these clones, ZAXF, was used to perform collagen-binding assay along with strain TOP10 harboring the vector pBAD/HisA (strain pBAD) and that harboring plasmid pSBP6 expressing another histidine-tagged protein (strain SBP6 (38)) as negative controls. Cells of these strains grown with or without $2x10^{-3}$ % arabinose as an inducer were collected, washed, and subjected to 6 cycles ultrasonication as described above to obtain crude cell-free extracts for the collagen-binding assay. Induction of the histidine-tagged proteins was confirmed by SDS-PAGE and CBB staining before the assay.

Binding of recombinant Cnm to extracellular matrix (ECM) proteins.

An ELISA used to analyze the binding ability of recombinant protein to immobilized ECM proteins was carried out according to the procedure described recently (22) with slight modifications. Briefly, ELISA plates (Code 3801-096, Asahi Techno Glass Corporation, Funabashi city, Japan) were coated with 1μg of ECM proteins or bovine serum albumin (BSA) in 100μl of PBS (50 mM potassium phosphate, pH 7.2; 150mM NaCl) and incubated overnight at 4ºC. After washing with PBST (PBS with 0.01% Tween 20) and blocking with 5% BSA, varying amounts of cell-free extract (1-10μg protein in 20μl of PBS containing 0.1% BSA) were added to the wells and incubated for 1.5 h at 37ºC. Bound protein was detected by Anti-His HRP Conjugates (Qiagen) antibody.

Binding of wild type and mutant whole cells of S. mutans to ECM proteins.

An ELISA was used to evaluate the binding abilities of Z1 and 05A02 whole cells to immobilized ECM proteins. The ELISA was performed according to the procedure described previously (30) with a slight modification. ELISA plates were coated with ECM proteins, washed, and blocked as described above. Z1 and 05A02 whole cells were harvested from overnight cultures, washed three times with PBS, and adjusted to a turbidity of 1.0 on a spectorophotometer (Ubest35, JASCO Corporation, Tokyo, Japan), equivalent to approximately 1×10^9 cfu/ml. A 0.9 ml portion of the cell suspemtion was biotin-labeled by mixing with a 0.1 ml PBS containing 0.1μg of NHS-LC-Biotin (Pierce, Rockford, Ill.). Labeled cells were washed in the inner tubes of Ultrafree-CL centrifugal filter devices (0.22μm, Millpore Corporation, Bedford, MA) by three rounds of filtration and resuspension of the cells. Approximately 2×10^8 labeled cells were used for the binding assay which was performed by incubation in the ECM protein-coated ELISA plates for 1h at 37°C. Bound cells were detected with Streptavidin-HRP Conjugates (Amersham Biosciences, Piscataway, NJ).

Nucleotide sequence accession number.

The *cnm* nucleotide sequence data reported in this report will appear in the DDBJ, EMBL and GenBank nucleotide sequence databases under the accession number AB102689.

Results and Discussion

Isolation of the 120 kDa protein from wall samples.

Wall samples from strains Z1 and UA159 were prepared and analyzed by SDS-PAGE as described in Materials and Methods. A 180 kDa protein band corresponding to the surface protein antigen of *S. mutans* designated PAc, I/II, B, or Sr (24, 31, 32, 42) was clearly detected in the wall samples of strain UA159. In contrast, this protein band was only faintly observed in extracts of Z1 while a smaller m.w. band, around 120 kDa, was observed independent of the growth phase of the Z1 as shown in Fig.1. This protein was not a degradation product of the PAc protein, because the *pac*-deleted mutant of Z1 still expressed this protein (data not shown).

We selected 14 each of typical cold-agglutination-positive and negative phenotypic strains and examined whether or not the 120 kDa protein band was detected by SDS-PAGE and CBB staining. Results indicated a complete correlation between cold-agglutination-positive phenotype and expression of the 120 kDa

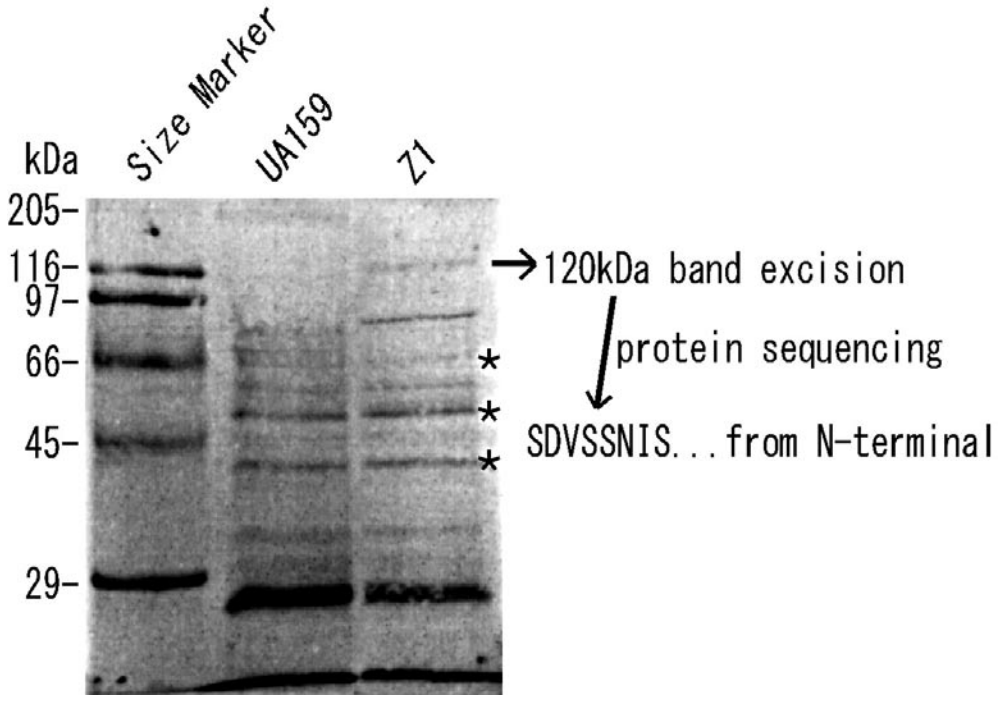

Fig.1. Protein bands visualized in the cell wall fraction of *S. mutans* Z1 and UA159 after SDS-PAGE. Wall protein samples from *S. mutans* strains Z1 and UA159 were separated by-SDS-PAGE and transferred to the PVDF membrane as described in the text. Asterisks indicate 60 kDa, 50 kDa, and 40 kDa bands probably corresponding to 60 kDa heat-shock protein, enolase, and glyceraldehyde-3-phosphate dehydrogenase, respectively. The partial N-terminal amino acid sequence of the Z1-specific 120 kDa protein is determined to be SDVSSNIS.

bands (data not shown). Therefore, we hypothesized that the 120 kDa protein could be involved in the cold-agglutination phenotype of this species. The 120 kDa band was not observed in the sample concentrated from culture supernatant fluid of strain Z1 and was not present in a wall fraction from the mutant in which the sortase gene was inactivated. These findings suggested that the 120 kDa protein was likely to be a wall-anchored protein possessing the LPXTG motif, and to be involved in cold-agglutination.

To determine the N-terminal amino acid sequence, the 120 kDa protein band of strain Z1 was isolated as described in Materials and Methods. The amino acid sequencing by Edman degradation revealed eight amino acid residues (SDVSSNIS) as a partial amino terminal amino acid sequence of the protein (Fig.1.), and the sequence was searched in the *S. mutans* strain UA159 genome database. However, no sequence corresponding to the determined sequence could be detected. A candidate gene encoding a 120 kDa protein with the LPXTG motif at its C-terminal region was sought in all six reading frames translated from the *S. mutans* whole genome sequence at the University of Oklahoma's Advanced Center for Genome (1). However, no such candidate was detected. A search of the identified octapeptide sequence, SDVSSNIS, with TBLASTN program in the same database was also negative. Therefore, we expected that this protein would not be coded by the chromosome of strain UA159, and that it might be a new member of the wall-anchored proteins expressed in a specific population of the species *S. mutans.*

Isolation of cold-agglutination-negative mutants.

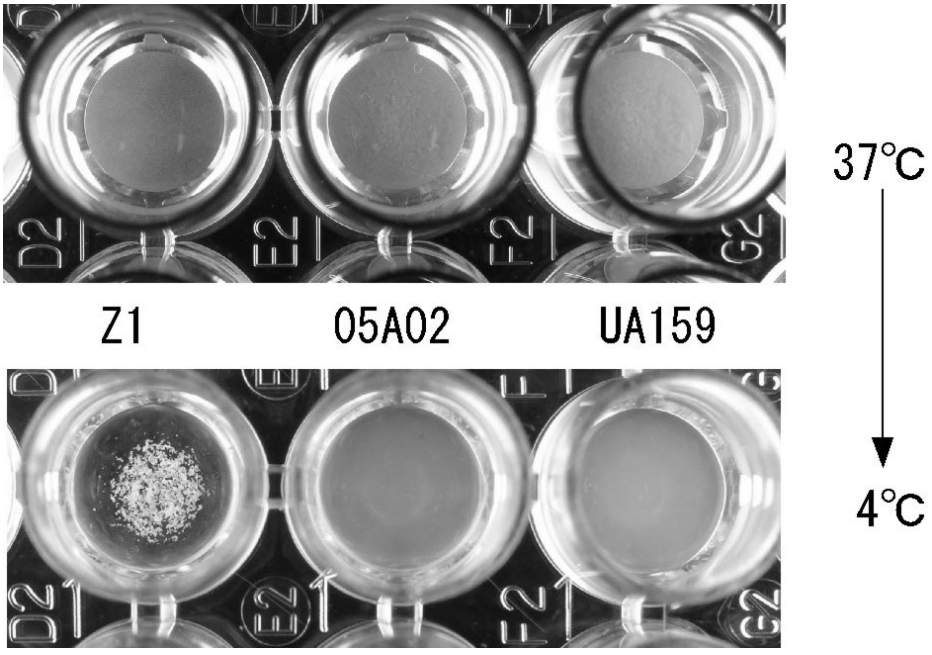

Fig.2. Cold agglutination assay on *S. mutans* Z1 and its transposon mutant. *S. mutans* strain Z1 cells grown overnight in the TH broth showed clumps (we designated this as cold-agglutination) when incubated at lower than 25 ºC for several h, while mutant 05A02 did not. Appearance of UA159 cell treated similarly resembled that of 05A02. These phenotypes were not influenced by growth phase, growth condition, or subculturing, and were specific for each strain.

In order to identify genes encoding the 120 kDa protein responsible for cold-agglutination, we utilized a random mutagenesis involving *in vitro* transposition (2).

In vitro transposition of the *Himar1* minitransposon from plasmid pJFP2 into chromosomal DNA of strain Z1 and subsequent transformation of strain Z1 were performed as described in Materials and Methods. Transposition of the minitransposon was reported to be highly random (2) and when applied this to the *S. mutans* genomic DNA, we confirmed this randomness by Southern hybridization analyses on transposon mutants (data not shown).

Microplate wells exhibiting no agglutination in cold agglutination assay were easily distinguished by our procedure. Approximately 2,000 transposon mutants were screened from the transformation experiments and we could identify 3 cold-agglutination-negative mutants. Typical appearances in microplate wells of cultures both positive and negative for agglutination are shown in Fig.2. We confirmed by PCR amplification using primers srt5' and srt3' (Table 1) that the transposon insertions in the chromosome of the three mutants were not within the sortase gene region, while a sortase mutant of strain Z1 exhibited cold-agglutination negative phenotype. One of the agglutination-negative mutants, designated 05A02, was selected for further characterization.

Akerley and Lampe (2) reported that they obtained approximately 800 transposon mutants in *H. influenzae* using this method under conditions where they obtained 10^6 transformants per 1 μg of a control DNA. Kitten (T. Kitten, Abstr. 80th General Session of the Internatl. Assoc. for Dent. Res., abstr. 0092, 2002) also reported that he obtained approximately 700-1500 transposon mutants in *S. sanguis* under similar conditions. In our case, approximately 800-1600 transposon mutants were obtained using *S. mutans* strain Z1 as a host under similar conditions. This

efficiency was comparable to those observed in the former two species, and should be sufficient for applying this method to chromosomal DNA of this strain as a random mutagenesis method. Randomness of this transposition is theoretically ensured because the target sequence is dinucleotide, TA, and appeared to be true in *S. mutans* Z1 chromosomal DNA from the findings that all of randomly selected transposon mutants exhibited different banding patterns in the Southern blot analysis of their chromosomal DNAs. No further transposition should occur within the recipient cells where no transposase exists, since the procedure of transposition manipulated *in vitro* is separated from the procedure for introduction of the mutated host DNA with minitransposon back into the host cells. An additional merit is easiness to analyze chromosomal DNA following the transformation procedure because of small size (approx. 2 kb including the kanamycin resistant gene functioning in the *S. mutans* cells) of this minitransposon. With these merits, we were successfully able to obtain three mutants that did not exhibit cold agglutination, and to identify the gene designated *cnm* from one of the mutants much more easily than our previous random mutagenesis experiment using pVA891 suicide vector (36), where we obtained many deletion- and duplication-mutants as well as mutants in which pVA891 was simply inserted into chromosomal DNA by the Campbell-like mechanism. Therefore, we concluded that this *in vitro* transposition method is well applicable to *S. mutans* if strains of interest are transformable with relatively good efficiencies.

Identification of the responsible gene for cold-agglutination.

According to the results from the Southern blot analysis of the *Hpa*I, *Pvu*II, and *Ssp*I digested chromosomal DNA fragments from mutant 05A02 using the kanamycin resistant gene as a probe, these restriction sites upstream and downstream the minitransposon insertion site were mapped (Fig.3).

Sequencing of this region revealed an 1617 nt open reading frame (ORF) beginning with an ATG and terminating with a TGA codon (data not shown). A nucleotide sequence homologous to this ORF was not detected in the UA159 genome database. This ORF encoded a 538 amino acid protein with a calculated molecular weight of 57,192, which was extremely different from the observed molecular size of the candidate protein product detected in the SDS-PAGE described above. The minitransposon insertion positions in the other two mutants also occurred within the same ORF (Fig.3) and were confirmed by sequencing of the region around the insertions following PCR amplifications with primers DSHpa2F and DSHpa1R. The 120 kDa protein was missing in any of the three transposon mutants. A potential ribosome-binding site (AGGA), and a promoter-like sequence (TTGACA-N_{16}-TATAAT) were identified at 9 bp and 39 bp upstream the ATG initiation codon of the gene, respectively (data not shown). In addition, a terminater-like sequence (ΔG=70.6 J) was detected 20 bp downstream the termination codon, suggesting the ORF to be monocistronic. Analysis of the deduced amino acid sequence revealed that the first 32 amino acids of the putative protein were consistent with a hydrophobic signal peptide. This was followed by the octapeptide that shared complete identity with the N-terminal amino acid sequence obtained from sequencing of the isolated 120 kDa protein (SDVSSNIS) described above. A C-terminal LPXTG motif (LPSTG), a recognition sequence for sortase that covalently tethers surface proteins to the peptidoglycan was located at amino acid residues 507-511 (Fig.3, nt 1519-1533), followed by putative hydrophobic membrane spanning and charged membrane anchor regions. Therefore, the gene encodes a strain-specific new member of wall-anchored proteins of *S. mutans* and was designated *cnm* because of the amino acid sequence similarity and collagen-binding function of the protein encoded by this gene as described below.

The 1617 nt *cnm* gene was not capable of coding for a protein with the molecular weight of 120 kDa which corresponds to the size observed on SDS-PAGE. The *cnm* nucleotide sequence has tandem 21 nt repeats and subsequent 19.7 repeats of 18 nt. In fact, these repeats produced difficulties in our nucleotide sequencing but we detected no artificial deletion during sequencing and even confirmed the size

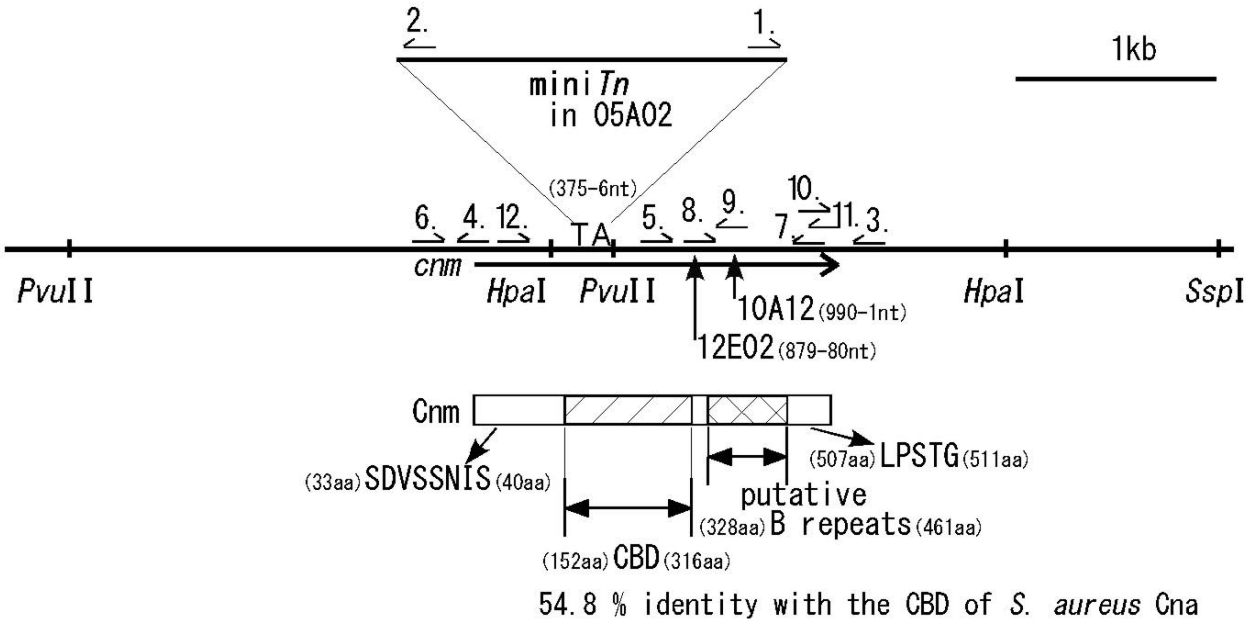

Fig.3. The restriction map around the Minitransposon insertion site in mutant 05A02 and location of primers designed for identification of the ORF. Minitransposon (mini*Tn*) from pJFP2 was inserted at the TA dinucleotide depicted in the Figure. Mini*Tn* insertion sites in the other mutants (10A12 and 12E02) are depicted with the vertical arrows. The thick lined arrow depicts the direction and region of the *cnm* gene. The rectangle depicts the Cnm protein corresponding to the gene. Locations of the mature N-terminal sequence and LPXTG motif of the amino acid sequence deduced from the gene are represented by SDVSSNIS and LPSTG, respectively. The putative collagen-binding and B repeats domains are depicted with the boxes. The numbers with 'nt' and 'aa' in parentheses indicate the *cnm* gene nucleotide numbers starting from the first base of the initiation codon and the Cnm amino acid numbers starting from the precursor N-terminal, respectively. Half head arrows below the numbers indicate approximate PCR primer locations and their directions (5'->3'). 1., 2tp1; 2., 2tp2; 3., DSHpa1R; 4., DVPvII1R; 5., DSHpa1F; 6., DVPvII2F; 7., DSHpa2R; 8., DSHpa2F; 9., DSHpa3R; 10., DSHpa3F; 11., 120KD_Rv; 12., 120kDFwFu. *Pvu*II, *Hpa*I and *Ssp*I indicate respective restriction enzyme recognition sites.

corresponding to the repeats by PCR amplification with primers closely situated to the both ends of this repeating region (DSHpa2F, DSHpa2R in Table 1). Surprisingly, the 120 kDa protein isolated from the wall of *S. mutans* Z1 cells was encoded by the 1617 nt *cnm* gene. The 120 kDa wall-protein was prepared following release from the cell wall by digestion with muramidase treatment. Although the wall proteins isolated by such procedures often yielded larger sizes than predicted (21, 37), the size of 120 kDa encoded by the *cnm* gene is more than twice the calculated molecular weight of the mature protein (51 kDa without peptidoglycan moieties). Wall-anchored proteins were reported to be released to the supernatant without tethering to the cell wall when the sortase gene was inactivated (3, 13, 14, 17). However, no 120 kDa size band could be recognized in a CBB stained gel of the electrophoresed concentrated supernatant of the sortase negative mutant of strain Z1 (srt-Z1). The size of the released protein in culture supernatants of the srt-Z1 mutant as well as that of the wall-anchored one from the wild type remains to be determined with antiserum to this protein and such approaches are currently in progress. The difference between the observed and calculated size indicates that this protein may have been modified.

The amino acid sequence similarity of the Cnm protein to collagen-binding adhesins.

The DNA databases were searched for proteins with the similar amino acid sequence deduced from the *cnm* gene. Similar sequences were unexpectedly found in a group of collagen-adhesin proteins, which are also wall-anchored proteins, from staphylococci and enterococci. In addition, another collagen-adhesin protein from *Streptococcus equi* was reported very recently (16). The target sequence regions most similar to that of *S. mutans cnm* gene product were those corresponding to the collagen-binding domains (CBD) in collagen-adhesin precursor proteins (Cna) from *Staph*. *aureus* strain FDA 574 (54.8 % identity) and MRSA strain MW2. The sequences with next similarty were the CBDs of the *Enterococcus faecium* (Acm; 48.8 % identity) and *Streptococcus equi* (Cne; 48.2 % identity), collagen-adhesin precursor proteins recently reported (16, 22). The CBD of the *Enterococcus faecalis* (Ace; 31.5 % identity) was less similar to that of *S. mutans* Cnm. Amino acid sequences of CBDs of Cnm, Cna, Acm, Cne and Ace are aligned in Fig.4.

The Cnm protein shared high homology to collagen-binding adhesins from *Staph. aureus, E. faecium,* and *S. equi*. In particular, 165 amino acid sequence from residues 152 to 316 of the Cnm protein was highly homologous to amino acid sequence of the CBDs of these collagen-binding adhesins. In addition, of the seven amino acids that are critical for collagen-binding by Cna of *Staph. aureus* (27, 45), three amino acids (tyrosine, arginine, and phenylalanine at positions 176, 190, and 192 of Cnm in Fig.4), which form the walls of the groove in Cna to accep collagen molecules (45), were conserved in all of the five CBDs, and another residue (asparagine at position 194 of Cnm) was present in four CBDs except for that of *S. equi.* The other two asparagines and tyrosin at residues 223, 278, and 233 of Cna were not conserved among the other CBDs. These residues may be complemented by other amino acid residues in Cnm, Acm, Cne and Ace.

Another characteristic sequence of the Cnm

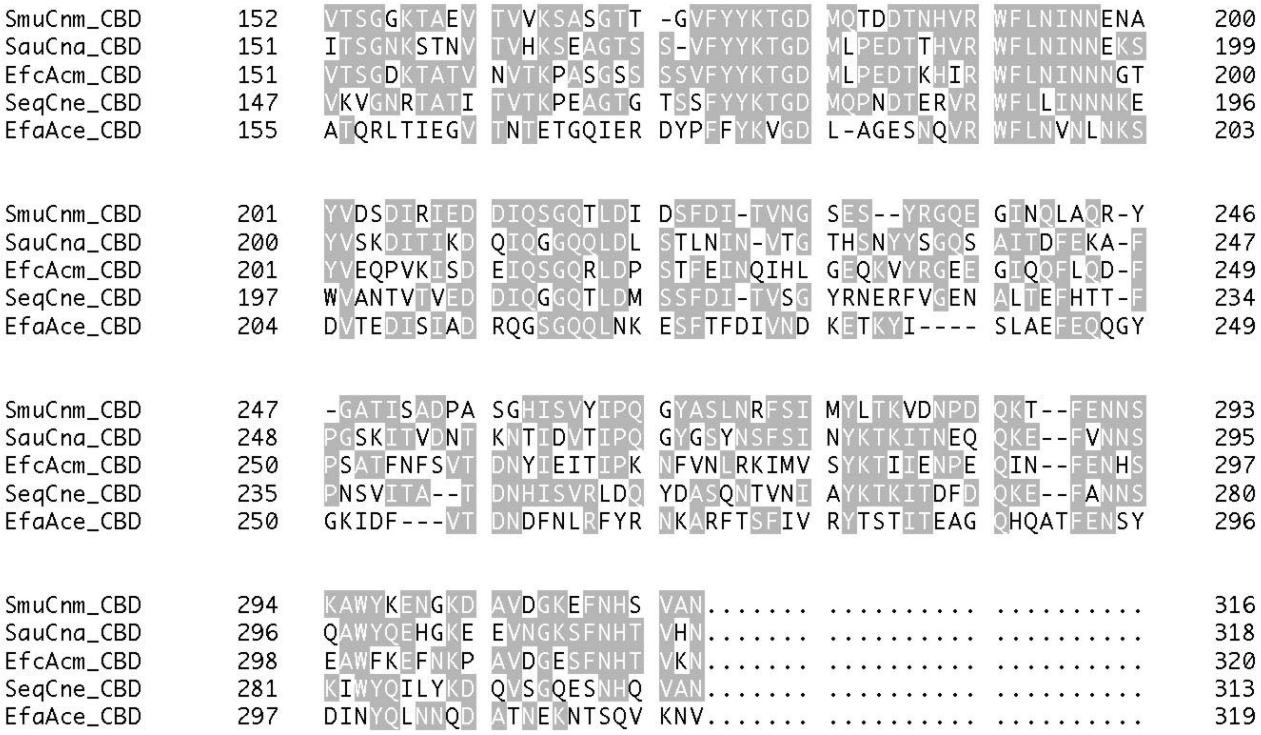

Fig.4 Alignment of amino acid sequence of Cnm CBD with that of CBDs of previously identified collagen-binding adhesins. All five amino acid sequences were numbered from the initiation codon of the precursor proteins. The putative amino acid seqnence of CBD identified from the Cnm was aligned with that of CBDs of collagen binding adhesins of *Staph. aureus*, *E. faecium*, *S. equi*, and *E. faecalis* by using the DNASIS-Mac program. Identical amino acid residues are indicated by letters on a gray background.

protein was found in the C-terminal region as a repetitive sequence (Fig.3), which consists of tandem TTTTE(K/A)P, and subsequent 19 TTTE(A/S/T)P repeats .

Collagen-adhesin molecules from *Staph. aureus* (Cna) (26), *E. faecium* (Acm) (22), *S. equi* (Cne) (16) and *E. faecalis* (Ace) (29) contained the B repeat regions following the A domain containing the CBD. However, the number of repeats and the lengths of the repeating units were dependent on bacterial species variation. The B repeat domains of collagen-adhesin proteins in these four bacterial species contained 0.5 to 4.5 repeating units of 47- to 110-residue-long. *S. mutans* Cnm contained two 7-residue and 19 6-residue repeating units located between the putative CBD and C-terminal wall-associated domain being rich in proline and lysine residues. This repeating unit region of the Cnm protein may correspond to the B domain of the collagen-adhesins. Therefore, we conclude that the characteristic domain structure of the Cnm protein as well as the homology of its putative CBD was over all conserved.

Collagen-binding assay.

Based on the similarities of N-terminal amino acid sequence deduced from the *cnm* gene to the CBD in collagen-adhesin precursor proteins, a 5' *cnm* gene region corresponding to the mature N-terminal region-containing putative CBD region was amplified by PCR and subcloned to pBAD/HisA expression vector for use to overexpress the protein. The resultant plasmid was designated pZAXF. Since the ZAXF protein expression was easily confirmed by CBB staining of electrophoresed SDS polyacrylamide gels, we initially attempted to purify the protein using a commercially available ProBond resin column (Invitrogen). However, the protein was aggregated immediately after elution with imidazol which is recommended by the supplier. Furthermore, the protein obtained by pH elution (pH=4.0) did not exhibit any binding activity to collagen. Therefore, we used the crude *E. coli* extracts prepared as described in Materials and Methods. The ZAXF protein bound to immobilized collagen type I in a concentration dependent manner and also to laminin with lesser extent but not to fibronectin or BSA (Fig.5A). Protein from ZAXF cells grown in the absence of arabinose (uninduced ZAXF) and those from strains pBAD and SBP6 cells grown in the presence of $2x10^{-3}$ % arabinose did not exhibit binding to collagen type I and laminin (Fig.5B).

Biotin-labeled *S. mutans* Z1 whole cells bound collagen type I and laminin and interacted with fibronectin to a lesser extent (Fig.5C). In contrast, mutant 05A02 cells bound only to fibronectin with similar binding activity as Z1 cells. The binding profiles of both the assays with recombinant protein and the assays with whole cells were comparable.

Specific binding assays using crude *E. coli* extracts containing a recombinant CBD domain (ZAXF protein) revealed that the *S. mutans* Cnm protein is a new member of the collagen-binding adhesin family. It is of interest that the ZAXF protein exhibited also an affinity to laminin. This was compatible not only with the demonstrated relative collagen-and laminin-binding properties of intact cells of Z1 and no such properties of its *cnm* mutant 05A02 but also with the similar fibronectin-binding abilities retained by both strains.

Occurrence of the cnm gene among S. mutans strains.

To evaluate the occurrence of the *cnm* gene among different *S. mutans* strains, Southern blot analysis of *Hin*dIII-digested chromosomal DNA fragments from laboratory strains and isolates including UA159 and Z1 was carried out using the *cnm* gene fragment as a probe. Five out of the 14 strains examined were *cnm*-positive (Fig.6), and exhibited cold-agglutination and collagen/laminin-binding activities, while the other 9 strains did not exhibit these phenotypes. Interestingly, three of the five positive strains were serotype e or f (LM7, OMZ175, and Z1) but no clonality has been observed among these *cnm*-positive strains analyzed by amplified fragment length polymorphism(AFLP).

Switalski *et al*.(44) reported a decade ago that approximately 20 % of *S. mutans* strains tested were able to bind collagen-coated substratum and tooth root particles. This ratio was comparable to our results and

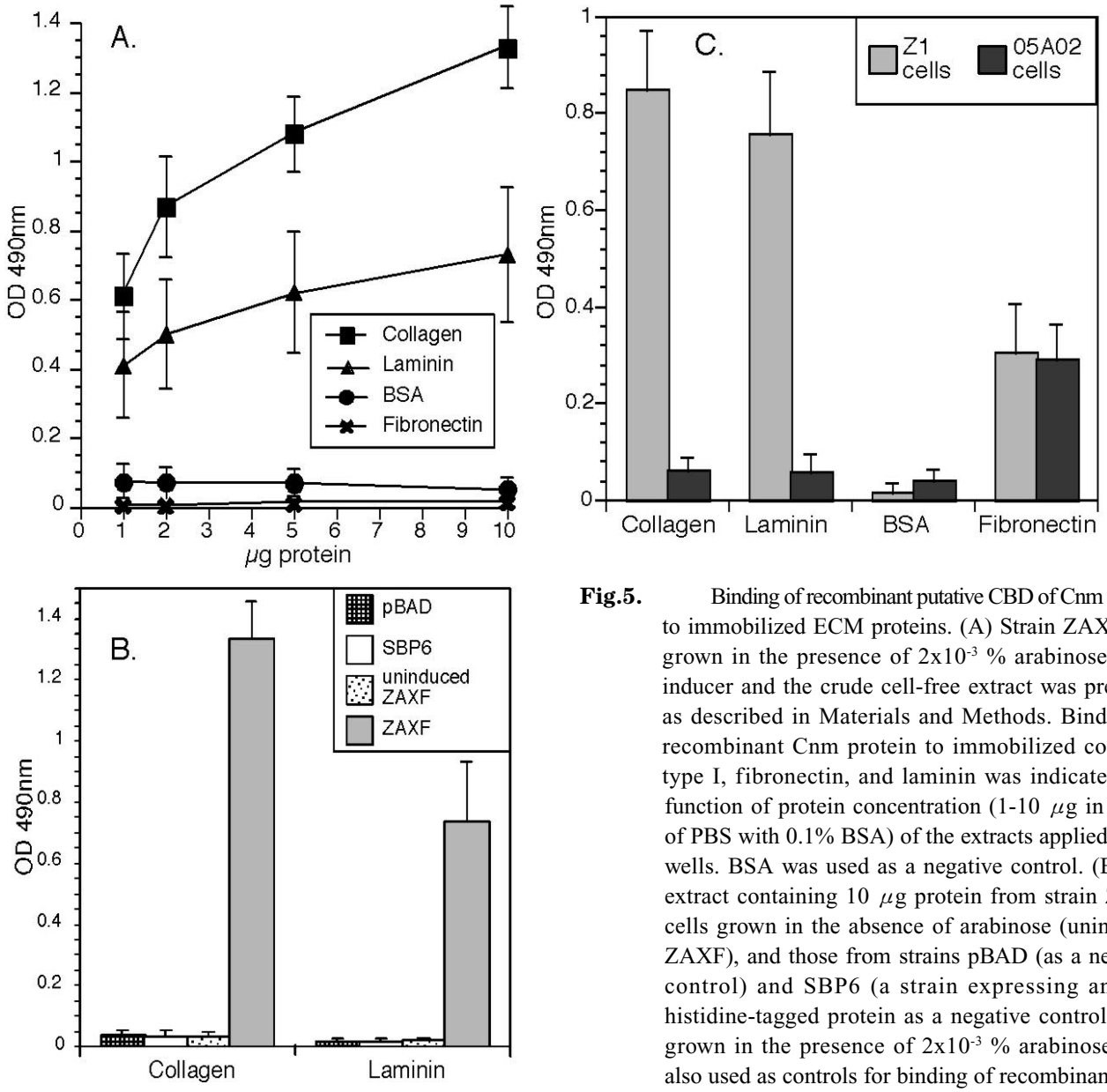

Fig.5. Binding of recombinant putative CBD of Cnm protein to immobilized ECM proteins. (A) Strain ZAXF was grown in the presence of $2x10^{-3}$ % arabinose as an inducer and the crude cell-free extract was prepared as described in Materials and Methods. Binding of recombinant Cnm protein to immobilized collagen type I, fibronectin, and laminin was indicated as a function of protein concentration (1-10 μg in 20 μl of PBS with 0.1% BSA) of the extracts applied to the wells. BSA was used as a negative control. (B) The extract containing 10 μg protein from strain ZAXF cells grown in the absence of arabinose (uninduced ZAXF), and those from strains pBAD (as a negative control) and SBP6 (a strain expressing another histidine-tagged protein as a negative control) cells grown in the presence of $2x10^{-3}$ % arabinose were also used as controls for binding of recombinant Cnm protein to collagen type I and laminin. (C) Biotin labeled strains Z1 and 05A02 whole cells were examined for binding to the ECM proteins as described in the text. Relative binding was measured by monitoring absorbance at 490nm following the peroxidase reaction for 3 min in the assays using the recombinant Cnm protein and for 4 min in the assays using whole cells with o-phenylenediamine and H_2O_2, which were terminated with addition of 2M H_2SO_4. All OD_{490nm} values were corrected for the response of peroxidase activities with the respective ECM proteins. Data points represent the means of OD_{490nm} values ± standard deviation in more than three independent experiments.

also to those of Liu *et al*. (18) indicating that 2 strains (B14; serotype e and OMZ175; serotype f) out of 8 *S. mutans* strains tested bound type I collagen. Interestingly, strain OMZ175 was one of the five *cnm* gene-positive strains in our study. In addition, strain ATCC10449 which is one of the *cnm* gene-negative strains was included in the six strains that did not bind collagen in their study. Taken together these results suggested that collagen-binding of *S. mutans* cells may be mediated by the Cnm protein.

Chromosome walking upstream and downstream from the *cnm* gene in strain Z1 with partial sequencing

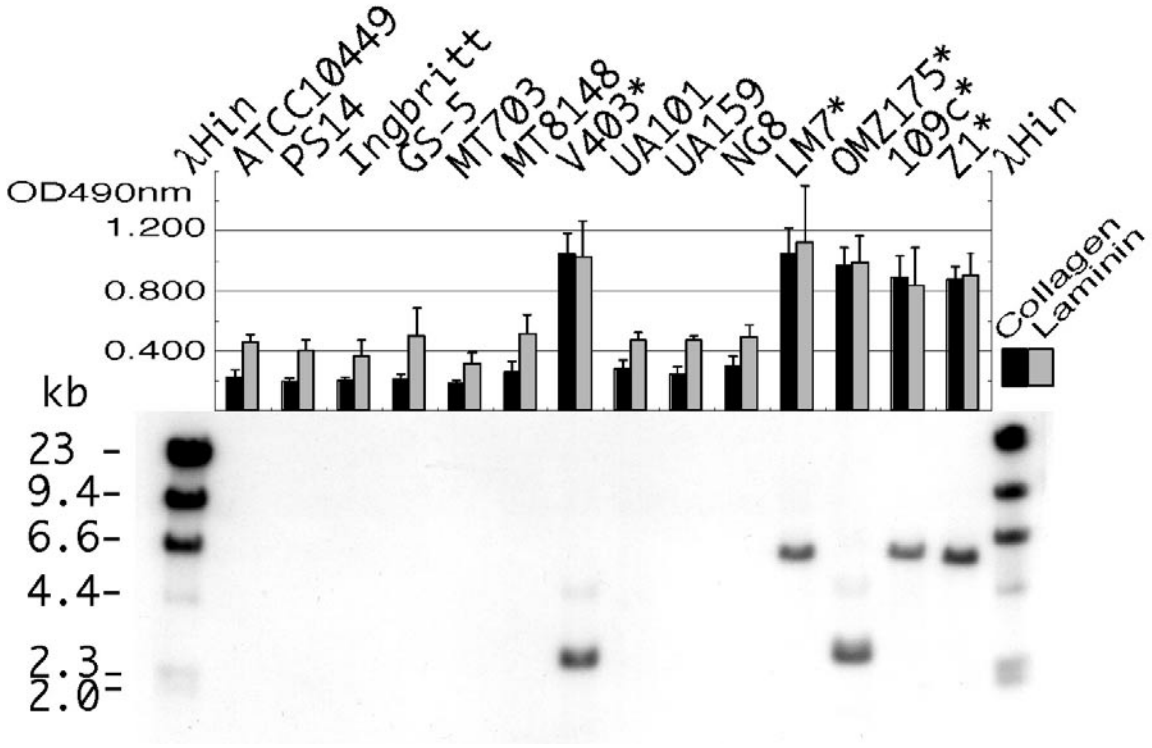

Fig.6. Occurrence of the *cnm* gene in various strains *S. mutans*. *Hind*III-digested chromosomal DNA fragments from reference strains, including strain UA159, and several natural isolates in addition to strain Z1 were analyzed by Southern hybridization under high stringency conditions with the *cnm* gene fragment as a probe. Asterisks indicate the *cnm* gene-positive strains. Binding assays of the strains to collagen/laminin were carried out as described in the legend for Fig. 5. The data represent the means of OD_{490nm} values ± standard deviation of four (collagen) or three (laminin) independent experiments.

indicated that an approximately 10 kb nucleotide sequence was missing from the chromosome of strain UA159 probably at a position within the 1940 to 1950 kb region. However, the precise comparison of these regions in strains UA159 and Z1 should be performed by sequencing the entire region detected in strain Z1, and is currently under way. At present, it is not clear whether this region was deleted in UA159 or acquired by Z1 from other species in the environment.

Very recently, Hubble *et al*. (11) reported the significant role in pathogenicity of collagen-binding protein Ace of *E. faecalis*, which is regarded as a major pathogenic organism of root canals or periapical foci by binding to dentin. *S. mutans* is considered to be a major pathogenic organism of dentin caries, *e.g.* root surface caries, although it alone does not cause tooth decay to a significant extent (9). The binding capacity of *S. mutans* cells to collagen, which is a major organic component of cementum and dentin, should be important in the etiology of root surface caries. Therefore, it will be important in future studies to correlate the presence of *cnm*-positive *S. mutans* strains with the events of root surface caries.

Oral viridans streptococci are pathogen associated with infective endocarditis and the binding abilities of these organisms to subendothelial matrix proteins including collagen, sialoproteins, fibronectin, and laminin as well as blood derived fibrinogen (fibrin) are regarded as potential virulent factors (4, 8, 20, 39, 43, 46). Since *S. mutans* is responsible for 8-18 % of total streptococcal endocarditis cases (33), the Cnm protein may be an important factor, although extracellular protein antigen I/II was reported to be involved in binding of *S. mutans* cells to extracellular matrix

protein (4, 19). Beg *et al*.(4) observed that cells of *S. mutans* strain M51, which was isolated from the peripheral blood of an infective endocarditis patient bound collagen type I, fibronectin, laminin, and fibrinogen in descending order, while the laboratory strain NG8 (*cnm*-negative, Fig.6) bound fibronectin better than others. Therefore, it will be of interest to compare the percentage of the *cnm* gene positive streptococcus strains isolated from infective endocarditis patients with that from healthy people.

Conclusion

We identified a novel 120 kDa protein detected in the wall preperation from *S. mutans*. This protein was not one of the unexpected intracellular proteins but a true wall protein classified as wall-anchored proteins of Gram-positive bacteria. We isolated the gene *cnm* encoding a 120 kDa wall-anchored protein involved in cold-agglutination of *S. mutans* by *in vitro* mutagenesis using the *Himar1* minitransposon. The *cnm* gene encoded a new strain-specific member of collagen-binding adhesin family proteins from *S. mutans.* Since this family genes have not yet been reported from other viridans streptococci in human oral indigenous flora, it is of interest to determine whether *cnm* homologues are present in salivary-or plaque-residing organisms besides *S. mutans.*

References

(1) Ajdic, D., McShan, W.M., McLaughlin, R.E., Savic, G., Chang, J., Carson, M.B., Primeaux, C., Tian, R., Kenton, S., Jia, H., Lin, S., Qian, Y., Li, S., Zhu, H., Najar, F., Lai, H., White, J., Roe, B.A., and Ferretti, J.J. 2002. Genome sequence of *Streptococcus mutans* UA159, a cariogenic dental pathogen. Proc. Natl. Acad. Sci. U S A **99**: 14434-14439.

(2) Akerley, B.J., and Lampe, D.J. 2002. Analysis of gene function in bacterial pathogens by GAMBIT. Methods Enzymol. **358**: 100-108.

(3) Barnett, T.C., and Scott, J.R. 2002. Differential recognition of surface proteins in *Streptococcus pyogenes* by two sortase gene homologs. J. Bacteriol. **184**: 2181-2191.

(4) Beg, A.M., Jones, M.N., Miller-Torbert, T., and Holt, R.G. 2002. Binding of *Streptococcus mutans* to extracellular matrix molecules and fibrinogen. Biochem. Biophys. Res. Commun. **298**: 75-79.

(5) Bentley, R.W., Leigh, J.A., and Collins, M.D. 1991. Intrageneric structure of Streptococcus based on comparative analysis of small-subunit rRNA sequences. Int. J. Syst. Bacteriol. **41**: 487-494.

(6) Burne, R.A., and Penders, J.E. 1992. Characterization of the *Streptococcus mutans* GS-5 *fruA* gene encoding exo-beta-D-fructosidase. Infect. Immun. **60**: 4621-4632.

(7) Burne, R.A. 1998. Oral streptococci : products of their environment. J. Dent. Res. **77**: 445-452.

(8) Chia, J.S., Yeh, C.Y., and Chen, J.Y. 2000. Identification of a fibronectin binding protein from *Streptococcus mutans.* Infect. Immun. **68**: 1864-1870.

(9) Dung, T.Z., and Liu, A.H. 1999. Molecular pathogenesis of root dentin caries. Oral Dis. **5**: 92-99.

(10) Ferretti, J.J., Russell, R.R., and Dao, M.L. 1989. Sequence analysis of the wall-associated protein precursor of *Streptococcus mutans* antigen A. Mol. Microbiol. **3**: 469-478.

(11) Hubble, T.S., Hatton, J.F., Nallapareddy, S.R., Murray, B.E., and Gillespie, M.J. 2003. Influence of *Enterococcus faecalis* proteases and the collagen-binding protein, Ace, on adhesion to dentin. Oral Microbiol. Immunol. **18**: 121-126.

(12) Igarashi, T., Yamamoto, A., and Goto, N. 1995. Sequence analysis of the *Streptococcus mutans* Ingbritt *dexA* gene encoding extracellular dextranase. Microbiol. Immunol. **39**: 853-860.

(13) Igarashi, T., Asaga, E., and Goto, N. 2003. The sortase of *Streptococcus mutans* mediates cell wall anchoring of a surface protein antigen. Oral Microbiol. Immunol. **18**: 266-269.

(14) Igarashi, T., Asaga, E., Sato, Y., and Goto, N. 2004. Inactivation of *srtA* gene of *Streptococcus mutans* inhibits dextran-dependent aggregation by glucan-binding protein C. Oral Microbiol.

Immunol. **19**: 57-60.
(15) Lampe, D.J., Churchill, M.E., and Robertson, H.M. 1996. A purified mariner transposase is sufficient to mediate transposition in vitro. Embo J. **15**: 5470-5479.
(16) Lannergard, J., Frykberg, L., and Guss, B. 2003. CNE, a collagen-binding protein of *Streptococcus equi.* FEMS Microbiol. Lett. **222**: 69-74.
(17) Lee, S.F., and Boran, T.L. 2003. Roles of sortase in surface expression of the major protein adhesin P1, saliva-induced aggregation and adherence, and cariogenicity of *Streptococcus mutans*. Infect. Immun. **71**: 676-681.
(18) Liu, T., Gibbons, R.J., and Hay, D.I. 1990. *Streptococcus cricetus* and *Streptococcus rattus* bind to different segments of collagen molecules. Oral Microbiol. Immunol. **5**: 143-148.
(19) Love, R.M., McMillan, M.D., Park, Y., and Jenkinson, H.F. 2000. Coinvasion of dentinal tubules by *Porphyromonas gingivalis* and *Streptococcus gordonii* depends upon binding specificity of streptococcal antigen I/II adhesin. Infect. Immun. **68**: 1359-1365.
(20) Lowrance, J.H., Baddour, L.M., and Simpson, W.A. 1990. The role of fibronectin binding in the rat model of experimental endocarditis caused by *Streptococcus sanguis.* J. Clin. Invest. **86**: 7-13.
(21) Mazmanian, S.K., Liu, G., Jensen, E.R., Lenoy, E., and Schneewind, O. 2000. *Staphylococcus aureus* sortase mutants defective in the display of surface proteins and in the pathogenesis of animal infections. Proc. Natl. Acad. Sci. U S A **97**: 5510-5515.
(22) Nallapareddy, S.R., Weinstock, G.M., and Murray, B.E. 2003. Clinical isolates of *Enterococcus faecium* exhibit strain-specific collagen binding mediated by Acm, a new member of the MSCRAMM family. Mol. Microbiol. **47**: 1733-1747.
(23) Navarre, W.W., and Schneewind, O. 1999. Surface proteins of gram-positive bacteria and mechanisms of their targeting to the cell wall envelope. Microbiol. Mol. Biol. Rev. **63**: 174-229.
(24) Okahashi, N., Sasakawa, C., Yoshikawa, M., Hamada, S., and Koga, T. 1989. Molecular characterization of a surface protein antigen gene from serotype c *Streptococcus mutans*, implicated in dental caries. Mol. Microbiol. **3**: 673-678.
(25) Pancholi, V., and Chhatwal, G.S. 2003. Housekeeping enzymes as virulence factors for pathogens. Int. J. Med. Microbiol. **293**: 391-401.
(26) Patti, J.M., Jonsson, H., Guss, B., Switalski, L.M., Wiberg, K., Lindberg, M., and Hook, M. 1992. Molecular characterization and expression of a gene encoding a *Staphylococcus aureus* collagen adhesin. J. Biol. Chem. **267**: 4766-4772.
(27) Patti, J.M., House-Pompeo, K., Boles, J.O., Garza, N., Gurusiddappa, S., and Hook, M. 1995. Critical residues in the ligand-binding site of the *Staphylococcus aureus* collagen-binding adhesin (MSCRAMM). J. Biol. Chem. **270**: 12005-12011.
(28) Perry, D., and Kuramitsu, H.K. 1981. Genetic transformation of *Streptococcus mutans*. Infect. Immun. **32**: 1295-1297.
(29) Rich, R.L., Kreikemeyer, B., Owens, R.T., LaBrenz, S., Narayana, S.V., Weinstock, G.M., Murray, B.E., and Hook, M. 1999. Ace is a collagen-binding MSCRAMM from *Enterococcus faecalis*. J. Biol. Chem. **274**: 26939-26945.
(30) Ruhl, S., Sandberg, A.L., Cole, M.F., and Cisar, J.O. 1996. Recognition of immunoglobulin A1 by oral actinomyces and streptococcal lectins. Infect. Immun. **64**: 5421-5424.
(31) Russell, M.W., Bergmeier, L.A., Zanders, E.D., and Lehner, T. 1980. Protein antigens of *Streptococcus mutans*: Purification and properties of a double antigen and its protease-resistant component. Infect. Immun. 28: 486-493.
(32) Russell, R.R. 1979. Wall-associated protein antigens of *Streptococcus mutans.* J. Gen. Microbiol. **114**: 109-115.
(33) Ryd, M., Schennings, T., Flock, M., Heimdahl, A., and Flock, J.I. 1996. *Streptococcus mutans* major adhesion surface protein, P1 (I/II), does not contribute to attachment to valvular vegetations or to the development of endocarditis in a rat model. Arch. Oral Biol. **41**: 999-1002.
(34) Sambrook, J., Fritsch, E.F., and Maniais, T. 1989. Molecular cloning−A Laboratory Manual, 2nd Ed. Cold Spring Harbor Laboratory Press, Cold

Spring Harbor, NY.
(35) Sato, Y., Yamamoto, Y., and Kizaki, H. 1997. Cloning and sequence analysis of the *gbpC* gene encoding a novel glucan-binding protein of *Streptococcus mutans*. Infect. Immun. **65**: 668-675.
(36) Sato, Y., Yamamoto, Y., and Kizaki, H. 2000. Construction of partial duplication mutants (merodiploid mutants) to investigate function of genes in vivo: identification of a regulatory gene for the glucan-binding protein C of *Streptococcus mutans.* FEMS Microbiol. Lett. **186**: 187-191.
(37) Sato, Y., Okamoto, K., and Kizaki, H. 2002. *gbpC* and *pac* gene mutations detected in *Streptococcus mutans* strain GS-5. Oral Microbiol. Immunol. **17**: 263-266.
(38) Sato, Y., Senpuku, H., Okamoto, K., Hanada, N., and Kizaki, H. 2002. *Streptococcus mutans* binding to solid phase dextran mediated by the glucan-binding protein C. Oral Microbiol. Immunol. **17**: 252-256.
(39) Sciotti, M.A., Yamodo, I., Klein, J.P., and Ogier, J.A. 1997. The N-terminal half part of the oral streptococcal antigen I/IIf contains two distinct binding domains. FEMS Microbiol. Lett. **153**: 439-445.
(40) Shibata, Y., Ozaki, K., Seki, M., Kawato, T., Tanaka, H., Nakano, Y., and Yamashita, Y. 2003. Analysis of loci required for determination of serotype antigenicity in *Streptococcus mutans* and its clinical utilization. J. Clin. Microbiol. **41**: 4107-4112.
(41) Shklair, I.L., and Keene, H.J. 1974. A biochemical scheme for the separation of the five varieties of *Streptococcus mutans*. Arch. Oral Biol. **19**: 1079-1081.
(42) Sommer, P., Bruyere, T., Ogier, J.A., Garnier, J.M., Jeltsch, J.M., and Klein, J.P. 1987. Cloning of the saliva-interacting protein gene from *Streptococcus mutans.* J. Bacteriol. **169**: 5167-5173.
(43) Sommer, P., Gleyzal, C., Guerret, S., Etienne, J., and Grimaud, J.A. 1992. Induction of a putative laminin-binding protein of *Streptococcus gordonii* in human infective endocarditis. Infect. Immun. **60**: 360-365.
(44) Switalski, L.M., Butcher, W.G., Caufield, P.C., and Lantz, M.S. 1993. Collagen mediates adhesion of *Streptococcus mutans* to human dentin. Infect. Immun. **61**: 4119-4125.
(45) Symersky, J., Patti, J.M., Carson, M., House-Pompeo, K., Teale, M., Moore, D., Jin, L., Schneider, A., DeLucas, L.J., Hook, M., and Narayana, S.V. 1997. Structure of the collagen-binding domain from a *Staphylococcus aureus* adhesin. Nat. Struct. Biol. **4**: 833-838.
(46) Takahashi, Y., Konishi, K., Cisar, J.O., and Yoshikawa, M. 2002. Identification and characterization of *hsa*, the gene encoding the sialic acid-binding adhesin of *Streptococcus gordonii* DL1. Infect. Immun. **70**: 1209-1218.

Analysis of Target Protein of *Staphylococcus hyicus* Exfoliative Toxins (SHETs)

Hisaaki Sato

Department of Veterinary Microbiology, School of Veterinary Medicine and Animal Sciences, Kitasato Uiversity, Towada, Aomori 034-8628, Japan

Introduction

Staphylococcus hyicus is known to be a causative agent of exudative epidermitis in pigs (1). Exudative epidermitis is generalized infection of the skin, characterized by greasy exudation, exfoliation, vesicle formation and crusting (2). Such clinical features closely resemble those of staphylococcal scalded skin syndrome in humans (3). In both diseases, the typical clinical signs are caused by staphylococcal exfoliative toxins (4, 5). *S. aureus* exfoliative toxins (ETs) are divided into four serotypes (ETA, ETB, ETC and ETD) (6−9), while *S. hyicus* exfoliative toxins (SHETs) are divided into five serotypes (SHETA, SHETB, ExhA, ExhC, ExhD) (10−12). The toxic activity and molecular weight of ETs and SHETs are extremely similar (5, 10). However, the two toxins differ widely in their susceptible animal species and antigen specificity (10, 11). The animal species susceptible to ET are humans and mice , while those susceptible to SHETs are pigs and chickens.

The homologies of amino acid sequences between ETs and SHETs are comparatively low (30% to 60%) (13, 14), but conservative regions are retained in these ET and SHET molecules (14). The catalytic triads that are related to the activity of serine proteases exist in all these toxin molecules, but these toxins do not exhibit caseinolytic activity (15, 16). Therefore, it seems that the major activity of exfoliative toxins is proteolytic activity, and that the target substance of exfoliative toxins is unique. One of the desmosomal proteins, desmoglein 1 (DSG1), is thought to be a target substance of ETs (17), although many proteins, such as profilaggrin (18), filaggrin (18), α-melanocyte-stimulating hormone (α-MSH) (19) and β-melanocyte-stimulating hormone (β-MSH) (19) are also possible target substances. Degradation of DSG1 by ETs results in destruction of desmosome (17). Destruction of desmosome in the upper layer of the stratum spinosum causes intraepidermal splitting (20). Such a toxic mechanism has been revealed for ETs, but not for SHETs.

The toxic mechanism of SHETs might be different from that of ETs, since the two toxins differ each other in their molecular compositions and susceptible animal species. In the present study, therefore, I attempted to analyze the mechanism of toxic action of SHETs by searching the target substance in the skin of the susceptible animal species.

Materials and Methods

Bacterial strains.

S. hyicus strains P-1 (3) and P-23 (11), isolated from pigs affected with exudative epidermitis, were used for preparation of SHET serotype A (SHETA) and serotype B (SHETB), respectively. These strains were lyophilized and stored at 4ºC. The lyophilized bacteria were suspended in heart infusion broth (Becton, Dickinson and Company; BD, Sparks, MD, U.S.A.) and cultured on heart infusion agar (BD) at 37ºC for 18 h. The grown bacteria were then suspended in 20% glycerol and stored at −80ºC.

Animals.

One hybrid piglet (Large Yorkshire×Landrace, two weeks old) bred on a Kitasato University farm, 21 day-old chickens (White Leghorn; Kanto Shokkei, Tokyo, Japan) and SPF suckling mice (BALB/c; Japan SLC, Hamamatsu, Japan) were used for extraction of proteins from skin. Ten SPF adult mice each (BALB/c, female[;] Japan SLC) were used for production of anti-SHETA antibody, anti-SHETB antibody and anti-P40 antibody.

Preparation of proteins from skin.

The skin of chickens, mice, and pig was cut into small pieces, suspended in 10 volumes of Dulbecco's phosphate buffered saline without $CaCl_2$ and $MgCl_2$ (PBS) and homogenized with Universal homogenizer (Nihon Seiki, Tokyo, Japan). This suspension was centrifuged at 10,000×*g* for 30 min, and the supernatant was designated the homogenate (HOMO). Small pieces of skin were suspended in 10 volumes of 0.1 M NaOH, stirred at 37ºC for 2 h and centrifuged at 10,000×*g* for 30 min. The supernatant of this suspension was collected and designated the alkaline extract (AE). Small pieces of skin were also suspended in 10 volumes of 20 mM EDTA, stirred at 37ºC for 2 h and centrifuged at 10,000×*g* for 30 min. The supernatant of this suspension was collected and designated the EDTA extract (EE).

Sodium dodecyl sulfate polyacrylamide gel electrophoresis (SDS-PAGE).

SDS-PAGE was performed at room temperature by the methods of Laemmli (21) and Sato et al. (5). A mixture of 0.05 ml of 500 mM Tris-HCl (pH 6.8), 0.08 ml of 10% SDS, 0.02 ml of 2-mercaptoethanol and 0.05 ml of 0.02% bromothymol blue in 80% glycerol was added to 0.2 ml of protein sample solution and incubated at 37ºC for 2 h. Then the solution was cooled, layered on 12.5% SDS-polyacrylamide gel slabs and run at 30 mA per gel. For detection of protein, proteins in the gel slabs were stained with 0.05% Coomassie brilliant blue R-250 (CBB; E. Merck AG Inc., Dermstadt, Germany) and decolorized with a 7% acetic acid solution. For Western blotting or the toxin-binding test, proteins in the gel were transferred to polyvinylidene difluoride (PVDF) membranes with an electro-blotting apparatus (HorizBlot; Atto Corp., Tokyo, Japan).

Purification of P40 (SHET-binding 40kD protein).

After electrophoresis of EE, the gels corresponding to the 40 kDa bands were cut out and cut into small pieces. The pieces of these gels were suspended in 10 volumes of 1% SDS in 20 mM Tris-HCl (pH 8.0) and incubated at room temperature overnight with gentle shaking. The suspension was dispensed in an inner tube with a membrane filter (0.45 μm pore size) in a test tube and centrifuged at 400×*g* for 15 min. The filtrate through the membrame filter was concentrated to 2 ml with a UP-20 ultrafilter (Toyo Roshi Co., Ltd., Tokyo, Japan), and 250 μl of this filtrate was dispensed in an Eppendorf tube. One ml of cold acetone was added, and the filtrate was kept at -80°C for 1 h. After centrifugation at 10,000×*g* for 15 min, the precipitates were dissolved in 10 mM Tris-HCl (pH 7.5) and designated P40. The P40 from chickens, mice, and the piglet were designated chicken P40, mouse P40, and pig P40.

Production of antibodies to SHETA, SHETB, and chicken P40.

The SHETA and SHETB were isolated and purified by the methods described previously (10, 11) (see later section). The purified SHETA and SHETB were converted to toxoids by treatment with 0.8% formalin at 37ºC for 50 h. Fifty mg of SHETA or SHETB toxoids were mixed with the same volume of Freund's incomplete adjuvant (BD), and were inoculated intraperitoneally to SPF adult mice once a week for 4 weeks. At 4 days after the fourth injection, sarcoma 180 cells (10^6 cells/0.5 ml) were injected into the mice intraperitoneally. After 3 days, the mice were inoculated subcutaneously with the toxoid as a booster. Most of the mice become to have distended abdomens within 10

days after inoculation of sarcoma cells. At that time, the ascitic fluid was withdrawn into a 10-ml syringe by paracentesis through an 18-gauge needle. The ascitic fluids were pooled and centrifuged at 1,500×*g* for 20 min to remove cellular components. The blood was obtained by cardiac puncture from each of the immunized mice, and the serum was separated. The ascitic fluid and serum were then pooled and designated anti-SHETA or anti-SHETB antibody. SPF adult mice were immunized with chicken P40 in the same manner, and 10 days after the inoculation of sarcoma cells, the ascitic fluid and serum collected from the mice were pooled and designated anti-P40 antibody.

Isoelectric focusing of chicken P40.

SDS remaining in chicken P40 preparation was removed by SDS-Out sodium dodecyl sulfate precipitation reagent (Pierce Biotechnology, Inc., Rockford, IL, U.S.A.). This solution was added to an equal volume of IEF sample buffer pH 3−7 (Invitrogen Inc., Carlsbad, CA, U.S.A.) and applied to Novex IEF pH 3−7 gel (Invitrogen) in an XCell SureLock Mini-Cell (Invitrogen). The upper buffer chamber was filled with 200 ml of 1×IEF Cathode Buffer pH 3−7 (Invitrogen) and the lower buffer chamber was filled with 600 ml of 1×IEF Anode Buffer (Invitrogen). Then, samples in the gel were run at 100 V for 1 h, 200 V for 1 h and 500 V for 2 h. After isoelectric focusing, the proteins in the gel were transferred to PVDF membranes with a HorizBlot electroblotting apparatus (Atto).

Preparation of SHETA- and SHETB-affinity columns.

Anti-SHETA IgG and anti-SHETB IgG were purified from anti-SHETA and anti-SHETB antibodies by Protein G Sepharose 4 Fast Flow (Amersham Biosciences, Piscataway, NJ, U.S.A.) column chromatography. Twenty ml of anti-SHETA IgG and anti-SHETB IgG solutions (5 mg/ml) were each mixed with 10 ml of CNBr-activated Sepharose 4B (Amersham) and incubated at room temperature for 2 h. Then, the Sepharose gel coupled with anti-SHETA IgG or anti-SHETB IgG mounted in column was blocked with 0.2 M glycine buffer (pH 8.3), washed with 0.5% NaCl in 0.1 M $NaHCO_3$ (pH 8.3) and 0.5 M NaCl in 0.1 M acetic acid (pH 4.0), and equilibrated with 10 mM Tris-HCl buffer (pH 7.5). The columns were designated the SHETA-affinity column and SHETB-affinity column, respectively.

Purification of SHETs.

S. hyicus strains P-1 and P-23 grown on heart infusion agar were harvested and suspended in PBS at a concentration of 10^9 CFU/ml. One ml of these suspensions was added to 100 ml of TY broth (22) and cultured at 37ºC for 18 h with shaking at 120 oscillations/min. After centrifugation of these bacterial cultures at 10,000×*g* for 20 min, the supernatants were passed through membrane filters (Toyo Roshi; 0.45 μm pore size). Then, the filtrates were fractionated with 75% saturated ammonium sulfate at 4ºC. After centrifugation at 10,000×*g* for 30 min, the precipitates were resolved in a small amount of 10 mM Tris-HCl (pH 7.5). These solutions were applied on a SHETA-affinity column or SHETB-affinity column and washed with 10 mM Tris-HCl (pH 7.5). Then, SHETA or SHETB were eluted with 10 mM Tris-HCl supplemented with 2.5 M NaSCN. Each eluate was dialyzed against 10 mM Tris-HCl at 4ºC overnight and used as SHETA and SHETB, respectively.

Western blotting.

Western blotting was carried out by the methods of Towbin et al. (23) and Tanabe et al. (10). After electrophoresis (or isoelectric focusing) of each sample (HOMO, AE, EE and P40), proteins in the gel were transferred onto a PVDF membrane (Atto). A portion of the membrane was stained with CBB and decolorized with a 7% acetic acid solution. The remaining membrane was then cut into 1 cm-width strips and incubated in 25% Block Ace (Dainippon Pharmaceutical Co., Ltd., Osaka, Japan) at room temperature for 1 h. The anti-SHETA or anti-SHETB antibody or anti-P40 antibody at 1:2,000 dilution in 10% Block Ace was mounted onto each strip and incubated at 37ºC for 1 h. After washing with 0.05% Tween 20 in PBS (T-PBS), 1:2,000-diluted peroxidase-conjugated anti-mouse IgG

was mounted onto each strip and incubated at 37ºC for 1 h. After washing with T-PBS, the substrate solution (0.05% 3, 3'-diaminobenzidine and 0.01% H_2O_2 in 50 mM Tris-HCI; pH 7.7) was mounted on each strip and incubated at room temperature. When the color reaction reached a maximum, each strip was washed with tap water to stop the reaction.

Toxin-binding test.

Three hundred μl of SHETA or SHETB solution (200 μg/ml) was mounted on HOMO, AE, EE or P40 (after electrophores)-transferred PVDF membrane strips and incubated at 37ºC for 2 h. After washing with T-PBS, the anti-SHETA or anti-SHETB antibody at 1:2,000 dilution in 10% Block Ace was mounted onto each strip and incubated at 37ºC for 1 h. After washing with T-PBS, 1:2,000-diluted peroxidase-conjugated anti-mouse IgG was mounted onto each strip and incubated at 37ºC for 1 h. After washing with T-PBS, the substrate solution (0.05% 3, 3'-diaminobenzidine and 0.01% H_2O_2 in 50 mM Tris-HCI; pH 7.7) was mounted on each strip and incubated at room temperature. When the color reaction reached a maximum, each strip was washed with tap water to stop the reaction.

In vitro digestion of P40 with SHETs.

One hundred μl (200 μg/ml) of chicken P40 was mixed with 100 μl of SHETA (300 μg/ml) or SHETB (300 μg/ml) and incubated at 37ºC for 2 h. Then, the mixed solution was layered on 12.5% SDS-polyacrylamide gel slabs and run at 30 mA per gel. After electrophoresis, the proteins in gels were transferred onto PVDF membranes. Each membrane was cut into 1 cm-width strips, and some strips were stained with CBB and decolorized with a 7% acetic acid solution. The remaining strips were used for the Western blotting using anti-P40 antibody.

Determination of N-terminal amino acid sequence of chicken P40.

The chicken P40 purified by isoelectric focusing was subjected to SDS-PAGE, transferred to PVDF membranes, stained with CBB at room temperature for 1 min and destained with 0.7% acetic acid at room temperature for 30 sec. Stained bands were cut out and sequenced by Edman degradation on the PPSQ-23 Protein Sequencer (Shimadzu Corp., Kyoto, Japan). The online software program FASTA (web address: http://fasta.genome.jp) was used to search for proteins possessing sequences similar to the amino terminal amino acid sequence of chicken P40. The alignment of amino acid sequences of chicken P40 with those of DSG1 of various animal species and analysis of the isoelectric points of DSG1s of various animal species were carried out by Genetyx- Win Ver. 6.1 (Genetyx Inc., Tokyo, Japan).

Results

Detection of SHET-binding protein.

The binding of SHETA to protein extracted from the skin of chickens is shown in Fig. 1. The EDTA extract (EE), homogenate (HOMO) and alkaline extract (AE) gave numerous protein bands (lanes 1, 3 and 5) on SDS-polyacrylamide gels after electrophoresis. However, SHETA bound a 40 kDa protein in EE alone (lane 2), and did not bind any protein in either HOMO or AE (lanes 4 and 6). Therefore, the 40 kDa protein is thought to be a SHET-binding protein and was designated P40.

The binding of SHETA to P40 from the three animal species (chicken P40, mouse P40 and pig P40) and the binding of anti-P40 antibody to chicken P40, mouse P40 and pig P40 are shown in Fig. 2. The SHETA bound to 40 kDa bands of chicken P40 (lane 2), mouse P40 (lane 4) and pig P40 (lane 6). In Western blotting, anti-P40 antibody bound to the 40 kDa bands of chicken P40 (lane 1), mouse P40 (lane 3) and pig P40 (lane 5).

The binding of SHETB and anti-P40 antibody to P40 from the three animal species is also shown in Fig. 3. The SHETB bound to 40 kDa bands of chicken P40 (lane 2), mouse P40 (lane 4) and pig P40 (lane 6). In Western blotting, anti-P40 antibody also bound to 40 kDa bands of chicken P40 (lane 1), mouse P40 (lane 3)

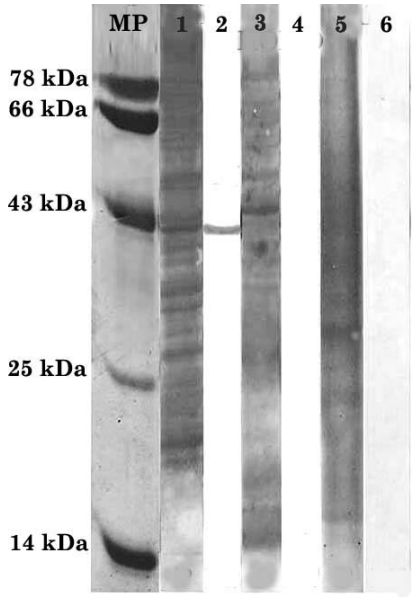

Fig. 1. Binding of SHETA to protein extracted from the skin of 1-day-old chickens. Lane MP, molecular weight marker; Lanes 1 and 2, EDTA extract (EE); Lanes 3 and 4, homogenate (HOMO); Lanes 5 and 6, alkaline extract (AE). Lanes 1, 3 and 5, CBB stain; Lanes 2, 4 and 6, toxin binding test.

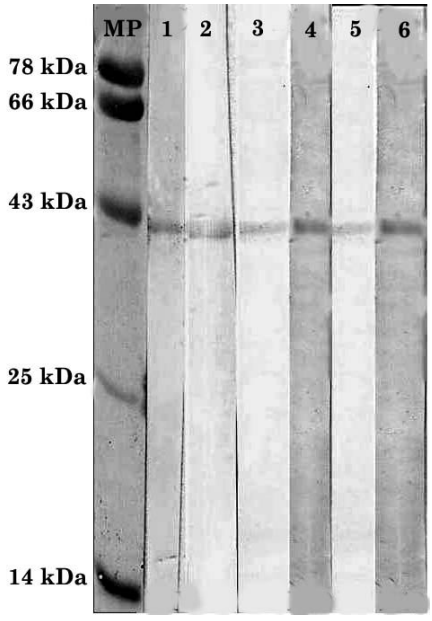

Fig. 2. Binding of SHETA and anti-P40 antibody to P40 from three animal spesies. Lane MP, molecular weight marker; Lanes 1 and 2, chicken P40; Lanes 3 and 4, pig P40; Lanes 5 and 6, mouse P40. Lanes 1, 3 and 5, anti-P40; Lanes 2, 4 and 6, toxin binding test.

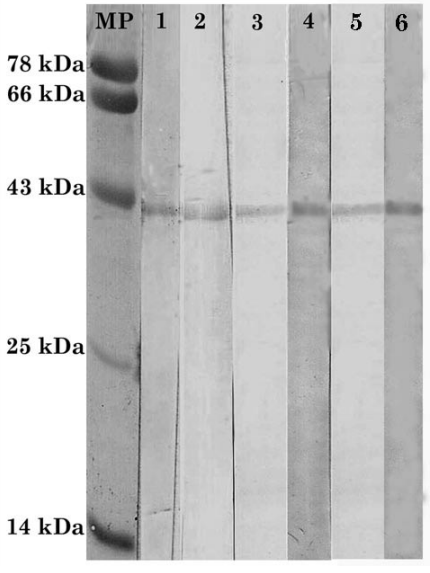

Fig. 3. Binding of SHETB and anti-P40 antibody to P40 from three animal spesies. Lane MP, molecular weight marker; Lanes 1 and 2, chicken P40; Lanes 3 and 4, pig P40; Lanes 5 and 6, mouse P40. Lanes 1, 3 and 5, anti-P40; Lanes 2, 4 and 6, toxin binding test.

and pig P40 (lane 5). Therefore, the antigeni specificity and molecular composition of the P40s from the three animal species seem to be similar, and all these P40s are SHET-binding proteins.

In vitro digestion of P40 with SHETs.

The results of *in vitro* digestion of chicken P40 with SHETA and SHETB are shown in Fig. 4 and Fig. 5, respectively. After incubation of chicken P40 with SHETA (Fig. 4), the 40 kDa band (lane 2) was degraded to a 35 kDa band (lane 3). In Western blotting of the SHETA-digested chicken P40, anti-P40 antibody bound to a 35 kDa band (lane 4). After incubation of chicken P40 with SHETB (Fig. 5), the 40 kDa band (lane 2) was also degraded to a 35 kDa band (lane 3) which bound anti-P40 antibody in Western blotting (lane 4).

The results of *in vitro* treatment of mouse P40 with SHETA are shown in Fig. 6. After incubation of

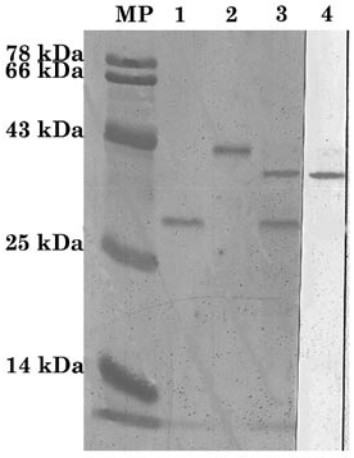

Fig. 4. In vitro digestion of chicken P40 with SHETA. Lane MP, molecular weight marker; Lane 1, SHETA (CBB stain); Lane 2, chicken P40 (CBB stain); Lane 3, chicken P40 digested with SHETA; Lane 4, Western blotting with anti-P40 antibody on SHETA-digested chicken P40.

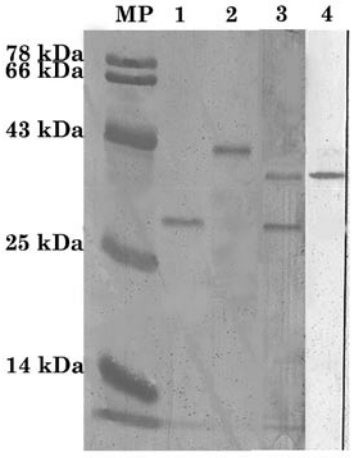

Fig. 5. In vitro digestion of chicken P40 with SHETB. Lane MP, molecular weight marker; Lane 1, SHETB (CBB stain); Lane 2, chicken P40 (CBB stain); Lane 3, chicken P40 digested with SHETB; Lane 4, Western blotting with anti-P40 antibody on SHETB-digested chicken P40.

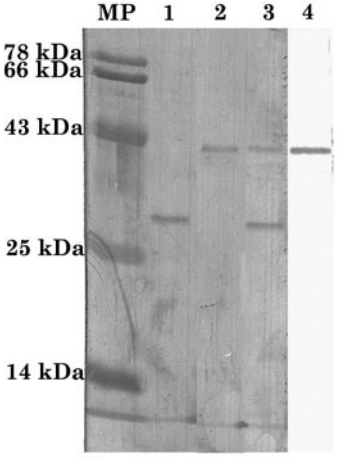

Fig. 6. In vitro treatment of mouse P40 with SHETA. Lane MP, molecular weight marker; Lane 1, SHETA (CBB stain); Lane 2, mouse P40 (CBB stain); Lane 3, mouse P40 treated with SHETA; Lane 4, Western blotting with anti-P40 antibody on SHETA-treated mouse P40.

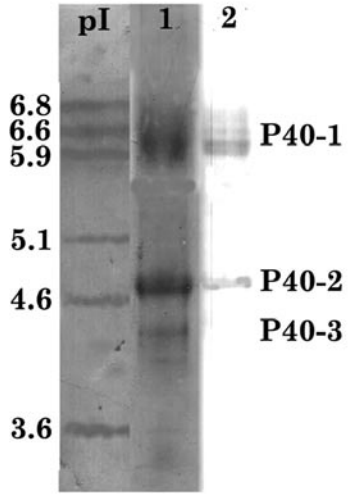

Fig. 7. Results of isoelectric focusing of chicken P40. Lane pI, pI marker; Lane 1, chicken P40 stained with CBB after run; Lane 2, chicken P40 subjected to SHETA-binding test after run.

mouse P40 with SHETA, the 40 kDa band (lane 2) was not degraded (lane 3). In Western blotting of the SHETA-treated mouse P40, anti-P40 antibody bound to a 40 kDa band (lane 4).

Therefore, it is thought that the SHET-binding protein, P40, is a target substance of SHET, and SHET can digest P40 of SHET- susceptible animal species, but not P40 of non-susceptible animal species.

Composition of chicken P40 analyzed by isoelectric focusing.

The results of isoelectric focusing of chicken P40 are shown in Fig. 7. The chicken P40 gave three major protein (P40-1, P40-2 and P40-3) bands. The P40-2 and P40-3 bands were composed of one protein, but the P40-1 band was composed of many proteins (lane 1). The SHETA bound to the P40-1 and P40-2 proteins, but not to P40-3 (lane 2). The isoelectric points of P40-1, P40-2 and P40-3 were 6−6.7, 4.7 and 4.3, respectively. Therefore, P40-2, one of the SHET-binding proteins, was used for further analysis of P40.

Identification of chicken P40-2

The N terminal amino acid sequence of P40-2 determined by Edman degradation was ALGQDLEKKL (Ala-Leu-Gly-Gln-Asp-Leu-Glu-Lys-Lys- Leu). In the analysis using the FASTA system, bovine desmoglein 1 (DSG1) and canine DSG1 were found to have amino acid sequences similar to this short sequence of P40-2.

The alignment of the N terminal amino acid sequence of P40-2 with the complete amino acid sequences of the extracellular region of bovine DSG1 (BoDSG1), canine DSG1 (CaDSG1), human DSG1 (HuDSG1) and murine DSG1 (MuDSG1) is shown in

```
BoDSG1 NITSIVDREVTPFFIIYCRALNSLGQDLEKPLELRVRVLDINDNPPVFSMSTFVGEIEEN 120
CaDSG1 NITSIVDREITPFFIIYCRALNSLGQDLERPLELRVRVLDINDNPPVFSMSTFVGQIEEN 120
HuDSG1 NITSIVDREVTPFFIIYCRALNSMGQDLERPLELRVRVLDINDNPPVFSMATFAGQIEEN 120
MuDSG1 NITSIVDREVTPFFIIYCRALNAQGQDLENPLELRVRVMDINDNPPVFSMTTFLGQIEEN 120
P40-2  ----------------------ALGQDLEKKL---------------------------
       *********.*********** .***** .*******.*********** ** *.****

BoDSG1 SNANTLVMVLNATDADEPNNLNSKIAFKIIRQEPSDSPMFIINRYTGEIRTMNNFLDREQ 180
CaDSG1 SNANTLVMRLNATGADEPNNLNSKIAFKIIRQEPSDSPMFIINRNTGEIRTMNNFLDREQ 180
HuDSG1 SNANTLVMILNATDADEPNNLNSKIAFKIIRQEPSDSPMFIINRNTGEIRTMNNFLDREQ 180
MuDSG1 SNANTLVMKLNATDADEPNNLNSMIAFKIIRQEPSDSPMFIINRKTGEIRTMNNFLDREQ 180
       ******** ****.*********.******************** ***************

BoDSG1 YGQYSLAVRGSDRDGGADGMSAECECNIKILDVNDNIPYMELPTQSISIEENSLNSNLLQ 240
CaDSG1 YSQYSLAVRGSDRDGGADGMSAECECNIKILDVNDNIPYMEPSSHMVRIEENALSQNLVE 240
HuDSG1 YGQYALAVRGSDRDGGADGMSAECECNIKILDVNDNIPYMEQSSYTIEIQENTLNSNLLE 240
MuDSG1 YSQYSLVVRGSDRDGGADGMSAESECSITILDVNDNIPYLEQSSYDIEIEENALHSQLVQ 240
       * **.*.****************.**.*.**********.* ..  . *.** * ..*

BoDSG1 IRVIDLDEEFSANWMAVIFFISGNEGNWFEIEMNERTNVGTLKVVKPLDFEAMNNLQLSL 300
CaDSG1 IRVIDLDEEFSANWMAVIFFISGNEGGWFDIEMNERTNVGILKVIKPLDYEAVQNLQLSL 300
HuDSG1 IRVIDLDEEFSANWMAVIFFISGNEGNWFEIEMNERTNVGILKVVKPLDYEAMQSLQLSI 300
MuDSG1 IRVIDLDEEFSDNWKAIIFFISGNEGNWFEIEMNERTNVGTLKVVKPLDYEAMKNLQLSI 300
       ***********.**.*.*********.**.********** ***.****.**. .****

BoDSG1 GVRNKAEFHQSIMSQYKLTATAISVTVLNVVEGSVFRPGSKTFVVNSNMGQNYKIGEYVA 360
CaDSG1 GVRNKADFHHSIMSQYKVTATAISVTVLNVIEGSVFRPGSKTYVVRSDMGQNYKVGDFVA 360
HuDSG1 GVRNKAEFHHSIMSQYKLKASAISVTVLNVIEGPVFRPGSKTYVVTGNMGSNDKVGDFVA 360
MuDSG1 GVRNVAEFHQSIISQYRLTATMVTVTVLNVIEGSVFRPGSKTFVVDSRMEANHRVGEFVA 360
       ****.*.** **.***...*....******.**.******** ** . *. * ..* .**

BoDSG1 WDLDANRPSTTVRYVMGRNPTDLLAIDSKTAIITLRNKVTMEQYKILGGKYQGTILSIDD 420
CaDSG1 TDLDTGLASTTVRYVMGNNPANLLNVDSKTGVITLRNKVTMEQYEMLNGKYQGTILSIDD 420
HuDSG1 TDLDTGRPSTTVRYVMGNNPADLLAVDSRTGKLTLKNKVTKEQYNMLGGKYQGTILSIDD 420
MuDSG1 TDLDTGRASTNVRYEMGNNPENLLVVDSRTGIITLRNRVTMEQYQRLNGEYKGTVLSIDD 420
       .***... **.***.**.**  ** .** *. .**.*.**.***  * *.*.**.*****

BoDSG1 ALQRTCTGTIVINLENGGWKTERPNVNGS--TTSAYGLTSGGVTTNGYTTGGGVGTVTFA 478
CaDSG1 ALQRTCTGTININIDLQGSGWEKDSEKVTSSQNSGSSTGDSSGGTGGGGRENPSEGDTTTNT 480
HuDSG1 NLQRTCTGTININIQSFGNDDRTNTEPNTKITTNTGRQESTSSTNYDTSTTSTDSSQVYS 480
MuDSG1 SLQRTCTGTIVIELSGTGWVPGSDGGGSS--SGSGGNRDPVTNGYQGTSTVGPQRVTGSG 478
                *********  *  .   *.       .   .    .     .  .

BoDSG1 VGTNGYGVGTGVYQPLRDNVH----------------                        499
CaDSG1 GGKTSTDYEDGETQTQSNNNHQELGSNNLSDNVH---                        514
HuDSG1 SEPGNGAKDLLSDNVH--------------------                        496
MuDSG1 GVTSSGGGSGVNNTPGRQNPLDEPEPEPFDITEDNVH                       515
```

Fig. 8. Alignment of amino acid sequences of the extracellular domain of BoDSG1, CaDSG1, HuDSG1 and MuDSG1 with amino terminal amino acid sequence of P40-2. Amino acids correspond to those of P40-2 are shown in bold letter. Identical and conservative amino acids are shown with asterisk and dot, respectively. ET cleavage site is shown with underline.

Fig. 8. The amino terminal residue of P40-2 corresponds to the position of the 83rd amino acid in the extracellular region of these four DSG1s. The homologies of the amino acid sequence of P40-2 to those of the corresponding region in BoDSG1, CaDSG1, HuDSG1 and MuDSG1 were 80%, 70%, 60% and 70%, respectively. The homologies of the amino acid sequence of HuDSG1 to those of BoDSG1, CaDSG1 and MuDSG1 were 75.0%, 78.7% and 71.7%, respectively.

A schematic diagram of the extracelluar domains of HuDSG1 is shown in Fig. 9. The extracellular region of the mature protein of HuDSG1 is composed of four extracellular cadherin domains (EC1 to EC4) and an extracellular anchor (EA). The ETs clove HuDSG1 between E (glutamic acid) and G (glycine) in the EC3 domain. This sequence is located at 332nd and 333rd amino acid residues of HuDSG1, BoDSG1, CaDSG1 and MuDSG1 (Fig. 8).

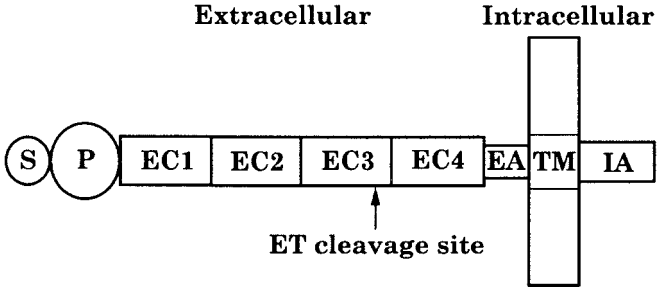

Fig. 9. Schematic diagram of the extracellular domains of HuDSG1. S, signal peptide; P, premature protein; EC1 to EC4, extra-cellular cadherin domains; EA, extracellular anchor; TM, transmembrane protein; IA, intracellular anchor.

Discussion

It is well known that ETs have no caseinolytic activity, but possess a motif related to serine protease in their molecules (16). The SHETs also possess a protease motif (14), but have no caseinolytic activity (15). Therefore, the mechanism of toxic action of ETs and SHETs seems to be the same, and the major activity of ETs and SHETs seems to be proteolysis. These findings indicate that casein is not the target substance of ET and SHET, and the target substance would be a unique protein. Many proteins, such as filaggrin and profilaggrin (18), α-MSH and β-MSH (19) and DSG1 (17), are thought to be candidates for the target protein of ET. Recently Hanakawa et al. (24) proved that ET bound DSG1 and clove it between E (glutamic acid) and G (glycine) in the EC3 domain. The cleavage of DSG1 caused destruction of desmosome (17), which in turn resulted in intraepidermal splitting in the upper layer of the stratum spinosum (20). However, such mechanisms in the toxic action of SHET have not yet been explored. Moreover, the animal species susceptible to SHET differ from those susceptible to ET (15). In addition, the homologies between the amino acid sequences of ETs and SHETs are low (15, 16). We therefore speculated at first that the target protein of SHETs might not be DSG1.

The SHETA and SHETB bound a 40 kDa protein extracted from the skin of chickens with EDTA. This SHET-binding 40-kDa protein was designated P40. The SHETA and SHETB bound to P40s from non-susceptible animals (mice) as well as those from susceptible animals (chickens). The antibody to chicken P40 also bound to mouse P40 as well as chicken P40. The SHETA and SHETB degraded chicken P40 to the 35 kDa protein, whereas SHETA and SHETB could not degrade mouse P40. Hanakawa et al. (25) reported that ETA bound HuDSG1, MuDSG1 and CaDSG1. In their report, ETA digested HuDSG1, but not CaDSG1. If P40 was in fact DSG1, SHETA would be expected to digest chicken P40 but not mouse P40. The chicken P40 gave three major proteins (P40-1, P40-2 and P40-3) in isoelectric focusing. The SHETA bound to P40-1 and P40-2, but not to P40-3. The P40-1 and P40-2 were therefore considered to be target proteins of SHET. The P40-2 was composed of one protein, while P40-1 was composed of many proteins. The isoelectric points of P40-1 and P40-2 were 6−6.7 and 4.7, respectively. The isoelectric points of DSG1 and DSG3 of various animal species were 4.6 to 4.8 and were identical to that of P40-2.

The amino terminal amino acid sequence (ALGQDLEKKL) of P40-2 well matched the 73rd-82nd amino acid residues of BoDSG1, CaDSG1, HuDSG1 and MuDSG1. The homologies of the amino acid sequence of P40-2 to those of BoDSG1, CaDSG1,

HuDSG1 and MuDSG1 were 80%, 70%, 60% and 70%, respectively. Therefore, P40-2 is thought to be a part of chicken DSG1. The complete peptide sequence of chicken DSG1 has not been determined yet. However, the homologies of DSG1s from four animal species (bovine, canine, human and murine DSG1s) are very high (70 to 80%). These results suggest that DSG1 is a target substance of SHET as well as that of ET.

Hanakawa et al. (24) reported that the 84 kDa band of recombinant HuDSG1 (rHuDSG1) was split into 50 kDa and 34 kDa bands after digestion with ETA. The 50 kDa protein is an amino terminal fragment and the 34 kDa protein is a carboxy terminal fragment. The 50 kDa fragment is composed of propeptide and EC1 to EC3, while the 34 kDa fragment is composed of EC4 and EA. The molecular weight of the amino terminal fragment estimated from the amino acid sequence of HuDSG1 is 40 kDa. The increase of molecular weight (10 kDa) of rHuDSG1 from that estimated by the amino acid sequence of HuDSG1 was due to glycosylation of rHuDSG1 during the expression process in insect cells. After digestion of chicken P40 with SHETA and SHETB, the 40 kDa band was degraded to 35 kDa. If the amino acid sequence of chicken DSG1 is similar to that of HuDSG1, SHET will cut it in two at the ET cleavage site of DSG1, and the molecular weight of the amino terminal fragment of chicken P40 estimated from the amino acid sequence would be 28 kDa. If the glycosylated form of chicken DSG1 was digested with SHETs, the molecular weight of the amino terminal fragment would be 35 kDa.

Conclusion

Staphylococccus hyicus exfoliative toxin serotype A (SHETA) and serotype B (SHETB) bound the 40 kDa protein extracted from the skin of 1-day-old chicken. This SHET-binding 40 kDa protein was designated chicken P40. The SHETA and SHETB bound P40s from the skin of susceptible animals (chickens and pigs) and those of non-susceptible animal species (mice). The antibody to chicken P40 reacted to chicken P40, pig P40 and mouse P40. The SHETA and SHETB could degrade chicken P40, but not mouse P40. The chicken P40 gave three major bands in isoelectric focusing. The isoelectric point of P40-2, the second band formed on isoelectric focusing gels of chicken P40, is 4.7. The amino terminal amino acid sequence of P40 well matched the 73rd-82nd amino acid residues of BoDSG1, CaDSG1, HuDSG1 and MuDSG1. These findings suggest that the target protein of SHET is DSG1 of susceptible animals.

References

(1) Sompolinsky, D.: De l'impetigo contagiosa suis et du *Micrococcus hyicus* n. sp. Schweiz. Arch. Tierheilkd. **95** :302−309, 1953.

(2) Jones, L. D.: Exudative epidermitis of pigs. Am. J. Vet. Res. **17**:179−193, 1956.

(3) Sato, H., Tanabe, T., Nakanowatari, M., Oyama, J., Yamazaki, N., Yoshikawa, H., Yoshikawa, T., Koyama, H. & Saito, H.: Isolation of *Staphylococcus hyicus* subsp. *hyicus* from pigs affected with exudative epidermitis and experimental infection of piglets with isolates. Kitasato Arch. Exp. Med. **63**:119−130, 1990.

(4) Melish, M. E. & Glasgow, L. A.: The staphylococcal scalded skin syndrome: development of an experimental model. N. Engl. J. Med. **282**:1114−1119, 1970.

(5) Sato, H., Tanabe, T., Kuramoto, M., Tanaka, K., Hashimoto, T. & Saito, H.: Isolation of exfoliative toxin from *Staphylococcus hyicus* subsp. *hyicus* and its exfoliative activity in the piglet. Vet. Microbiol. **27**:263−275, 1991.

(6) Kondo, I., Sakurai, S. & Sarai, Y.: Purification of exfoliatin produced by *Staphylococcus aureus* of bacteriophage group 2 and its physicochemical properties. Infect. Immun. **8**:156−164, 1973.

(7) Kondo, I., Sakurai, S. & Sarai, Y.: New type of exfoliatin obtained from staphylococcal strains belonging to phage groups other than group II, isolated from patients with impetigo and Ritter's disease. Infect. Immun. **10**:851−861, 1974.

(8) Sato, H., Matsumori, Y., Tanabe, T., Saito, H., Shimizu, A. & Kawano, J.: A new type of staphylococcal exfoliative toxin from a *Staphylococcus*

aureus strain isolated from a horse with phlegmon. Infect. Immun. **62**:3780−3785, 1994.
(9) Yamaguchi, T., Nishifuji, K., Sasaki, M., Fudaba, Y., Aspfelbacher, M., Takata, T., Ohara, M., Komatsuzawa, H., Amagai, M. & Sugai, M.: Identification of the *Staphylococcus aureus etd* pathogenicity island which encodes a novel exfoliative toxin, ETD, and EDIN-B. Infect. Immun. **70**:5835−5845, 2002.
(10) Tanabe, T., Sato, H., Kuramoto, M. & Saito, H.: Purification of exfoliative toxin produced by *Staphylococcus hyicus* and its antigenicity. Infect. Immun. **61**:2973−2977, 1993.
(11) Sato, H., Watanabe, T., Murata, Y., Ohtake, A., Nakamura, N., Aizawa, C., Saito, H. & Maehara, N.: New exfoliative toxin produced by a plasmid-carrying strain of *Staphylococcus hyicus*. Infect. Immun. **67**:4014−4018, 1999.
(12) Andresen, L. O.: Development and evaluation of an indirect ELISA for detection of exfoliative toxin ExhA, ExhB or ExhC produced by *Staphylococcus hyicus*. Vet. Microbiol. **68**:285−292, 1999.
(13) Watanabe, T., Sato, H., Hatakeyama, Y., Matsuzawa, T., Kawai, M., Aizawa, C., Danbara, H. & Maehara, N.: Cloning of the gene coding for *Staphylococcus hyicus* exfoliative toxin B and its expression in *Escherichia coli*. J. Bacteriol. **182**:4101−4103, 2000.
(14) Ahrens, P. & Andresen, L. O.: Cloning and sequence analysis of genes encoding *Staphylococcus hyicus* exfoliative toxin types A, B, C and D. J. Bacteriol. **186**:1833−1837, 2004.
(15) Sato, H.: Structure and activity of staphylococcal exfoliative toxins. Vet. Biochem (in Japanese with English abstract). **38**:1−11, 2001.
(16) Dancer, S. J., Garratt, R., Saladanha, J., Jhoti, H. & Evans, R. : The epidermolytic toxins are serine proteases. FEBS Let. **268**:129−132, 1990.
(17) Amagai, M., Matsuyoshi, N., Wang, Z. H., Andl, C. & Stanley, J. R.: Toxin in bullous impetigo and staphylococcal scalded-skin syndrome targets desmoglein 1. Nature Med. **6**:1275−1277, 2000.
(18) Smith, T. P. & Bailey, C. J.: Epidermolytic toxin from *Staphylococcus aureus* binds to filaggrins. FEBS Let. **194**:309−312, 1986.
(19) Rago, V. J., Vath, M. G., Tripp, J. T., Bohach, A. G., Ohlendorf, H. D. & Schlievert, M. P.: Staphylococcal exfoliative toxins cleave α- and β-melanocyte-stimulating hormones. Infect. Immun. **68**:2366−2368, 2000.
(20) Lillibridge, C. B., Melish, M. E. & Glasgow, L. A.: Site of action of exfoliative toxin in the staphylococcal scalded-skin syndrome. Pediatrics **50**:728−738, 1972.
(21) Laemmli, U. K.: Cleavage of structural proteins during the assembly of the head of bacteriophage T4. Nature **227**:680−685, 1970.
(22) Kapral, F. A. & Miller, M. M.: Product of *Staphylococcus aureus* responsible for the scalded-skin syndrome. Infect. Immun. **4**:541−545, 1971.
(23) Towbin, H., Staehelin, T. & Gordon, J.: Electrophoretic transfer of polyacrylamide gels to nitrocellulose sheets: procedure and some applications. Proc. Natl. Acad. Sci. U.S.A. **76**:4350−4354, 1979.
(24) Hanakawa, Y., Schechter, N. M., Lin, C., Garza, L., Li, H., Yamaguchi, T., Fudaba, Y., Nishifuji, K., Sugai, M., Amagai, M. & Stanley, J. R.: Molecular mechanisms of blister formation in bullous impetigo and staphylococcal scalded skin syndrome. J. Clin. Invest. **110**:53−60, 2002.
(25) Hanakawa, Y., Schechter, N. M., Lin, C., Nishifuji, K., Amagai, M. & Stanley, J. R.: Enzymatic and molecular characteristics of the efficiency and specificity of exfoliative toxin cleavage of desmoglein 1. J. Biol. Chem. **279**:5268−5277, 2004.

Roles of Transcription Factor c-Fos in Response to Bacterial Infection

Koichi Matsuo

Department of Microbiology and Immunology, School of Medicine, Keio University, Tokyo 160-8582, Japan

Introduction

Septic shock is a leading cause of death in intensive care units, and the incidence of sepsis as well as the number of sepsis-related deaths is on the rise (1). Septic shock represents a whole-body response to infection, and is manifested by changes in body temperature, blood pressure, heart rate, lung function, and in more severe forms, organ dysfunction and death. Sepsis by Gram-negative bacteria is one major cause of septic shock, and is specifically referred to as endotoxic shock. Lipopolysaccharide (LPS), or endotoxin, an outer cell-wall component of Gram-negative bacteria, is recognized by Toll-like receptor (TLR) 4 on various cell types, including macrophages, with the help of LPS-binding protein and CD14 (2). Signaling downstream of TLR4 involves molecules such as MyD88 and TRAF6, which eventually activate transcription factors, particularly Nuclear Factor-κB (NF-κB) and Activator Protein-1 (AP-1), causing production of pro-inflammatory cytokines such as interleukin (IL)-1, IL-6, IL-12, and tumor necrosis factor (TNF)-α as well as other inflammatory mediators like nitric oxide (NO). In addition, subsequent adaptive immune responses are induced in the host. TLR4 signaling also results in production of anti-inflammatory molecules, including IL-10. Endotoxic shock is a clinical manifestation of excess or unregulated production of inflammatory mediators (3).

c-Fos belongs to the Fos family of proteins which, together with the Jun family, make up the dimeric transcription factor AP-1. Fos and Jun family proteins all contain the highly conserved "basic leucine zipper" structure. The basic region is responsible for DNA-binding, and the leucine-zipper is for dimerization (4). c-Fos is induced by a variety of stimuli in diverse cell types, including keratinocytes and neurons. The most prominent phenotype of mice lacking c-Fos ($Fos^{-/-}$ mice) is osteopetrosis due to failure of osteoclast differentiation (5). In contrast to this crucial role in the osteoclast lineage, c-Fos does not appear essential for differentiation of macrophages which are derived from the same myeloid precursors as osteoclasts. However, several *in vitro* studies have indicated that c-Fos may have a regulatory role in macrophages (6-10)

In this study, we examined the role of c-Fos in the inflammatory response. Both *in vitro* and *in vivo*, the absence of c-Fos led to enhanced production of IL-6, IL-12 p40 and TNF-α, but decreased production of IL-10 in response to LPS. Consistently, $Fos^{-/-}$ mice displayed more profound hypothermic response to LPS than wild-type mice.

Materials and Methods

Mice.

$Fos^{+/+}$, $Fos^{+/-}$, and $Fos^{-/-}$ mice (11) of 129/BL6 mixed-background were bred and maintained under specific pathogen-free conditions in the mouse facility at Keio University School of Medicine. $Fos^{-/-}$ mice were provided with powder diet. All experiments were conducted in accordance with guidelines for animal use at the Keio University School of Medicine.

Peritoneal macrophages.

Peritoneal cells were harvested from mice by flushing peritoneal cavity with DMEM containing 10% FCS and antibiotics. The medium containing cells was then passed through a cell strainer (Falcon) to remove debris. Cells were counted and plated at 1×10^6 cells per well in 24-well tissue culture plates (Falcon). The cell sheets in the cultures were kept overnight, washed with PBS to remove non-adherent cells, and then fresh medium was added. These adherent cells were used as peritoneal macrophages (PMs).

LPS stimulation.

PMs were stimulated with 1 μg/ml *Salmonella enterica* serovar Typhimurium LPS (Sigma-Aldrich) in PBS for the indicated lengths of time. Where specified, PMs were serum-starved in DMEM without FCS for 2 h and then LPS was added to the starvation medium. In *in vivo* experiment, mice were injected i.p. with indicated doses of LPS in PBS and then sacrificed after approximately 3 h.

Western blot analysis.

PMs were lysed for 30 min on ice in RIPA buffer (1% deoxycholate, 150 mM NaCl, 1% NP-40, 0.1% SDS, 10 mM Tris; pH 7.4) supplemented with protease inhibitors (Roche) and phosphatase inhibitors (Sigma-Aldrich). Cell lysates were cleared by centrifugation at 23,000 × *g* for 30 min at 4ºC, and protein concentration was measured by Bradford assay. Proteins were separated on a 4-12% Bis-Tris gel (Invitrogen) and transferred to a nitrocellulose membrane (Amersham Biosciences). Membrane was probed with anti-c-Fos antibody (Ab-1, Oncogene), anti-phosphorylated ERK1/2 antibody (Cell Signaling Technology), anti-ERK1/2 antibody (Santa Cruz), and anti-actin antibody (Santa Cruz). Appropriate horse radish peroxidase-conjugated secondary antibodies and the ECL Western Blot Detection Kit (Amersham Biosciences) were used for visualization.

RT-PCR analysis.

PMs or spleens were collected and homogenized in 1 ml Isogen reagent (Nippon Gene), and total RNA was purified. cDNA was synthesized using the Enhance Avian HS RT-PCR kit (Sigma-Aldrich). Quantitative PCR was performed on an ABI PRISM 7000 using TaqMan Assay-on-demand kits (Applied Biosystems) for IL-1β, IL-6, IL-10, IL-12 p40, TNF-α, and GAPDH.

ELISA.

IL-1β, IL-6, IL-12 p40, and TNF-α levels in PM culture supernatants and in the serum were measured using ELISA sets (BD PharMingen). IL-10 was quantified using an ELISA kit (R&D Systems).

Body temperature measurement.

A telemetric radio transmitter (TA10ETA-F20, Data Sciences) for measuring body temperature (BT) was implanted subcutaneously on the back of each mouse under pentobarbital sodium anesthesia (30 mg/kg, i.p.) as described (12). Mice were individually housed unrestrained in cages inside of a chamber (MIR-553, Sanyo), wherein a light-dark cycle (LD 12:12; light on at 8:00) was maintained and temperature was kept at 24±1ºC. Food and water were supplied *ad libitum*. Mice were allowed at least 10 days to recover from surgery before data collection. BT was monitored continuously by receivers (CTR-86, Data Sciences) below the cages, and recorded every 5 min by a Data Quest analyzing system (Data Sciences). Where specified, polyclonal rabbit anti-mouse TNF-α antibody (1.0 mg/kg) (Genzyme) was injected to the mice i.p. as described (13).

Results

c-Fos expression in PMs following LPS stimulation.

We first examined expression of c-Fos as well as the MAP kinases ERK1/2 in response to LPS in PM culture at the protein level. c-Fos is known to be

regulated through phosphorylation by ERK1/2, which are themselves phosphorylated in response to various extracellular stimuli (14). Wild-type PMs were serum-starved to prevent serum-induction of c-Fos, and then stimulated with LPS. Western blotting showed that total ERK was equivalent in all samples, but phosphorylated ERK1/2 were detected only at 30 min and 1 h after stimulation. c-Fos was strongly visible at 1 h after stimulation (Fig. 1A). These data demonstrate that in PM cultures LPS induces c-Fos and its upstream kinases, supporting the notion that c-Fos is a downstream mediator of LPS-induced signaling.

Enhanced pro-inflammatory cytokine production in $Fos^{-/-}$ PMs.

To examine whether *in vitro* pro-inflammatory cytokine response is affected by lack of c-Fos, we stimulated PMs from adult wild-type and $Fos^{-/-}$ mice with LPS. Cells and culture supernatants were harvested at several time points over the course of 9 h, and IL-1β, IL-6, IL-12 p40 and TNF-α mRNA levels in cell homogenates were measured by quantitative RT-PCR, and protein levels in culture supernatant were quantified by ELISA (Fig. 1B). Production of IL-6, IL-12 p40, and TNF-α was significantly higher in $Fos^{-/-}$ compared to wild-type PMs at the protein level, and showed a similar tendency at the mRNA level. Differences in IL-1β production were not prominent. For each cytokine, mRNA peaked more rapidly in $Fos^{-/-}$ than in wild-type PMs. At the protein level, the difference in cytokine production between the two genotypes became apparent by 3 h after LPS stimulation, and persisted thereafter. These data suggest that c-Fos may suppress LPS-induced pro-inflammatory cytokine production in PMs.

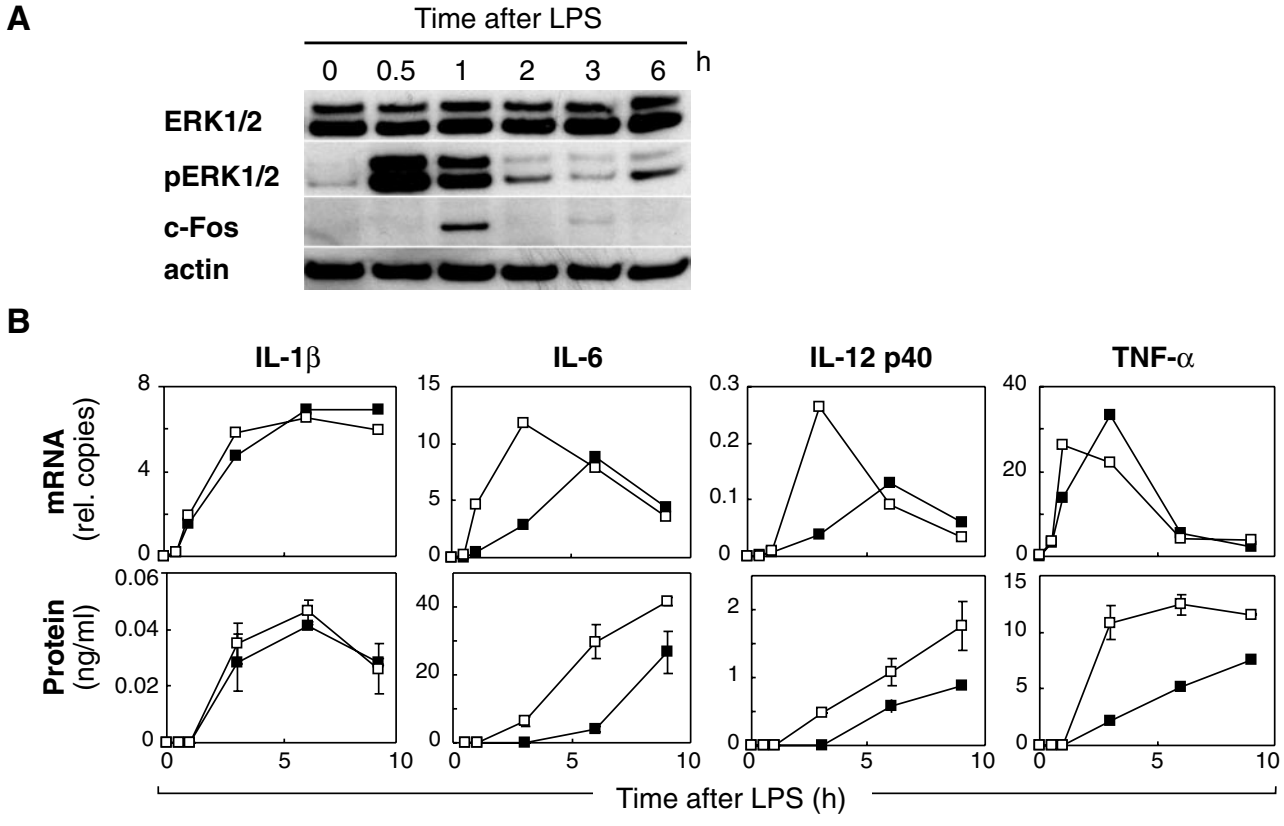

Fig. 1. *In vitro* LPS stimulation of PMs. (A) Western blot analysis of ERK1/2, phospho-ERK1/2, c-Fos, and actin. (B) Pro-inflammatory cytokine profiles of wild-type (closed box) and $Fos^{-/-}$ (open box) PMs as measured by quantitative RT-PCR and ELISA. Culture supernatant and cells were collected over a course of 9 h. Experiments shown are representative of two.

Increased serum pro-inflammatory cytokines in Fos$^{-/-}$ mice.

We next examined whether enhanced pro-inflammatory cytokine production could be observed in *Fos*$^{-/-}$ mice. We injected either PBS or 4 mg/kg LPS to *Fos*$^{+/+}$, *Fos*$^{+/-}$, and *Fos*$^{-/-}$ mice i.p.. Three hours after injection we collected blood and spleens from each mouse and measured IL-6, IL-12 p40, and TNF-α in the spleen cell homogenates at mRNA level and those in the sera at protein level. Serum levels of each of these cytokines were more elevated in *Fos*$^{-/-}$ mice than in wild-type controls after LPS stimulation (Fig. 2). Splenic mRNA levels also showed a tendency for elevation in *Fos*$^{-/-}$ mice. Interestingly, in heterozygous mice, both mRNA and protein levels of these cytokines tended to be intermediate to those of wild-type and *Fos*$^{-/-}$ mice (Fig. 2). These data suggest a converse correlation between systemic pro-inflammatory cytokine response to LPS and levels of c-Fos.

Decreased IL-10 production in Fos$^{-/-}$ PMs and Fos$^{-/-}$ mice.

IL-10, an anti-inflammatory cytokine produced by a variety of cells including macrophages, is known to inhibit production of IL-6, IL-12, and TNF-α (15-17). We measured IL-10 protein levels in PM culture supernatants over a 9 h period after LPS stimulation, as in Fig. 1B, by ELISA. Production of IL-10 was significantly lower in *Fos*$^{-/-}$ PMs compared to wild-type PMs (Fig. 3A). The difference in IL-10 production between the two genotypes was apparent by 1 h after LPS stimulation, and persisted thereafter. Consistently, serum level of IL-10 was also lower in *Fos*$^{-/-}$ mice following 3 h LPS stimulation (Fig. 3B). Thus, reduced expression of IL-10 may be the cause of increased IL-6, IL-12, and TNF-α in *Fos*$^{-/-}$ mice. In other words, c-Fos may enhance production of IL-10 thereby suppressing systemic pro-inflammatory cytokine production.

Profound LPS-induced hypothermia in Fos$^{-/-}$ mice.

Drastic BT changes, whether fever or hypothermia, are one of the hallmark signs of septic shock. To examine whether increased pro-inflammatory cytokine production observed in *Fos*$^{-/-}$ mice makes them more sensitive to septic shock, we stimulated wild-type and *Fos*$^{-/-}$ mice by i.p. injection

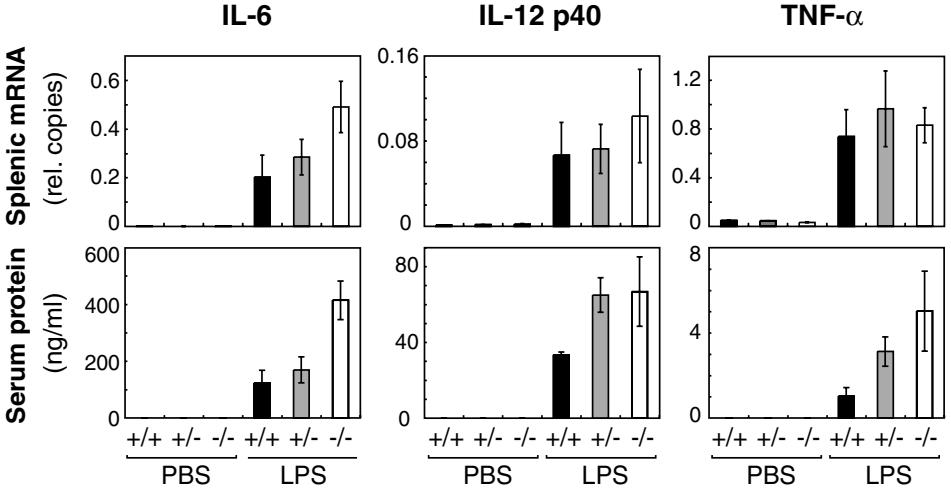

Fig. 2. LPS-induced pro-inflammatory cytokine response in mice. IL-6, IL-12 p40, and TNF-α at the splenic mRNA levels were measured by quantitative RT-PCR and those in the serum protein by ELISA. Wild-type (closed bar), heterozygous (gray bar), and *Fos*$^{-/-}$ (open bar) mice (n = 3 mice per bar) were stimulated for 3 h by i.p. injection of PBS or 4 mg/kg LPS. Results shown are representative of three experiments.

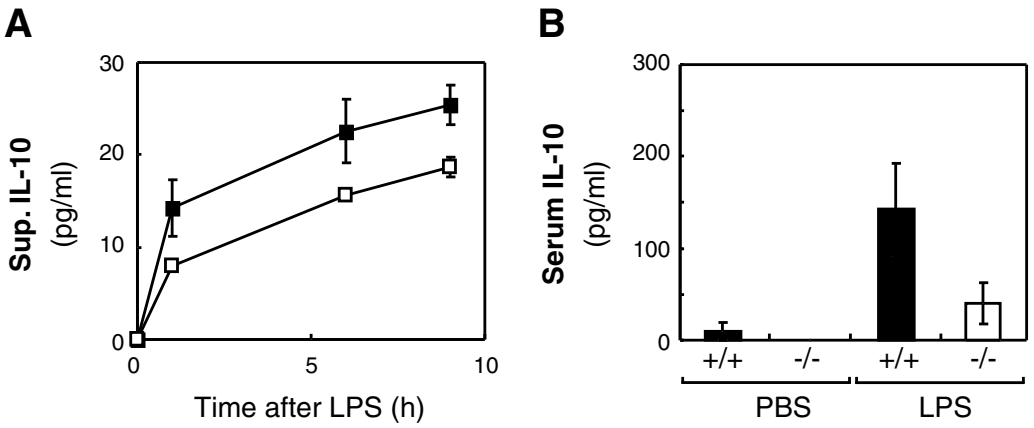

Fig. 3. IL-10 production in PMs and in mice after LPS stimulation. (A) IL-10 protein production after LPS stimulation in wild-type (closed box) and *Fos*$^{-/-}$ (open box) PMs measured by ELISA as in Fig. 1B. (B) Serum IL-10 protein levels were measured in wild-type (closed bar), and *Fos*$^{-/-}$ (open bar) mice (n = 5 mice per LPS-stimulated bar, 2 mice per non-stimulated bar) by ELISA as in Fig. 2. Results shown are representative of two experiments.

with 4 mg/kg LPS, and measured resulting changes in BT. LPS was administered at 13:00 for each experiment, in consideration of circadian rhythm. Following transient fever of 1-2ºC, hypothermia was observed in both genotypes (Fig. 4A). However, the severity of hypothermic response was much greater in *Fos*$^{-/-}$ mice, with BT reaching an average lowest value of 28ºC, versus only 32ºC in control mice.

To determine whether LPS-induced hypothermia is dose-dependent, we stimulated wild-type and *Fos*$^{-/-}$ mice with 0.1, 1 and 4 mg/kg doses of LPS, and measured BT changes. Drop in BT in *Fos*$^{-/-}$ mice showed a clear LPS dose dependence. Moreover, at each dose, hypothermia in *Fos*$^{-/-}$ mice exceeded that in wild-type mice (Fig. 4B).

Neutralization of TNF-α attenuates hypothermic response to LPS in Fos$^{-/-}$ *mice.*

TNF-α is known to induce hypothermia in mice (13). We attempted to counteract the hypothermic response to LPS by pre-treating both wild-type and *Fos*$^{-/-}$ mice with anti-TNF-α antibody 2 h prior to stimulation with 1 mg/kg LPS. As expected, anti-TNF-α antibody was effective in blunting hypothermic response in wild-type mice (data not shown). Figure 4C depicts hypothermic response in *Fos*$^{-/-}$ mice with or without anti-TNF-α antibody pre-treatment. Pre-treated mice showed less profound hypothermia (drop from 34 to 31ºC) than non-pretreated (drop from 34 to 29ºC). The rate of recovery back to baseline was also more rapid in pre-treated mice. These data indicate that enhanced TNF-α production is at least, in part, responsible for the intensity of the hypothermic response seen in *Fos*$^{-/-}$ mice.

Discussion

Several explanations for how c-Fos controls production of inflammatory mediators may exist. It has been reported that certain macrophage populations are increased in *Fos*$^{-/-}$ mice (5). We considered that increased macrophages could contribute to enhanced pro-inflammatory cytokine production in *Fos*$^{-/-}$ mice, so we examined both mRNA and surface expression of several macrophage markers by RT-PCR and FACS (data not shown). We found no consistent positive correlation between elevation of these markers and pro-inflammatory cytokine production. This is consistent with the idea that enhanced pro-inflammatory cytokine production in *Fos*$^{-/-}$ mice is a cell-level phenomenon.

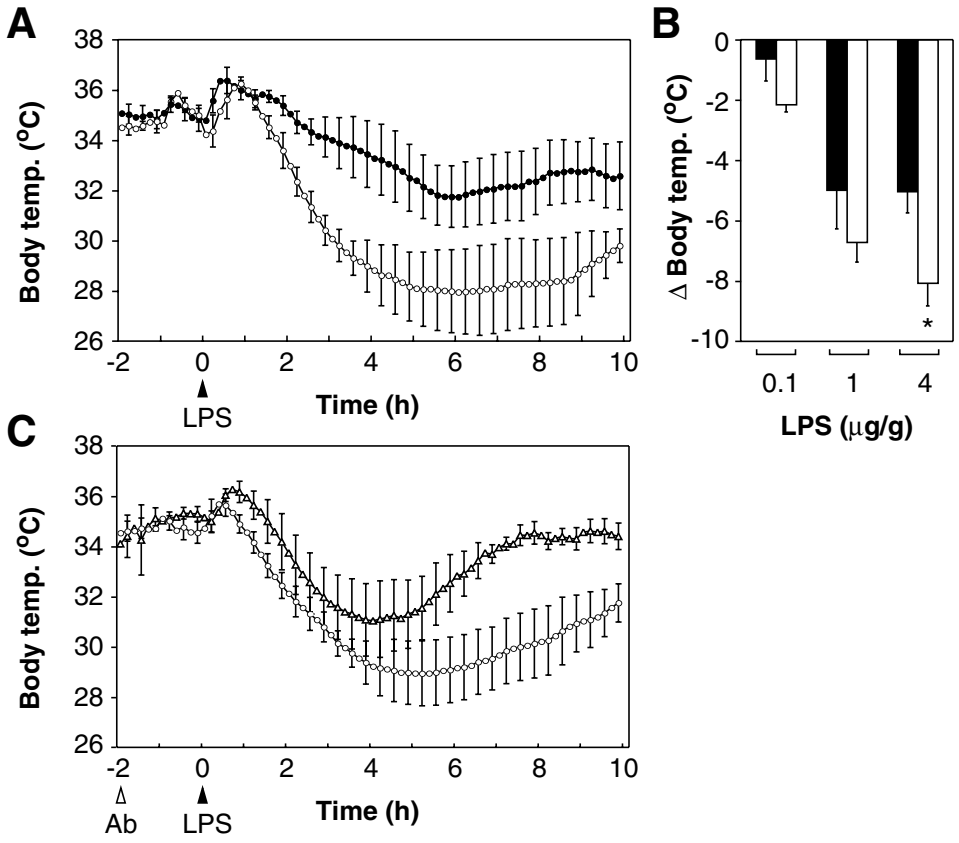

Fig. 4. BT changes after LPS injection. (A) Average BT changes in wild-type (closed circles) and *Fos*$^{-/-}$ (open circles) mice (n = 3 each) after i.p. injection of 4 mg/kg LPS. (B) Dose-dependence of hypothermic response in wild-type (black bar) and *Fos*$^{-/-}$ (open bar) mice (n = 3 per bar). (C) Attenuation of hypothermia in *Fos*$^{-/-}$ mice by i.p. injection of 1.0 mg/kg anti-TNF-α antibody 2 h prior to i.p. injection of 1 mg/kg LPS. Pre-treated and non-pretreated mice (n = 3 each) represented by open triangles and open circles, respectively.

At the cellular level, IL-10, IRAK-M, SOCS and Stat3 are among several molecules implicated in controlling response to LPS (15, 18-20). c-Fos likely acts via or in conjuction with several of these molecules. Furthermore, c-Fos itself is believed to suppress directly several inflammatory mediators, for example, it negatively regulates the *iNOS* promoter, preventing production of inducible nitric oxide synthase (iNOS), and consequently, its product, NO (8). c-Fos may also suppress IL-12 p40 at the promoter level (9).

In this report, we focus on c-Fos suppression of pro-inflammatory cytokine production via IL-10. However, we do not discount effects of c-Fos acting in conjunction with other regulatory molecules, or itself acting directly on pro-inflammatory cytokine production at the promoter level. We propose that the IL-10 pathway is one important mechanism via which c-Fos can control systemic inflammatory response. IL-10$^{-/-}$ mice (15) especially illustrate the importance of this regulatory pathway, as induction of sepsis in IL-10$^{-/-}$ mice can lead to 15-fold higher serum levels of IL-6 and TNF-α and greater sensitivity to septic shock (21). Interestingly the mechanisms by which IL-10 suppresses each cytokine varies quite greatly (16, 17). In reality, control of pro-inflammatory cytokine production involving c-Fos is likely a result of several mechanisms working in conjunction.

Osteoimmunology is the concept that bone-and immune-regulation are closely linked. Several

molecules including IFN-β, IFN-γ, RANKL, TRAF6, NFAT, NF-κB, and c-Fos are important in osteoimmunology (22, 23). c-Fos is necessary for determining cell fate towards osteoclastic differentiation at the macrophage-osteoclast lineage bifurcation. However, even in macrophages which have chosen the immune lineage versus osteoclast, c-Fos appears to suppress persistently immune function. This contrasting role of c-Fos in cells derived from the same myeloid lineage is intriguing; depending on the nature of the signal it receives, c-Fos can be either a positive or negative regulator—RANKL signaling causes c-Fos to promote osteoclast differentiation, but LPS signaling causes c-Fos to suppress inflammation. Signaling via c-Fos appears to be a point of interface between the immune and skeletal systems, and the mechanisms by which divergence in signaling occurs need to be further studied.

Conclusion

In conclusion, we have found that lack of c-Fos results in enhanced inflammatory response *in vitro* and *in vivo*, establishing c-Fos as a negative regulator in LPS-signaling. These findings provide deeper insight into the complex pathways underlying inflammation and septic shock

This work was done in collaboration with Neelanjan Ray, Vanderbilt University School of Medicine, and Masayoshi Kuwahara, Department of Comparative Pathophysiology, Graduate School of Agricultural and Life Sciences, The University of Tokyo.

References

(1) Martin, G.S., D.M. Mannino, S. Eaton, and M. Moss. 2003. The epidemiology of sepsis in the United States from 1979 through 2000. *N Engl J Med* **348**: 1546−1554.

(2) Medzhitov, R. 2001. Toll-like receptors and innate immunity. *Nat Rev Immunol* **1**: 135−145.

(3) Cohen, J. 2002. The immunopathogenesis of sepsis. *Nature* **420**: 885−891.

(4) Chinenov, Y., and T.K. Kerppola. 2001. Close encounters of many kinds: Fos-Jun interactions that mediate transcription regulatory specificity. *Oncogene* **20**: 2438−2452.

(5) Grigoriadis, A.E., Z.Q. Wang, M.G. Cecchini, W. Hofstetter, R. Felix, H.A. Fleisch, and E.F. Wagner. 1994. c-Fos: a key regulator of osteoclast-macrophage lineage determination and bone remodeling. *Science* **266**: 443−448.

(6) Roy, S., R. Charboneau, K. Cain, S. DeTurris, D. Melnyk, and R.A. Barke. 1999. Deficiency of the transcription factor c-fos increases lipopolysaccharide-induced macrophage interleukin 12 production. *Surgery* **126**: 239−247.

(7) Roy, S., R. Charboneau, D. Melnyk, and R.A. Barke. 2000. Interleukin-4 regulates macrophage interleukin-12 protein synthesis through a c-fos mediated mechanism. *Surgery* **128**: 219−224.

(8) Okada, S., S. Obata, M. Hatano, and T. Tokuhisa. 2003. Dominant-negative effect of the c-fos family gene products on inducible NO synthase expression in macrophages. *Int Immunol* **15**: 1275−1282.

(9) Matsumoto, M., D. Einhaus, E.S. Gold, and A. Aderem. 2004. Simvastatin augments lipopolysaccharide-induced proinflammatory responses in macrophages by differential regulation of the c-Fos and c-Jun transcription factors. *J Immunol* **172**: 7377−7384.

(10) Agrawal, S., A. Agrawal, B. Doughty, A. Gerwitz, J. Blenis, T. Van Dyke, and B. Pulendran. 2003. Cutting Edge: different toll-like receptor agonists instruct dendritic cells to induce distinct Th responses via differential modulation of extracellular signal-regulated kinase-mitogen-activated protein kinase and c-Fos. *J Immunol* **171**: 4984−4989.

(11) Wang, Z.Q., C. Ovitt, A.E. Grigoriadis, U. Mohle-Steinlein, U. Ruther, and E.F. Wagner. 1992. Bone and haematopoietic defects in mice lacking *c-fos*. *Nature* **360**: 741−744.

(12) Ishii, K., M. Kuwahara, H. Tsubone, and S. Sugano. 1996. The telemetric monitoring of heart rate, locomotor activity, and body temperature in mice and voles (*Microtus arvalis*) during ambient

temperature changes. *Lab Anim* **30**: 7−12.
(13) Mizuno, T., Y. Kannan, M. Tokunaga, M. Moriyama, Y. Kiso, K. Kusakabe, J. Yamate, K. Kiyomiya, and T. Sugano. 2000. Role of hypothermia induced by tumor necrosis factor on apoptosis and function of inflammatory neutrophils in mice. *Am J Physiol Regul Integr Comp Physiol* **278**: R157−165.
(14) Murphy, L.O., S. Smith, R.H. Chen, D.C. Fingar, and J. Blenis. 2002. Molecular interpretation of ERK signal duration by immediate early gene products. *Nat Cell Biol* **4**: 556−564.
(15) Kuhn, R., J. Lohler, D. Rennick, K. Rajewsky, and W. Muller. 1993. Interleukin-10-deficient mice develop chronic enterocolitis. *Cell* **75**: 263−274.
(16) Denys, A., I.A. Udalova, C. Smith, L.M. Williams, C.J. Ciesielski, J. Campbell, C. Andrews, D. Kwaitkowski, and B.M. Foxwell. 2002. Evidence for a dual mechanism for IL-10 suppression of TNF-alpha production that does not involve inhibition of p38 mitogen-activated protein kinase or NF-kappa B in primary human macrophages. *J Immunol* **168**: 4837−4845.
(17) Zhou, L., A.A. Nazarian, and S.T. Smale. 2004. Interleukin-10 inhibits interleukin-12 p40 gene transcription by targeting a late event in the activation pathway. *Mol Cell Biol* **24**: 2385−2396.
(18) Kobayashi, K., L.D. Hernandez, J.E. Galan, C.A. Janeway, Jr., R. Medzhitov, and R.A. Flavell. 2002. IRAK-M is a negative regulator of Toll-like receptor signaling. *Cell* **110**: 191−202.
(19) Kubo, M., T. Hanada, and A. Yoshimura. 2003. Suppressors of cytokine signaling and immunity. *Nat Immunol* **4**: 1169−1176.
(20) Takeda, K., B.E. Clausen, T. Kaisho, T. Tsujimura, N. Terada, I. Forster, and S. Akira. 1999. Enhanced Th1 activity and development of chronic enterocolitis in mice devoid of Stat3 in macrophages and neutrophils. *Immunity* **10**: 39−49.
(21) Latifi, S.Q., M.A. O'Riordan, and A.D. Levine. 2002. Interleukin-10 controls the onset of irreversible septic shock. *Infect Immun* **70**: 4441−4446.
(22) Arron, J.R., and Y. Choi. 2000. Bone versus immune system. *Nature* **408**: 535−536.
(23) Matsuo, K., and N. Ray. 2004. Osteoclasts, mononuclear phagocytes, and c-Fos: new insight into osteoimmunology. *Keio J Med* **53**: 78−84.

Comparison between Antigen-Presenting Activities of Dendritic Cells and those of Langerhans Cells, and Activation of T Cells by Antigen Trans-loaded from Langerhans Cells to Dendritic Cells

Hiroshi Kawasaki

Department of Clinical Immunology and AIDS Research Center, The Institute of Medical Science, The University of Tokyo, 4-6-1 Shirokanedai, Minato, Tokyo 108-8639, Japan

ABSTRACT Evidence obtained from experiments on animals suggests that epidermal Langerhans cells (LCs) and dermal dendritic cells (DCs) play a crucial role in epicutaneous immune responses. However, the mechanism underlying the induction of the epicutaneous immune response in humans remains obscure. To clarify the mechanism responsible for the induction of Ag-specific immune response in epidermis in the human system, we examined the role of the interplay between DCs and LCs, both derived from human peripheral blood (PB) monocytes, in vitro. DCs exhibited more potent expression of the MHC product and costimulatory molecules than LCs. LCs were less effective for the internalization of exogenous Ag, and the activation of allogeneic and autologous Ag-specific T cells than DCs. DCs and LCs expressed different chemokine receptor repertoires and showed responsiveness to different chemokine repertoires. LCs can transfer unprocessed Ag to DCs via cell to cell contact, and these Ag-*trans*-loaded DCs induced Ag-specific T cell response. Thus, cross-priming between DCs and LCs is crucial for the induction of epicutaneous immune responses.

Introduction

Dendritic cells (DCs) are unique professional major APCs capable of stimulating naive T cells in the primary immune response, and are more potent APCs than peripheral blood (PB) monocytes/macrophages or B cells (1-3). Characterization of DCs is difficult because they represent only a small subpopulation that includes interdigitating cells in lymphoid organs, blood DCs, Langerhans cells (LCs) in the epidermis of the skin, and dermal DCs (1-3).

A series of previous studies have shown that human PB monocytes cultured with GM-CSF and IL-4 (GM-CSF/IL-4) give rise to immature DCs (iDCs) (4, 5), and these cells exhibited characteristic features of dermal DCs, including i) a vigorous endocytic ability, ii) high production of proinflammatory cytokines, and iii) a potent chemotactic response to inflammatory chemokines, including RANTES and macrophage inflammatory protein (MIP)-1α via their receptors (CCR-1 and CCR-5) (4-12). The development of iDCs

Abbreviations used in this paper: BM, bone marrow; CB, cord blood; CD40L; CD40 ligand; CHS, contact hypersensitivity; CLA, cutaneous lymphocyte-associated antigen; cIgG, control IgG; CM, conditioned medium; DCs, dendritic cells; DMEC, dermal microvascular endothelial cells; E-cad, E-cadherin; FITC-OVA, FITC labeled-OVA; HPF, high power field; HPC, hematopoietic stem cell; iDCs, immature DCs; LCs; Langerhans cells; mDCs, mature DCs; MIP, macrophage inflammatory protein; PB, peripheral blood; TT, tetanus toxin.

into mature DCs (mDCs) requires various stimuli, including bacterial components (e.g., LPS), proinflammatory cytokines (e.g., TNF-α), and cognate $CD4^+$T cell help via CD40/CD40 ligand (CD40L) interaction, and these events are accompanied by the upregulation of MHC products/costimulatory molecules leading to the enhancement of T cell-stimulatory ability as well as downmodulation of the abilities to internalize exogenous soluble Ag and to produce proinflammatory cytokines (4-6, 8). This maturation process also involves the downregulation of the expressions of CCR-1 and CCR-5, which results in defective chemotactic responses to inflammatory chemokines, but the acquisition of CCR-7 expression and the responsiveness to MIP-3β, specifically secreted at the T cell-rich area in the secondary lymphoid tissues. Thus acquisition of CCR-7 expression and responsiveness to MIP-3β leads these cells to home into these areas via interaction of CCR-7 and MIP-3β (9-12). These properties were thought to cause accumulation of Ag-loaded mDCs in T cell-dependent areas of the secondary lymphoid tissues where these cells prime naive T cells and induce immune responses.

LCs are member of the DC family present in the epithelium/epidermis, and this cell type specifically expresses E-cadherin (E-cad) and cutaneous lymphocyte-associated antigen (CLA), which are supposed to be relevant to their unique localization (13-15). Recent studies have shown that human PB monocytes cultured with GM-CSF, IL-4 and TGF-β1 (GM-CSF/IL-4/TGF-β1) differentiate into immature LCs (iLCs), and the exposure to immune/inflammatory signals turns iLCs into mature LCs (mLCs) (13-15). An analysis of the chemokine responsiveness of LCs revealed that iLCs predominantly express CCR-6 and respond to MIP-3α, which is produced by keratinocytes and dermal microvascular endothelial cells (DMEC) (15, 16), while mLC migrate to MIP-3β via CCR-7 (16). Morphologic evidence from studies on animal models implies that epidermal LCs travel via lymphatic vessels into T cell-dependent areas of secondary lymphoid tissues where they are thought to act as professional APCs (interdigitating dendritic cells) following epicutaneous sensitization (17-19). However, the mechanism underlying initiation of the epicutaneous immune response involving dermal DCs and epidermal LCs in humans is still unclear, because human LCs apparently exhibit several distinct properties compared with those of animals (14, 20). Furthermore, the difference in the properties between human dermal DCs and epidermal LCs also remains unclear.

To examine the role of DCs and LCs in the initiation of the epicutaneous immune response in humans, we performed a comparative study of the putative DCs and LCs generated from PB monocytes in vitro. Our findings suggest that the interaction between DCs and LCs may play a crucial role in the initiation of epicutaneous immune responses.

Materials and Methods

Media and Reagents.

The medium used throughout was RPMI 1640 supplemented with 2 mM L-glutamine, 50 μg/ml streptomycin, 50 U/ml penicillin, and 10% heat inactivated FCS. GM-CSF, IL-2, IL-4, IL-10, TNF-α, TGF-β1, RANTES, MIP-1α, MIP-3α and MIP-3β were purchased from Pepro Tech. (London, England). FITC-labeled OVA (FITC-OVA) was purchased from Molecular Probes, Inc. (Eugene, OR).

In vitro generation and culture of human DCs and LCs.

iDCs and iLCs were obtained by culturing peripheral blood monocytes with GM-CSF (50 ng/ml) and IL-4 (50 ng/ml) (21, 22) or GM-CSF (50 ng/ml), IL-4 (50 ng/ml) and TGF-β1 (50 ng/ml) for 7 days, respectively. For the preparation of mDCs or mLCs, cells were subsequently cultured with TNF-α (50 ng/ml) for another 3 days. In another experiment, iDCs and iLCs were treated with immobilized control mouse IgG (cIgG; Sigma, St. Louis, MO) or mAb to CD40 (50 μg/ml) (BD Pharmingen, San Diego, CA) for 3 days. Cell differentiation was monitored by light microscopy, and the resultant cells were used for subsequent experiments.

Preparation of T cells.

PB T cells and cord blood (CB) T cells were isolated from PBMCs and CBMCs as described previously (23). These T cell preparations were typically > 98 % pure as indicated by anti-CD3 mAb (BD Pharmingen) staining.

Flow cytometry.

For surface marker analysis, DCs or LCs were cultured with the following mAbs conjugated to FITC or PE for direct staining: CD1a and CD83 (Coulter Immunology, Hialeah, FL), CDD11c, CD40, CD80, CD86, HLA-DR, CLA and CCR-5 (BD Pharmingen). Cells were also stained with the corresponding FITC- or PE-conjugated isotype-matched control mAb (BD Pharmingen). For indirect staining, cells were incubated with biotin conjugated anti-CCR-1 mAb (R&D System, Minneapolis, MN), anti-CCR-6 mAb (R&D System) or anti-E-cad mAb (Chemicon International, Temecula, CA) plus FITC-conjugated avidin (BD Pharmingen) or goat anti-mouse IgG (BD Pharmingen). Analysis of fluorescence staining was performed with a FACSCalibur flow cytometer (Becton Dickinson, Mountain View, CA) and CELLQuest Software.

Endocytosis assay with FITC-OVA.

The methods used to determine the endocytotic activity have previously been described (23). Briefly, FITC-OVA was added to the cells (10^6) at a final concentration of 50 μg/ml. After incubation for 60 min at 37ºC, cells were washed four times with ice-cold PBS. The uptake of FITC-OVA by cells was measured, or a further chase in tracer-free medium was done for a specified period at 37ºC. Cells were then washed four times with ice-cold PBS, and the uptake of FITC-OVA was analyzed by flow cytometry.

Assay for transference of antigenic material to DCs by LCs.

iDCs or iLCs (10^6) were mixed with FITC-OVA (50 μg/ml)-pulsed iLCs or iDCs (10^6) prepared as above in 24-well plates (Costar) for 6 h at 37ºC. In another experiment, iDCs or iLCs (10^6) were added to the upper compartment of a 24-well Transwell cell culture chamber (Costar), and FITC-OVA-pulsed iLCs or iDCs (10^6) were loaded in the lower compartment (separated from upper chamber with 3.0-μm pore size membrane). The cultures were incubated for 6 h at 37º C. Subsequently, E-cad$^-$iDCs (>98 %) or E-cad$^+$iLCs (>98 %) were negatively or positively selected with anti-E-cad mAb in combination with anti-mouse IgG mAb conjugated immunomagnetic beads (Dynal, Oslo, Norway) according to the manufacturer's instruction manual. The endocytosis was measured as described above.

Stimulation of iDCs and iLCs.

iDCs and iLCs (5×10^6/5 ml) were unstimulated or stimulated with LPS (*E. coli* 0127B8; Sigma) (1 μg/ml) for 48 h at 37ºC. Cells were washed twice with cold PBS, collected and used for RNA extraction.

Culture of dermal fibroblasts and DMEC and preparation of conditioned medium (CM).

Normal human neonatal skin fibroblasts and DMEC were purchased from BioWhittaker (Walkersville, MD), and the culture of these cells was performed according to the manufacturer's instruction manual. Culture conditioned media were prepared as follows; normal human neonatal skin fibroblasts and DMEC (5×10^6) were unstimulated or stimulated with IL-1β and TNF-α (IL-1β/TNF-α) (50 ng/ml) in 5 ml of serum-free medium for 48 h at 37ºC. The supernatant was collected, and cell-free supernatants were obtained following centrifugation at 800 × *g* for 5 min and passage through a 0.22 μm filter (Milipore Corporation, Bedford, MA), then stored at −20ºC before use. In another experiment, cells were collected and used for RNA extraction.

Semiquantitative RT-PCR.

RNA from each sample (5×10^6) was isolated

using Trizol LS reagent (GIBCO BRL, Gaithersburg, MD). The first strand cDNA kit (SuperScript™ Preamplication System, GIBCO BRL) was used to make cDNA (10 μl) from 5 μg of each RNA. Amplification of each cDNA (1 μl) was performed with a SuperTaq Premix kit (Sawady Tech., Tokyo, Japan) using the specific primers for CCR-1, CCR-5, CCR-6 and CCR-7 (22). Specific primers for β-actin (Toyobo, Osaka, Japan) and other cytokines including GM-CSF, IL-1β, IL-6, TNF-α, IL-12p35, IL-12p40 (Continental Laboratory Products Inc., San Diego, CA), RANTES, MIP-1α (Biosource, Camarillo, CA) and MIP-3α (16) were also used for amplification. To activate DNA polymerase, preheating (95ºC for 5 min) was performed. The reaction mixture was then subjected to 30 cycles of PCR (22). PCR products were analyzed by electrophoresis through 2 % or 2.5 % agarose gels and visualized under UV light after ethidium bromide staining.

Assay for chemotaxis.

Chemotaxis of DCs and LCs to RANTES, MIP-1α, MIP-3α or MIP-3β (1-100 ng/ml) or CMs (two-fold dilutions with serum-free medium) from dermal fibroblasts or DMEC was determined as described previously (21, 22). The data were expressed as No. of migrated cells/high power field (HPF).

MLR.

Allogeneic PB T cells or CB T cells (10^5) were cultured in 96-well flat-bottom microplates (Coster) with irradiated (15Gy from a ^{137}Cs source) APCs (10^4). Thymidine incorporation was measured on day 5 by an 18-h pulse with [^{3}H]thymidine (1 μCi/well, specific activity, 5 Ci/mmol; Amersham Life Science, Buckinghamshire, UK).

Ag presentation assay with autologous Ag-specific T cells.

PBMCs were primed with tetanus toxin (TT) (Biogenesis, Poole, England) (1 μg/ml) for 3 wk in medium containing IL-2 (100 U/ml). Following this procedure, T cells (>95 % $CD3^+$ cells) isolated from the TT-primed PBMCs (23) were washed twice with PBS, before being cultured in medium for 5 days in the presence of IL-2 (10 U/ml). For preparation of Ag-pulsed DCs and LCs, iDCs and iLCs were cultured with TT (1 μg/ml) or TT-pulsed iLCs or iDCs for 24 h, and subsequently stimulated with TNF-α (50 ng/ml) for 3 days to induce mature type cells, which were then washed, and used as APCs. TT-primed T cells (10^5) were cultured with irradiated (15Gy) TT-loaded DCs and LCs (10^4), and [^{3}H]thymidine incorporation was measured on day 5.

Results

DCs and LCs exhibit distinct expression patterns of cell surface molecules.

Few studies have reported the difference in the properties between human DCs and LCs, and the role of these cell types in the initiation of epicutaneous immune response remains unclear. Human PB monocytes are reportedly to differentiate into two type of APCs, namely, iDCs and iLCs when monocytes are cultured with GM-CSF/IL-4 or GM-CSF/IL-4/TGF-β1, respectively (4, 5, 13-15). To address the difference in the biological properties between human DCs and LCs, we analyzed the phenotypes and functions of human monocyte-derived DCs and LCs. Figure 1*A* shows that both iDCs and iLCs expressed CD1a and CD11c while CLA and E-cad were expressed only on iLCs. Furthermore, iLCs exhibited lower expression levels of CD40, CD80, CD86 and HLA-DR than iDCs (Figure 1*B*). Stimulation of iLCs with TNF-α resulted in the enhancement of cell surface expression levels of CD40, CD80, CD86 and HLA-DR though these expression levels were lower than those of TNF-α-induced mDCs (Fig. 1*B*). Furthermore, TNF-α-induced mDCs and mLCs exhibited similar expression levels of CD83, which is known as a maturation marker for a family of DCs (5). We observed that the cell surface expression levels of CLA and E-cad were decreased in LCs following stimulation with TNF-α (Fig. 1*A*).

We also examined the effect of CD40 ligation, a

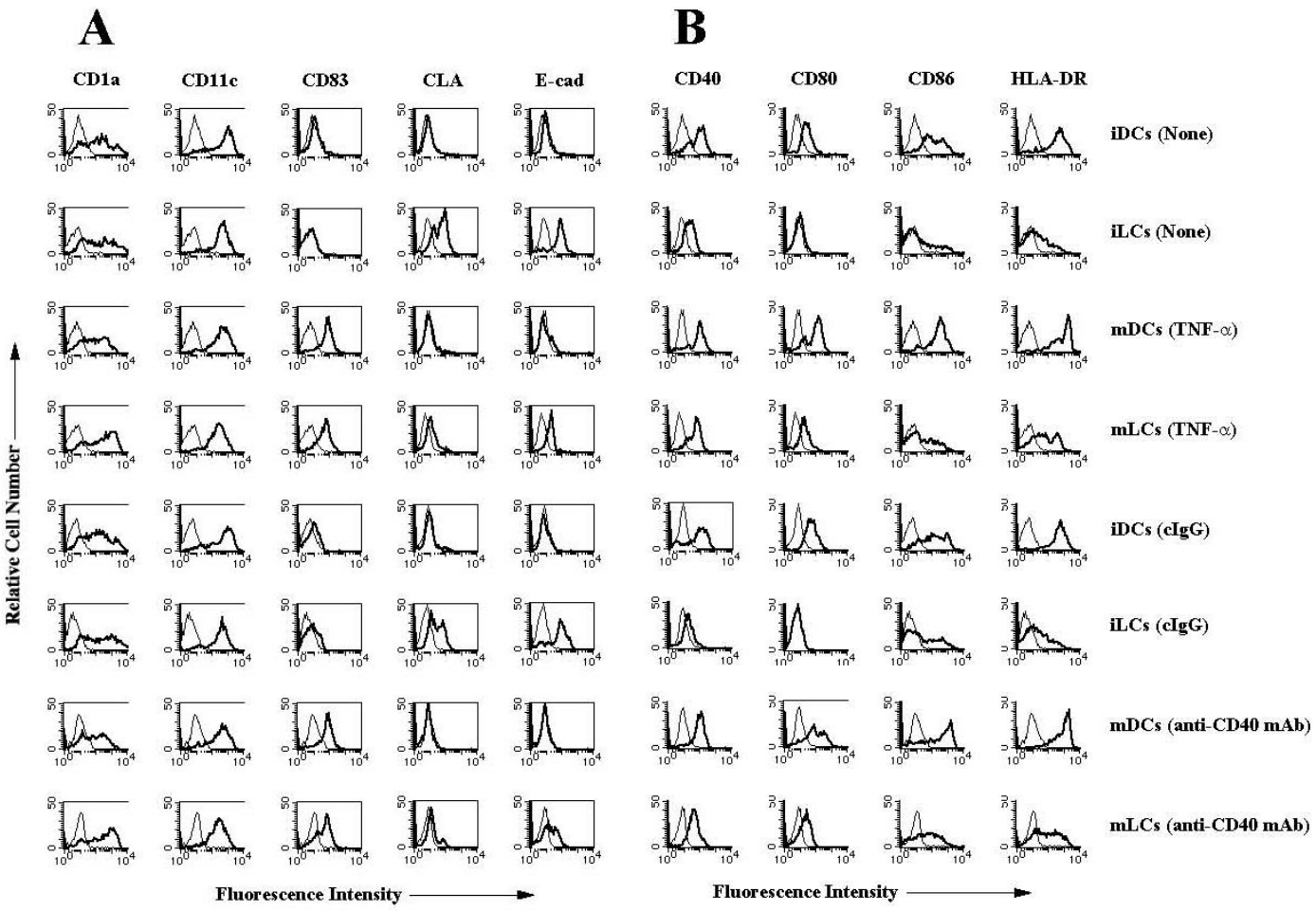

Fig. 1. Phenotypic profiles of DCs and LCs. Cells were stained with the stated mAbs against markers for the DC family (*A*) and HLA-DR and costimulatory molecules (*B*) (thick lines) or isotype-matched mAbs (thin lines), and cell surface expression was analyzed by FACS. The results are representative of ten experiments with similar results.

surrogate for T cell help, on the maturation of these cell types. The change in the expression levels of these cell surface molecules following CD40 ligation was more potent than that in TNF-α-induced mDCs and mLCs (Figure 1, A and B). Similar results were observed when iDCs and iLCs were stimulated with Con A-activated CD4+T cells expressing CD40L (data not shown).

LCs exhibit lower production of proinflammatory cytokines than DCs.

Little is known about the difference in the ability to produce inflammatory cytokines between DCs and LCs in humans. We therefore examined the LPS-induced production of GM-CSF, IL-1β, IL-6, TNF-α, IL-12p35 and IL-12p40 in iDCs and iLCs by semiquantitative RT-PCR. Fig. 2 shows that LPS significantly induced the transcripts of these proinflammatory cytokines in iDCs while this stimulation resulted in lower production levels in iLCs. These results indicate that the ability of iLCs to produce proinflammatory cytokines is less than that of iDCs. On the other hand, stimulation with LPS failed to induce these proinflammatory cytokines in mature status of both cell types (data not shown), indicating that, like in mDCs (8), the responsiveness to LPS is downregulated in mLCs.

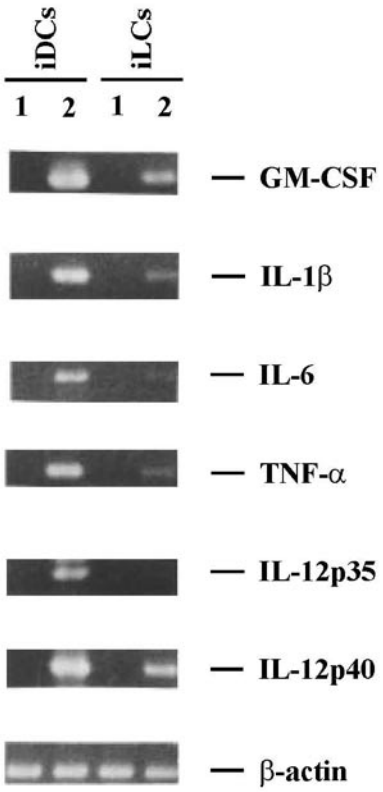

Fig. 2. Detection of LPS-induced proinflammatory cytokine production in iDC and iLCs. iDCs or iLCs (5×10^6) were either unstimulated (lane 1) or incubated with 1 μg/ml of LPS (lane 2) for 48 h at 37ºC. The expression of the indicated cytokine mRNA was detected by semiquantitative RT-PCR. The results of RT-PCR for β-actin demonstrate the loading of equal amounts of DNA on the gel. The results are representative of ten experiments with similar results.

Long-lasting retention of antigenic protein in iLCs.

iDCs capture and process Ags through their high endocytic capacity by receptor-mediated endocytosis, clathrin-coated pits pathway and fluid phase endocytosis (4, 24). Fig. 3*A* shows that iLCs exhibited less endocytosis of FITC-OVA than iDCs, and this ability was significantly decreased in the maturation status in both cell types.

To evaluate the kinetics of Ag internalization in iDCs and iLCs, both cell types were cultured with FITC-OVA for 1 h at 37ºC, washed twice with PBS, and the internalized FITC-OVA was chased in the tracer-free medium until the time points indicated (Fig.

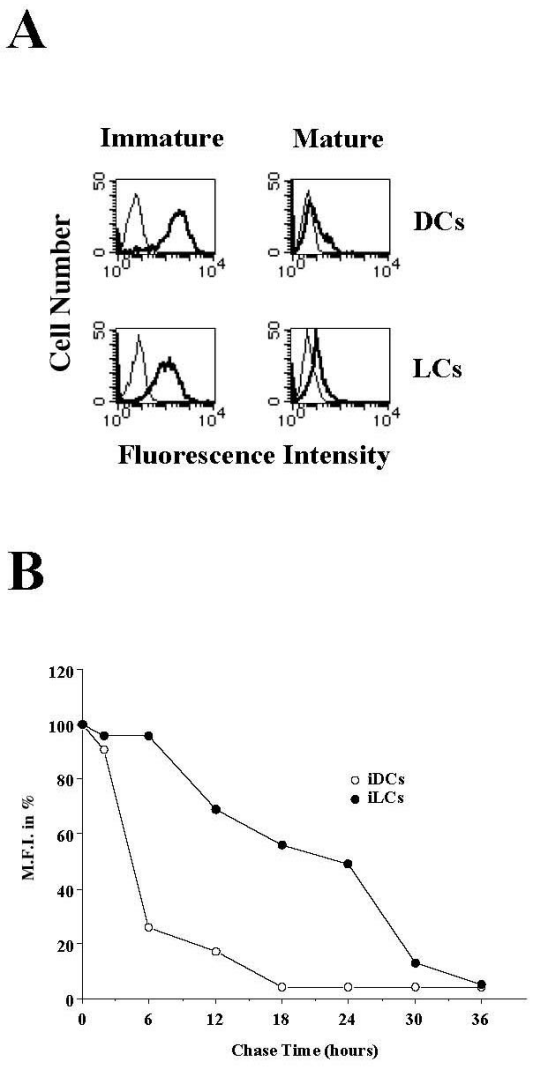

Fig. 3. Ag uptake and retention in DCs and LCs. DCs or LCs (10^6) were cultured with medium alone (thin lines in *A*) or FITC-OVA (50 μg/ml) (thick lines in *A*). After a 60-min pulse at 37ºC, cells were washed and subsequently measured (*A*) or chased in tracer-free medium until the indicated time point at 37ºC (*B*). The internalization of FITC-OVA by cells was analyzed by flow cytometry. The results are representative of five experiments with similar results.

3*B*). iDCs lost the internalized FITC-OVA rapidly, and little or no antigenic material was detected at 18 h after incubation. On the other hand, iLCs still contained large amounts of FITC-OVA at a chase of 6 h, indicating that this tracer was retained, and that the internalized FITC-OVA slowly decreased during the

36 h. These results indicate that iLCs retain unprocessed antigenic material longer than iDCs.

Differential chemokine responsiveness of DCs and LCs.

To clarify the difference in expression of chemokine receptor between DCs and LCs, the expression levels of CCR-1, CCR-5, CCR-6 and CCR-7 in DCs and LCs were determined by flow cytometry (Fig. 4). iDCs expressed higher levels of CCR-1 and CCR-5 than iLCs while CCR-6 expression was only detected in iLCs. Similar results were observed with transcriptional expression of CCR-1 and CCR-5 (data not shown). Interestingly, although the CCR-6 transcript was detected in both cell types, the expression level of this transcript was lower in iDCs than in iLCs (data not shown). We also observed CCR-7 transcript was not expressed in either cell type (data not shown). On the other hand, the expression levels of cell surface products and transcripts of CCR-1, CCR-5 and CCR-6 (data not shown) were decreased following maturation. Conversely, CCR-7 transcript was detected in mDCs and mLCs (data not shown), and the level of this expression in mDCs was more potent than mLCs.

We also compared the responsiveness of DCs and LCs to RANTES (ligand for CCR-1 and CCR-5), MIP-1α (ligand for CCR-1 and CCR-5), MIP-3α (ligand for CCR-6) and MIP-3β (ligand for CCR-7), and found that their chemokine responsiveness was associated with these chemokine receptor expression (Fig. 5). These results indicate that DCs and LCs exhibit different chemokine responsiveness via distinct

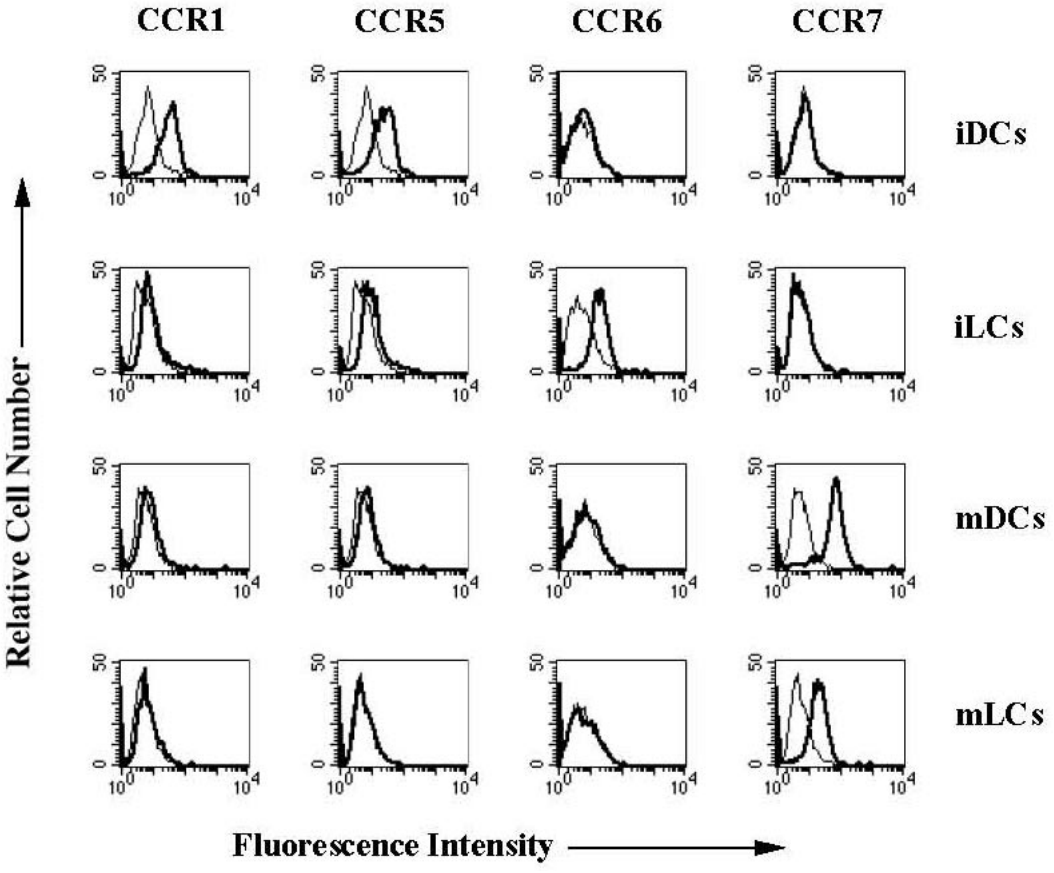

Fig. 4. Cell surface expression of chemokine receptors in DCs and LCs. Cells were stained with the stated mAbs (thick lines) or isotype-matched mAbs (thin lines), and their cell surface expression was analyzed by FACS. Data are represented by a histogram.

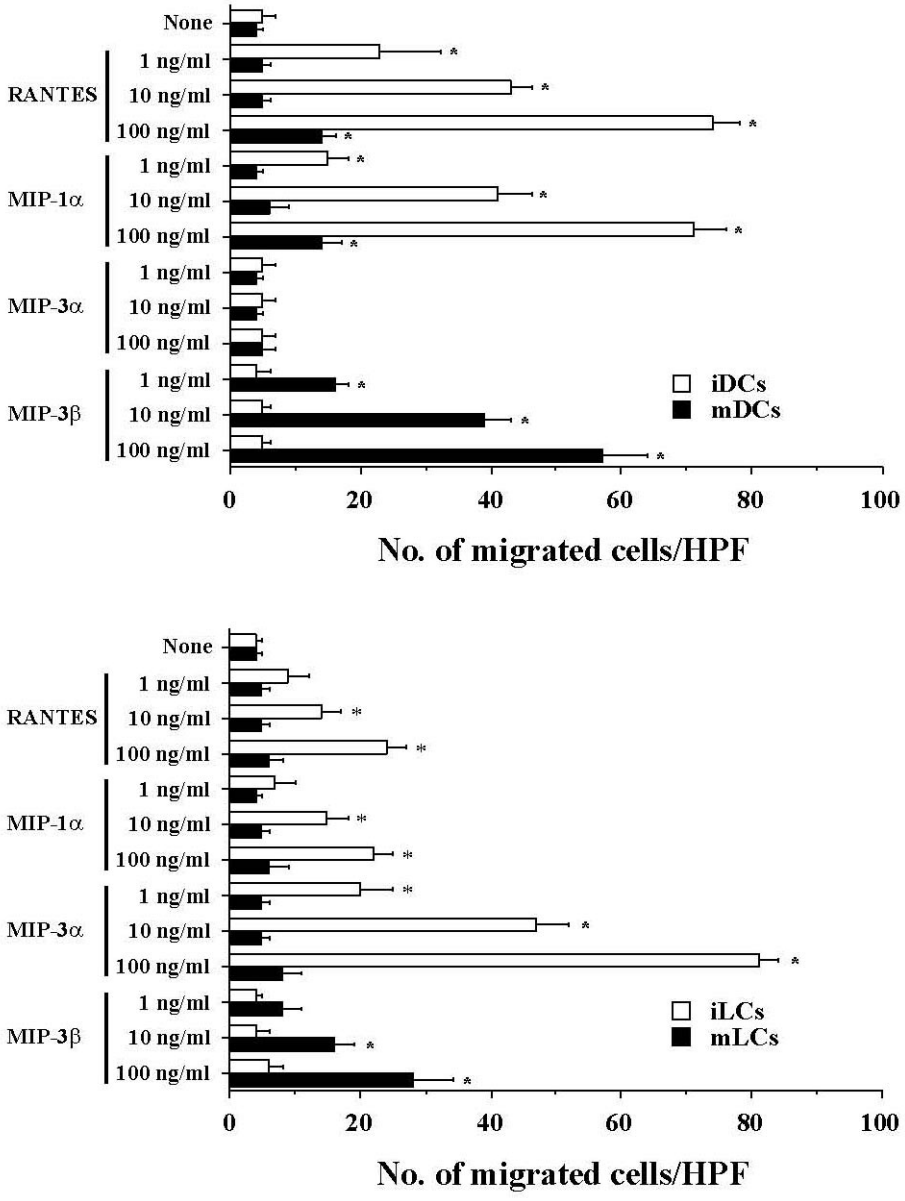

Fig. 5. Chemotactic responses of DCs and LCs to chemokines. Chemotaxis of DCs or LCs to RANTES, MIP-1α, MIP-3α or MIP-3β (1-100 ng/ml) was determined. The data is expressed as No. of migrated cells/high power field.The results are representative of five experiments with similar results.

chemokine receptor expression.

Previous studies have shown that dermal fibroblasts and DMEC produce various sets of chemokines, and the secretion of these chemokines is suggested to be crucial for the induction of epicutaneous immune response (16, 25). As shown in Fig. 6, dermal fibroblasts and DMEC did not express the transcripts of RANTES and MIP-1α while treatment with IL-1β/TNF-α induced expression of these transcripts in both cell types. Furthermore, DEMC constitutively expressed the transcripts of MIP-3α whereas treatment with IL-1β/TNF-α slightly enhanced this expression. On the other hand, little or no MIP-3α transcript was expressed in both unstimulated and IL-1β/TNF-α-stimulated dermal fibroblasts.

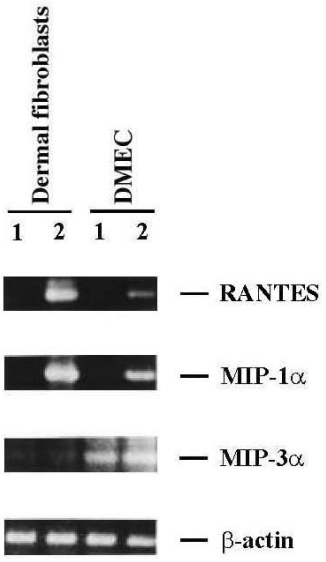

Fig. 6. Production of RANTES, MIP-1α and MIP-3α in inflamed dermal fibroblasts and DEMC. RNA was extracted from unstimulated (lane 1) or IL-1β/TNF-α-stimulated (lane 2) cells, and the expression of transcripts of RANTES, MIP-1α and MIP-3α was evaluated by semiquantitative RT-PCR. PCR products for RANTES (197 bp), MIP-1α (279 bp), MIP-3α (254 bp) and β-actin (645 bp) are shown. The results of RT-PCR for β-actin demonstrate the loading of equal amounts of DNA on the gel.

To assess the abilities of DCs and LCs to migrate into epicutaneous inflamed tissues, dermal fibroblasts and epithelial cells were unstimulated or stimulated with a combination of IL-1β/TNF-α, CM were collected, and the chemotaxis of DCs and LCs in response to these CM as chemoattractant were examined. Fig. 7 shows that iDCs responded to CM from IL-1β/TNF-α-stimulated dermal fibroblasts and DEMC while iLCs responded to CM from unstimulated and IL-1β/TNF-α-stimulated DEMC. Furthermore, their chemotactic migratory responses in the mature status were significantly reduced as compared with those of immature status of both cell types.

LCs are less effective for activation of allogeneic and Ag-specific T cells than DCs.

To compare the T cell-stimulatory abilities between DCs and LCs, allogeneic PB T cells and CB T cells (10^5) were cultured with immature and mature status of both cell types (DC or LC) (10^4), and T cell proliferative responses were measured on day 5. Fig. 8 shows that iLCs and TNF-α-induced mLCs elicited less T-cell proliferation than DCs. Furthermore, CD40 ligation enhanced the T-cell stimulatory capacity of LCs although significantly less than that of DCs.

To examine the abilities of DCs and LCs to activate Ag-specific T cells, immature status of both cell types were pulsed with TT for 24 h, and these TT-loaded cells were made to develop into their mature status by culturing with TNF-α for 3 days. Subsequently, TT-specific T cells were cultured with these APCs, i.e., TT-loaded mDCs or mLCs, and the T cell-proliferation was measured on day 5. Fig. 10 shows that TT-loaded mDCs induced a more potent activation of TT-specific T cells than TT-loaded mLCs

LCs transfer soluble Ag to DCs via cell to cell contact and transferred Ag-loaded DCs stimulate Ag-specific T-cell responses.

The findings that LCs retain unprocessed Ag for a long period and are less effective in the Ag-presentation to T cells than DCs led to hypothesis that LCs may transfer unprocessed Ag to DCs to initiate efficient Ag-specific T cell activation. To test this possibility, iDCs or iLCs were cultured with FITC-OVA-loaded iLCs or iDCs for 6 h at 37ºC, and the binding of transferred FITC-OVA to the respective cells was evaluated. Fig. 9 shows that cell to cell contact allowed iLCs to transfer FITC-OVA to iDCs whereas FITC-OVA-loaded iDCs did not transfer this Ag to iLCs in mixed culture. To show that the contact between iDCs and iLCs was essential, iDCs or iLCs were cultured in transwells with FITC-OVA-loaded iLCs or iDCs for 6 h at 37ºC in separate compartments. Little or no transference of FITC-OVA through the membrane separating two compartments was observed (Fig. 9).

To test the possibility that Ag transferred to DCs from LCs activate Ag-specific T cells, iDCs or iLCs were cultured with TT-loaded iLCs or iDCs for 6 h at 37ºC. These *trans*-Ag-loaded APCs were cultured with

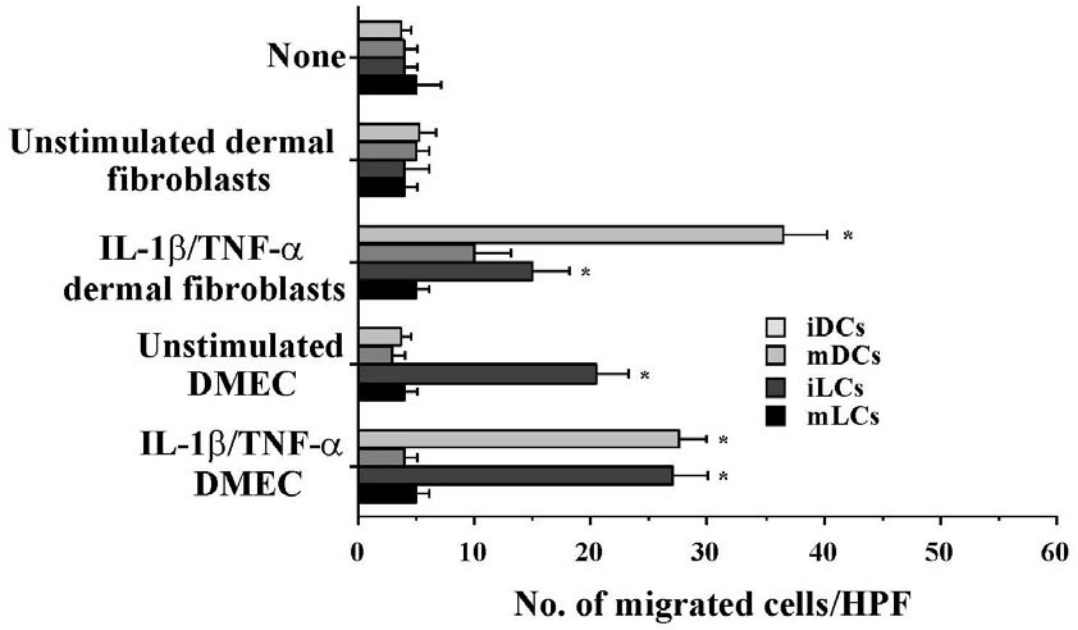

Fig. 7. Chemotactic migratory responses of DCs and LCs to IL-1β/TNF-α-stimulated dermal fibroblasts and DEMC. Chemotaxis of DCs or LCs to CM from unstimulated or IL-1β/TNF-α-stimulated dermal fibroblasts and DEMC was determined. The data is expressed as No. of migrated cells/high power field (HPF).The results are representative of five experiments with similar results.

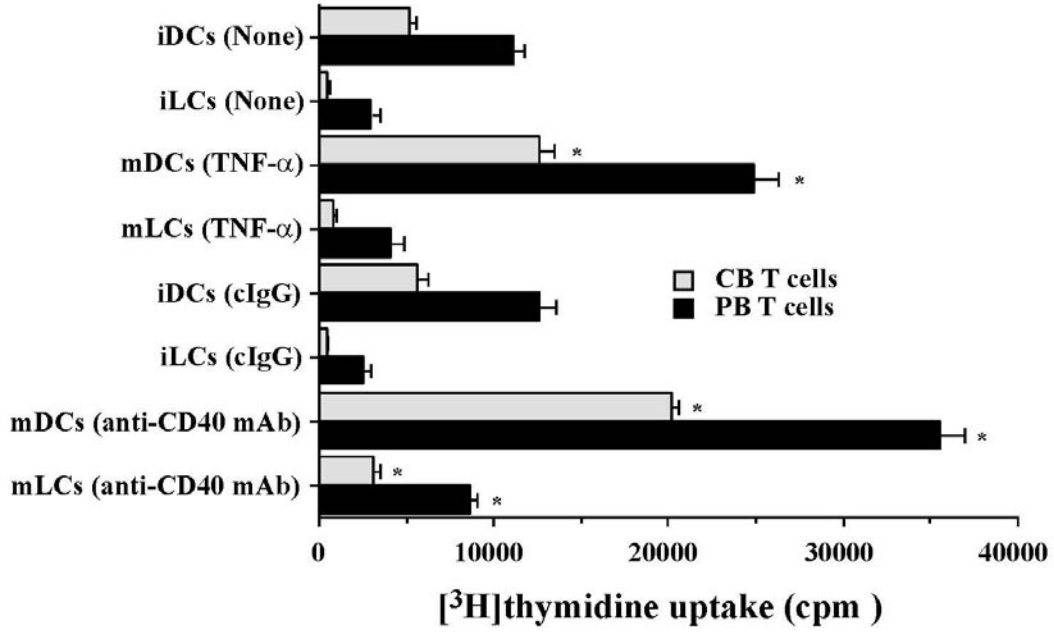

Fig. 8. Allogeneic T cell-stimulatory abilities of DCs and LCs. PB T cells or CB T cells (10^5) were cultured with irradiated APCs (10^4). The proliferative response was measured on day 5. Values are the mean ± SD obtained for triplicate cultures. Values of [^{3}H]thymidine incorporation into T cells or irradiated APCs were less than 1000 cpm. The results are representative of five experiments with similar results.

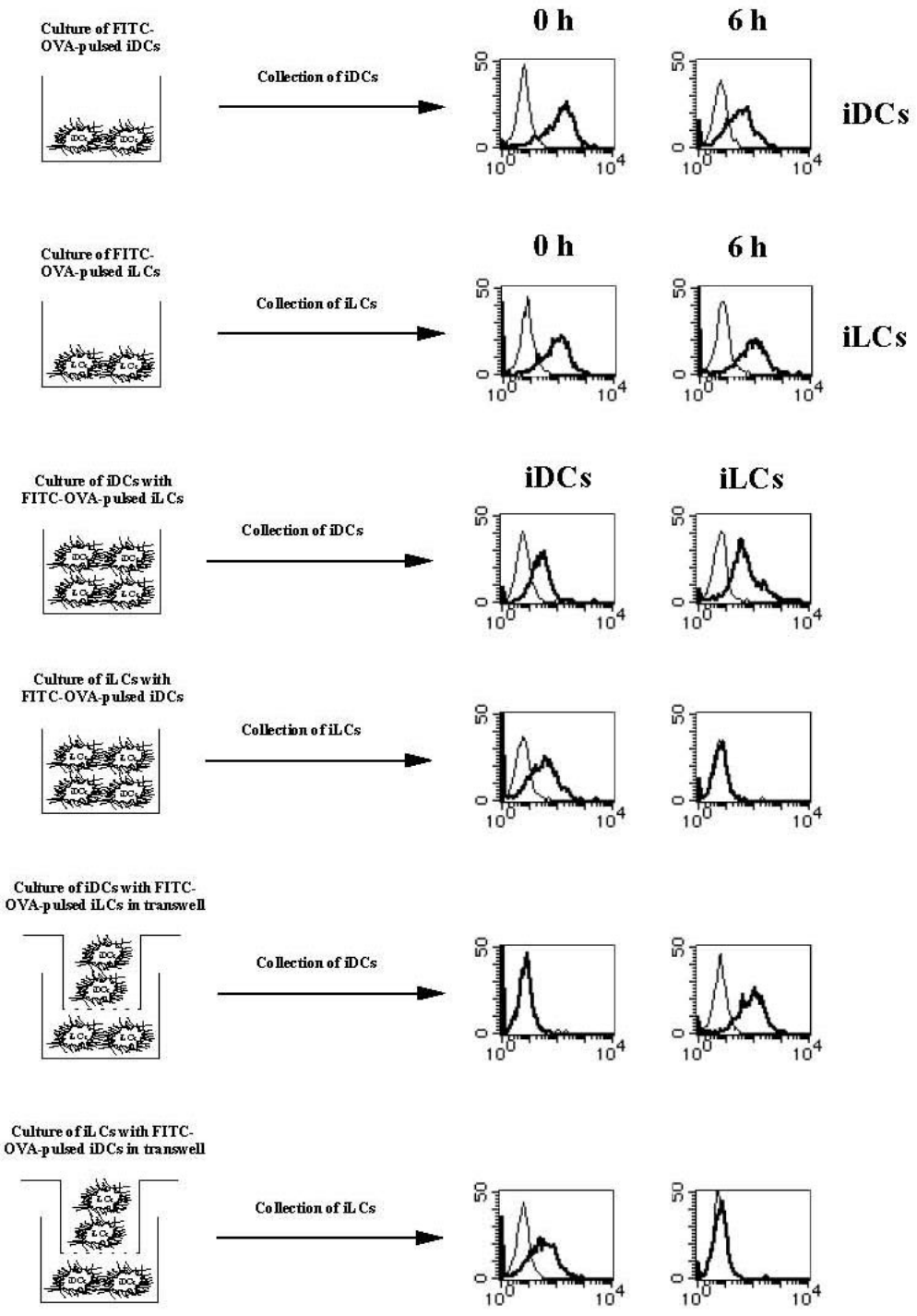

Fig. 9. iLCs transfer FITC-OVA to iDCs. iDCs or iLCs (10^6) were pulsed with FITC-OVA (50 μg/ml) for 60 min at 37ºC. Subsequently, iDCs or iLCs (10^6) were mixed cultured or separately cultured in Transwell cell culture chambers with the above described FITC-OVA-loaded iLCs or iDCs (10^6) for 6 h at 37ºC, and E-cad$^-$iDCs or E-cad$^+$iLCs were negatively or positively selected with anti-E-cad mAb and anti-mouse IgG mAb conjugated immunomagnetic beads. The FITC-OVA endocytosis by these cells was measured by FACS.

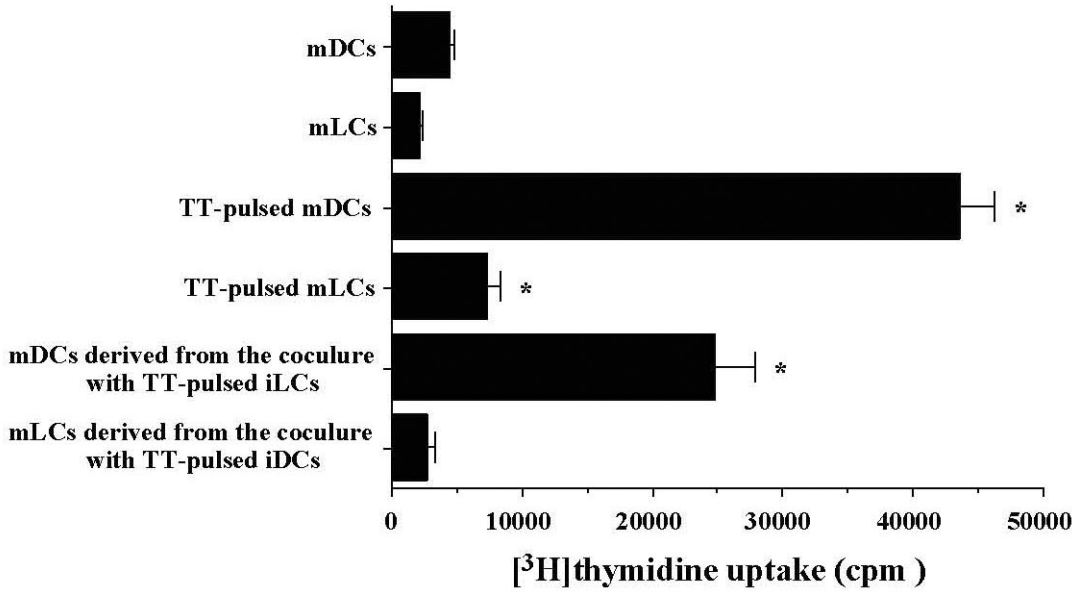

Fig. 10. DCs which received TT from LCs induce TT-specific T-cell proliferation. TT-loaded APCs and TT-primed T cells were prepared as described in *Materials and Methods*. TT-primed T cells were cultured with irradiated TT-loaded APCs. The proliferative response was measured on day 5. Values are the mean ± SD obtained for triplicate cultures. Values of [^{3}H]thymidine incorporation into TT-specific T cells or irradiated APCs were less than 2000 or 1000 cpm, respectively. The results are representative of five experiments with similar results.

TT-specific T cells for 5 days, and the T cell-proliferation was measured on day 5. Fig. 10 shows that iLC transferred TT to iDCs via cell to cell contact, and these *trans*-TT-loaded DCs elicited Ag-specific T-cell proliferation. We also observed that iLC isolated from culture with TT-loaded iDCs did not elicit Ag-specific T-cell proliferation. These results indicate that LCs directly transfer unprocessed Ag to DCs via cell to cell contact, and these DCs induce Ag-specific T cell activation.

Discussion

It has been shown in a certain artificial experimental systems (17-19) that at the port of Ag entry into epidermis, various types of APCs, including epidermal LCs, dermal macrophages and dermal DCs, capture the Ag and then migrate via the afferent lymphatics into the T cell-rich areas of regional lymph nodes. Recently, a minority of inflammatory monocytes were also shown to carry phagocytosed antigenic particles to lymph nodes and differentiate themselves into DCs in murine model (26). Analysis of these animal models suggests that these APCs present processed Ag to naive T cells and generate an Ag-specific primary T cell response (17-19). The present study addressed the hypothesis that the activation of Ag-specific T cells by DCs loaded with Ag transferred from LCs is one of the mechanisms for the initiation of epicutaneous immune responses in humans.

iLCs expressed significantly lower levels of HLA-DR and costimulatory molecules than iDCs. Stimulation of iLCs with TNF-α increased their expression levels but far lower than those in iDCs. Previous studies have shown that TNF-α-induced maturation of iDCs is mediated through p55 TNFR type I (p55TNFRI) whereas p75TNFRII involves the effect of TNF-α in iLCs (14). On the other hand, in contrast to the previous report (14), crosslinking of CD40 by immobilized CD40 mAb (artificial

condition) and activated T cells expressing CD40 (physiological condition) were insufficient for activation of LCs. This discrepancy might be due to the experimental desigh. Taken together, the difference in the mature status between DCs and LCs may be reflected by the respective usage of TNFR and the expression levels of CD40 as well as the basal expression levels of HLA-DR and costimulatory molecules.

The ability of iLCs as well as TNF-α- and CD40 ligation-induced mLCs to activate allogeneic T cells was less than that of their counterparts DCs. mLCs were also less potent in presenting Ag to TT-specific T cells than mDCs. Interestingly, DCs of immature and mature status induced a greater proliferation of allogeneic CB naive T cells than LCs did. These results suggest that in humas, DCs activate naive T cells as well as Ag-specific T cells more effectively than LCs. These phenomena imply that the low ability of LCs to stimulate T cell response may be the mechanism involved in the maintainance of immune homeostasis to prevent the induction and the development of allergic and autoimmune diseases in the epicutaneous tissues.

The chemokine-chemokine receptor system is thought to be one of the important mechanisms for the trafficking and the localization of DCs (9-12, 21, 22) and LCs (15). In association with chemokine receptor expressions in iDCs and iLCs, iDCs exhibited greater chemotactic migratory responses to RANTES and MIP-1α, but not to MIP-3α, while iLCs responded only to MIP-3α. Thus, difference in tissue distribution between iDCs and iLCs may be due to difference in chemokine responsiveness as well as in the expression of tissue-specific receptor including CLA and E-cad. On the other hand, we showed that CCR-6 expression and chemotaxis to MIP-3α as well as cell surface expression of CLA and E-cad were downregulated during the development of iLCs into mLCs. Therefore, loss of the responsiveness to MIP-3α as well as of the tissue adhesion mediated through CLA and E-cad is responsible for the departure of LCs from epidermis following exposure to exogenous Ag. Furthermore, we also showed that the transcriptional expression level of CCR-7 and MIP-3β responsiveness of mDCs were higher than those of mLCs. Thus, mDCs more efficiently home to T cell-rich areas of secondary lymphoid tissues to prime naive T cells than mLCs do.

We showed that the endocytosis by iLCs of FITC-OVA was less extensive than that by iDCs. Surprisingly, Ag-loaded iLCs interacted directly with iDCs and transfered the unprocessed Ag to them, and these trans-Ag-loaded mDCs induced Ag-specific T cell response, whereas mLCs failed to transfer processed Ag to mDCs (data not shown). Wykes *et al*. (27) have reported that splenic DCs interacted directly with naive B cells to transfer Ag and induced class switching in a primary T-dependent antibody response in vivo in murine model. On the other hand, Inaba *et al*. (28) have recently reported that B blasts transfer immunogenic peptide to murine allogeneic bone marrow (BM)-derived iDCs following the phagocytosis of B blasts by these DCs in vitro. Furthermore, they observed efficient uptake of donor migrating iDCs by recipient DCs in the T-cell area of lymph nodes when allogeneic DCs were injected into mice, implying that peripheral iDCs may transfer Ag to resident DCs in lymph nodes (28). Thus, these phenomena imply that transference of unprocessed and processed exogenous Ag among different types of APCs (cross-priming) should play a crucial role in the initiation and the regulation of the immune response.

The molecular mechanism by which LCs transfer unprocessed Ag to DCs remains unknown. We showed that LCs retained unprocessed Ag for a long period, whereas DCs internalized it quickly. Mommaas *et al*. (20) previously reported that LCs displayed lower level of the late endosomal/early lysosomal compartments than DCs, and these properties were involved in their defective abilities to process and present exogenous Ags. Therefore, these features of LCs may be involved in the transference of unprocessed Ag from iLCs to iDCs. Furthermore, fluorescence microscopic analysis showed that iLCs, but not iDCs, retain FITC-OVA around cell surface membrane for a long period (data not shown). Thus, direct membrane attachment of Ag may be responsible for this event because soluble proteins were internalized by macropinocytosis (4, 24). On the other hand, human DC can retain HIV in DC-SIGN, which acts as HIV-1-binding protein, and

subsequently this HIV can infect T cells adhering to the DCs (29). These phenomena led us to hypothesize that exogenous Ag occupies identified or unknown compartments used for the retention in iLCs, and that this unprocessed Ag escapes from the processing machinery and is subsequently transferred to iDCs. Further study will be needed to test this possibility.

We showed that MIP-3α transcript, but not the transcripts of other chemokines, was constitutively expressed in DMEC. Furthermore, inflammatory stimulation enhanced the expressions of RANTES and MIP-1α transcripts whereas this stimulation caused only a slight enhancement of the transcriptional expression of MIP-3α in DMEC. In dermal fibroblasts too, inflammatory stimulation upregulated transcriptional expressions of RANTES and MIP-1α, but not MIP-3α. iLCs only responded to CM from unstimulated and IL-1β/TNF-α-stimulated DEMC while iDCs migrated to CM from IL-1β/TNF-α-stimulated dermal fibroblasts and DEMC. It has been shown that iLCs present in epidermis without virtual inflammatory stimuli while other types of DCs emerge from transmigrated blood-derived precursors (e.g., monocytes) in the presence of inflammatory stimuli (16). Thus, constitutive production of MIP-3α in DMEC as well as expression of CLA, E-cad and CCR-6 in iLC may allow epidermal iLCs to anchor to epidermis in normal and inflammatory condition, while inflamed dermal fibroblasts and DMEC may attract dermal iDCs from other peripheral sites. Thus, dermal iDCs may interact directly with epidermal iLCs at the site of the inflamed DMEC. Collectively, these observations suggest several possible scenarios for the initiation of an epicutaneous immune response. First, epidermal iLCs, which are constitutively present in epidermis, capture and mainly retain, but partly process, antigenic materials during inflammation while dermal iDCs migrate from peripheral tissue into inflammatory epicutaneous sites, and capture and process soluble antigenic proteins efficiently. Second, epidermal LCs capture exogenous Ag and transfer its unprocessed form to dermal DCs, which act as *trans*-Ag-loaded dermal DCs in the inflamed DMEC. These cells are subsequently converted into dermal mDCs or epidermal mLCs by inflammatory stimuli, and lose their responsiveness to inflammatory chemokines, resulting in their departure from the inflamed epicutaneous sites. In turn, these APCs migrate through afferent lymph, and home into secondary lymphoid tissues via acquisition of the responsiveness to homeostatic chemokines. Ultimately, these Ag-presented mDCs and mLCs prime naive T cells in T cell-dependent areas of secondary lymphoid tissues to initiate immune responses at different efficiency.

In conclusion, our findings provide a novel mechanism for the initiation of epicutaneous immune responses. Clinical evidences suggest that various types of APCs, including dermal DCs and epidermal LCs, traffick from epicutaneous tissues to secondary lymphoid tissues in contact hypersensitivity (CHS), although their respective role in the initiation of cutaneous immune response remains unclear. Thus, further characterization of a group of DCs may provide further insights into the role of these cells in immune-related diseases.

Acknowledgments

We would like to thank Miss. M. Yamamoto for her excellent assistance. This work was supported by Grant-in-Aid for Scientific Research from the Ministry of Education, Science and Culture of Japan (13218027 to K. Sato and H. Kawasaki) and by a research grant from Waksman Foundation of Japan (to H. Kawasaki).
This work was done in collaboration with Katsuaki Sato*, Chikao Morimoto, Naohide Yamashita**, and Takami Matsuyama*. *Department of lmmunology and Medical Zoology, School of Medicine, Kagoshima University. **Department of Advanced Medical Science, The Institute of Medical Science, The University of Tokyo.

References

(1) Steinman, R. M. 1991. The dendritic cell system and its role in immunogenicity. *Annu. Rev. Immunol.* **9**: 271.
(2) Austyn, J. M. 1996. New insights into the mobilization and phagocytic dendritic cells. *J. Exp. Med.* **183**: 1287.

(3) Banchereau, J., and R. M. Steinman. 1998. Dendritic cells and the control of immunity. *Nature* **392**: 245.
(4) Sallusto, F., and A. Lanzavecchia. 1994. Efficent presentation of soluble antigen by cultured human dendritic cells is maintained by granulocyte/ macrophage colony-stimulating factor plus interleukin 4 and downregulated by tumor necrosis factor α. *J. Exp. Med.* **179**: 1109.
(5) Zhou, L.-J., and T. F. Tedder. 1996. $CD14^+$ blood monocytes can differentiate into functionally mature $CD83^+$ dendritic cells. *Proc. Natl. Acad. Sci. USA*. **93**: 2588.
(6) Koch, F., U. Stanzl, P. Jennewein, K. Janke, C. Heufler, E. Kaempgen, N. Romani, and G. Schuler. 1996. High level IL-12 production by murine dendritic cells: upregulation via MHC class II and CD40 molecules and downregulation by IL-4 and IL-10. *J. Exp. Med.* **184**: 741.
(7) Verhasselt, V., C. Buelens, F. Willems, D. D. Groote, N. Haeffner-Cavallon, and M. Goldman. 1997. Bacterial lipopolysaccharide stimulates the production of cytokines and the expression of costimulatory molecules by human peripheral blood dendritic cells. *J. Immunol.* **158**: 2919.
(8) Kalinski, P., J. H. N. Schuitemarker, C. M. U. Hilkens, E. A. Wierenga, and M. L. Kapsenberg. 1999. Final maturation of dendritic cells is associated with impaired responsiveness to IFN-γ and to bacterial IL-12 inducers: decreased ability of mature dendritic cells to produce IL-12 during the interaction with Th cells. *J. Immunol.* **162**: 3231.
(9) Sozzani, S., P. Allavena, G. D'Amico, W. Luini, G. Bianchi, M. Kataura, T. Imai, O. Yoshie, R. Bonecchi, and A. Mantovani. 1998. Differential regulation of chemokine receptors during dendritic cell migration: A model for their trafficking properties. *J. Immunol.* **161**: 1083.
(10) Chan, V. W. F., S. Kahtakota, M. C. Rohan, L. Panganiban-Lustan, J. P. Gardner, M. S. Wachowicz, J. A. Winter, and L. T. Williams. 1999. Secondary lymphoid-tissue chemokine (SLC) is chemotactic for mature dendritic cells. *Blood*. **93**: 3610.
(11) Cyster, J. G. 1999. Chemokines and the homing of dendritic cells to the T cell areas of lymphoid organs. *J. Exp. Med.* **189**: 447.
(12) Sozzani, S., P. Allavena, , A. Vecchi, and A. Mantovani. 1999. The role of chemokines in the regulation of dendritic cell trafficking. *J. Leuko. Biol.* **66**: 1.
(13) Geissmann, F., C. Prost, J.-P. Monnet, M. Dy, N. Brousse, and O. Hermine. 1998. Transforming growth factor β1, in the presence of granulocyte/ macrophage colony-stimulating factor and interleukin 4, induces differentiation of human peripheral blood monocytes into dendritic Langerhans cells. *J. Exp. Med.* **187**: 961.
(14) Geissmann, F., P. Revy, A. Regnault, Y. Lepelletier, M. Dy, N. Brousse, O. Hermine, and A. Durandy. 1999. TGF-β1 prevents the noncognate maturation of human dendritic Langerhans cells. *J. Immunol.* **162**: 4567.
(15) Yang, D., O. M. Z. Howard, Q. Chan, and J. J. Oppenheim. 1999. Immature dendritic cells generated from monocytes in the presence of TGF-β1 express functional CC chemokine receptor 6. *J. Immunol.* **163**: 1737.
(16) Charbonnier, A. -S., N. Kohrgruber, E. Kriehuber, G. Stingl, A. Rot, and D. Maurer. 1999. Macrophage inflammatory protein 3α is involved in the constitutive trafficking of Langerhans cells. *J. Exp. Med.* **190**: 1755.
(17) Kripke, M. L., C. G. Munn, A. Jeevan, J. -M. Tang, and C. Bucana. 1990. Evidence that cutaneous antigen-presenting cells migrate to regional lymph nodes during contact sensitization. *J. Immunol.* **145**: 2833.
(18) Roak, J. A., A. S. Rao, P. J. Morris, C. P. Larsen, D. F. Hankins, and J. M. Austyn. 1995. Dendritic cell loss from nonlymphoid tissue after systemic administration of lipopolysaccharide, tumor necrosis factor, and interleukin 1. *J. Exp. Med.* **181**: 2237.
(19) Sato, K., Y. Imai, and T. Irimura. 1998. Contribution of dermal macrophage trafficking in the sensitization phase of contact hypersensitivity. *J. Immunol.* **161**: 6835.
(20) Mommaas, A. M., A. A. Mulder, R. Jordens, C.

Out, M. C. A. A. Tan, P. Cresswell, P. M. Kluin, and Frits Koning. 1999. Human epidermal Langerhans cells lack functional monnose receptors and a fully developed endosomal/ lysosomal compartment for loading of HLA class II molecules. *Eur. J. Immunol.* **29**: 571.

(21) Sato, K., H. Kawasaki, H. Nagayama, R. Serizawa, J. Ikeda, C. Morimoto, K. Yasunaga, N. Yamaji, K. Tadokoro, T. Juji, and T. A. Takahashi. 1999. CC chemokine receptors, CCR-1 and CCR-3, are potentially involved in antigen-presenting cell function of human peripheral blood monocyte-derived dendritic cells. *Blood* **93**: 34.

(22) Sato, K., H. Kawasaki, H. Nagayama, M. Enomoto, C. Morimoto, K. Tadokoro, T. Juji, and T. A. Takahashi. 2000. TGF-β1 reciprocally controls chemotaxis of human peripheral blood monocyte-derived dendritic cells via chemokine receptors. *J. Immunol.* **164**: 2285.

(23) Sato, K., H. Kawasaki, H. Nagayama, M. Enomoto, C. Morimoto, K. Tadokoro, T. Juji, and T. A. Takahashi. 2001. Chemokine receptor expressions and responsiveness of cord blood T cells. *J. Immunol.* **166**: 1659.

(24) Lutz, M. B., P. Rovere, M. J. Kleijmeer, M. Rescigno, C. U. Abmann, V. M. J. Oorschot, H. J. Geuze, J. Trucy, D. Demandolx, J. Davoust, and P. Ricciardi-Castagnoli. 1997. Intracellular routes and selective retention of antigens in mildly acidic cathepsin D/lysosome-associated membrane protein-1/MHC class II-positive vesicles in immature dendritic cells. *J. Immunol.* **159**: 3707.

(25) Ebnet, K., K. D. Brown, U. K. Siebenlist, M. M. Simon, and S. Shaw. 1997. *Borrelia burgdorferi* activates nuclear factor-κB and is a potent inducer of chemokine and adhesion molecule gene expression in endothelial cells and fibroblasts. *J. Immunol.* **158**: 3285.

(26) Randolph, G. J., K. Inaba, D. F. Robbiani, R. M. Steinman, and W. A. Muller. 1999. Differentiation of phagocytic monocytes into lymph node dendritic cells in vivo. *Immunity* **11**: 753.

(27) Wykes, M., A. Pombo, C. Jenkins, and G. G. MacPherson. 1998. Dendritic cells interact directly with naive B lymphocytes to transfer antigen and initiate class switching in a primary T-dependent response. *J. Immunol.* **161**: 1313.

(28) Inaba, K., S. Turley, F. Yamaide, T. Iyoda, K. Mahnke, M. Inaba, M. Pack, M. Subklewe, B. Sauter, D. Sheff, M. Albert, N. Bhardwaj, I. Mellman, and R. M. Steinman. 1998. Efficient presentation of phagocytosed cellular fragments on the major histocompatibility complex class II products of dendritic cells. *J. Exp. Med.* **188**: 2163.

(29) Geijtenbeek, T. B. H., D. S. Kwon, R. Torensma, S. J. V. Vliet, G. C .F. V. Duijnhoven, J. Middel, I. L. M. H. A. Cornelissen, H. S. L. M. Nottet, V. N. KewalRamani, D. R. Littman, C. G. Figdor, and Y. Y. Kooyk. 2000. DC-SIGN, a dendritic cell-specific HIV-1-binding protein that enhances trans-infection of T cells. *Cell* **100**: 587.

Activation of JNK/SAPK and p38 MAPK Signal Transduction Pathways in the Mouse Brain upon Infection with Neurovirulent Influenza A Virus

Yoshinobu Kimura

Department of Microbiology, Fukui University School of Medicine, Fukui 910-1193, Japan

ABSTRACT The temporal and spatial distribution of active c-Jun N-terminal kinase (JNK) and p38 mitogen-activated protein kinase (MAPK) in the brain was investigated in an experimental virus-mouse system where neurovirulent influenza A virus caused lethal acute encephalitis. Following stereotactic microinjection of the virus into the olfactory bulb, virus-infected neurons appeared in several brain structures at the midbrain level, including the ventral tegmental area, amygdala and the pyramidal layer of the hippocampus. Infected neurons exhibited apoptosis on day 5 as evidenced by *in situ* detection of DNA fragmentation and active caspase-3. The stress-responsive JNK signal transduction pathway was activated in virus-infected neurons. Activation of p38 MAPK occurred widely in astrocytes on day 7 after infection. The active p38 MAPK in astrocytes showed no association with apoptosis but rather appeared to be involved in regulation of tumor necrosis factor-α production. These results indicate that these two stress-activated protein kinases may play distinct roles during the course of lethal acute influenza viral encephalitis.

Introduction

Increasing evidencs have suggested that neuronal apoptosis plays an important role in the pathogenesis of neurodegenerative, ischemic and prion diseases, as well as virus infections of the brain (1). However, knowledge is scarce on molecular mechanisms underlying the process of neuronal apoptosis induced by a wide range of insults given to the central nervous system (CNS). Elucidation of intracellular events during the process of neuronal apoptosis in the brain is essential for the establishment of effective therapeutic strategy against these disorders.

A mitogen-activated protein kinase (MAPK) superfamily protein functions as a serine threonine kinase which regulates intracellular signalling cascades and transmits extracellular stimuli from the plasma membrane into the nucleus. Extracellular signal-regulated kinases, the so-called classical MAPKs, are activated by mitogens and survival factors, and transduce signals to promote cell proliferation and survival (2). In contrast, c-Jun N-terminal kinase/stress-activated protein kinase (JNK/SAPK) and p38 MAPK become activated by a variety of stress signals, including ultraviolet irradiation, inflammatory cytokines and oxidative stimuli, and are implicated in the induction of apoptotic cell death (2, 3). Intriguingly, double-stranded RNA has also been shown to activate these kinases (4). Active JNK phosphorylates c-Jun and activating transcription factor-2 (ATF-2). The JNK signalling pathway stabilizes and activates the pro-apoptotic effector p53 and antagonizes the function of anti-apoptotic mediator Bcl-2 by phosphorylation (3). Phosphorylated c-Jun stimulates the transcription of several key target genes, including the death-inducer Fas ligand (5). Recent studies in various *in vitro* experimental systems have

provided strong evidence that the JNK signal transduction cascade mediates neuronal apoptosis (5-8). Activation of this pathway *in vivo,* especially in the brain, upon exposure to stress stimuli has not yet been addressed enough (9, 10). On the other hand, p38 MAPK regulates gene expression by phosphorylating some transcription factors, including cyclic AMP-responsive element binding protein, myocyte-enhancer factor 2C and ATF-2 (3). Significant function of the p38 MAPK pathway has been reported in the apoptotic cascade in cultured neurons (11-14). Axotomy-induced apoptosis of retinal ganglion cells in rats has also been attributed to activation of p38 MAPK, although the role played by p38 activation in apoptosis regulation differs in a cell-type- or a stimulation-dependent manner (15).

To clarify the underlying mechanisms whereby virus infection triggers neuronal apoptosis in the brain, we have investigated the activation kinetics of two apoptosis mediators, JNK/SAPK and p38 MAPK, during the course of lethal acute encephalitis in mine caused by neurovirulent influenza A virus infection (16). Here we show that the JNK/SAPK signal transduction cascade becomes activated in virus-infected neurons, while delayed and widespread activation of p38 MAPK occurs in astrocytes and evokes inflammatory responses in the mouse brain.

Materials and Methods

Experimental infection of animals.

The R404BP strain of influenza A virus (a kind gift from Dr. S. Nakajima, The Institute of Public Health, Japan) was propagated as described elsewhere (17). R404BP virus (10^5 p. f. u.) in 1 μl sterile phosphate-buffered saline (PBS) was injected stereotactically into the right olfactory bulb of specific-pathogen-free female C57BL/6 mice (Clea) at 4 weeks of age, as reported previously (17).

UV inactivation of virus.

Stock virus suspension was exposed to a 15 W UV lamp at a distance of 30 cm for 30 min at 4ºC with continuous and gentle stirring. After irradiation, infectivity was reduced to $<10^{-7}$ of the original.

Tissue processing.

Under deep anesthesia by intraperitoneal administration of 7.2 % chloral hydrate in PBS (0.05 ml g^{-1} body weight), mice were perfused transcardially with 3.7 % formaldehyde in PBS. Brains were soaked in 20 % sucrose in PBS at 4ºC overnight and frozen at −80ºC. Coronal sections of 14 μm thickness of brain tissue were cut at the midbrain level on a cryostat.

Dual immunofluorescent labelling.

Tissue slices were incubated in 5 % donkey serum (Chemicon International) containing 0.3 % Triton-X in PBS for 20 min and made to react with a mixture of appropriate combination of two primary antibodies diluted in 2 % donkey serum containing 0.3 % Triton-X in PBS at 4ºC overnight. The primary antibodies used in this study were goat polyclonal anti-influenza A virus antibody (working dilution of 1:500; Chemicon International), rabbit polyclonal anti-neuronal nitric oxide synthase (nNOS) antibody (working dilution of 1:100; Chemicon International), rabbit polyclonal anti-cloven caspase-3 (Asp^{175}) antibody (working dilution of 1:50; Cell Signalling Technology), rabbit polyclonal anti-JNK antibody (working dilution of 1:200; Cell Signalling Technology), rabbit polyclonal anti-p38 MAPK antibody (working dilution of 1:400; Santa Cruz), rabbit polyclonal anti-phospho-JNK (Thr^{183}/Tyr^{185}) antibody (working dilution of 1:200; Cell Signalling Technology), anti-phospho-c-Jun (Ser^{63}) antibody (working dilution of 1:200; Cell Signalling Technology), rabbit polyclonal anti-phospho-p38 MAPK (Thr^{180}/Tyr^{182}) antibody (working dilution of 1:200; Cell Signalling Technology), mouse monoclonal anti-glial fibrillary acidic protein (GFAP) antibodies cocktail (working concentration of 10 μg ml^{-1}; Pharmingen), goat polyclonal anti-tumor necrosis factor-α (TNF-α) antibody (working dilution of 1:200; Santa Cruz), and rabbit polyclonal anti-Fas ligand antibody (working dilution of 1:200; Wako Pure

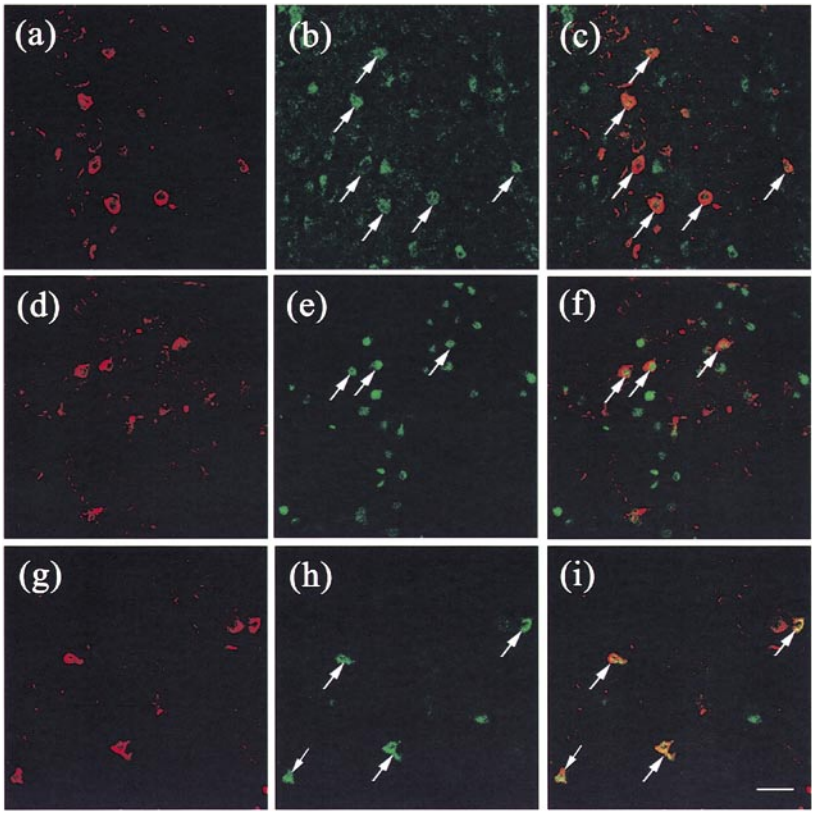

Fig. 1. Infection of neurons with the neurovirulent R404BP strain of influenza A virus and induction of neuronal apoptosis in the amygdala. (a) Infected cells. (b) Cells expressing nNOS molecules. (c) Overlapped [(a) and (b)] confocal image. Note that infected cells correspond with nNOS expression (arrows). (d) Infected neurons. (e) TUNEL-specific signals. (f) Overlapped [(d) and (e)] confocal image. Note that infected cells exhibit TUNEL-specific signals in a nuclear staining-manner (arrows). (g) Infected neurons. (h) Activated caspase-3. (i) Overlapped [(g) and (h)] confocal image. Note the cytoplasmic localization of activated caspase-3 in infected cells (arrows). The bar marker represents 20μm.

Chemical Industries). Then, tissue sections were incubated in appropitate secondary antibodies which had been affinity-purified and absorbed for dual immunolabelling (all diluted 1:100 in PBS supplemented with 0.3 % Triton-X; Chemicon International), including rodamine-labelled donkey anti-goat immunoglobulin, fluorescein-labelled donkey anti-rabbit immunoglobulin and rodamine-labelled donkey anti-mouse immunoglobulins. Binding was visualized under a confocal laser scanning microscope.

In situ detection of DNA fragmentation.

DNA fragmentation was detected by the terminal deoxynucleotidyl transferase-mediated dUTP nick end-labelling (TUNEL) method using the ApopTag Direct *In Situ* Apoptosis Detection kit (Intergen). Dual imaging for virus antigens and TUNEL reactions was carried out as described in a previous report (18).

Detection of mRNA for influenza A virus membrane protein 1 (M1) and TNF-α.

Total mRNA was extracted from brain tissue at the midbrain level using a mRNA Isolation kit (Roche). cDNA synthesis and successive polymerase chain reaction (PCR) were carried out with the One Step RNA PCR kit (AMV)(Takara), according to the

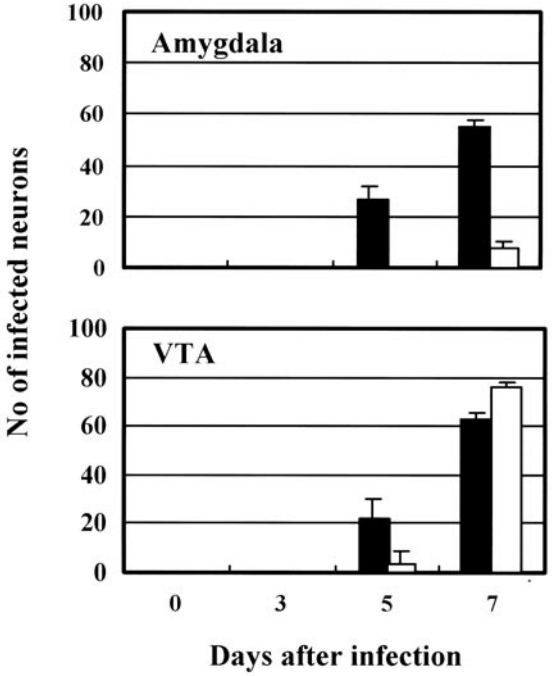

Fig. 2. Kinetics of the number of virus-infected neurons in the ipsilateral (closed bars) and contralateral (gray bars) amygdala and ventral tegmental area (VTA) on days 0, 3, 5 and 7 of infection (n=4). Virus-infected cells visualized by immunofluorescence were counted in the whole area of the section preparation. Data are expressed as the averages ± SEM.

manufacturer's instructions. Sequences of primer pairs were as follows: influenza A virus M1, 5'-GAGATCGCACAGAGA-3' and 5'-TCGTTGCATCTGCAC-3'(19); mouse TNF-α, 5'-CCTGTAGCCCACGTCGTAGC-3' and 5'-TTGACCTCAGCGCTGAGTTG-3' (20); and mouse β-actin, 5'-ATCTGGCACCACACCTTCTACA-3' and 5'-GTTTCATGGATGCCACAGGATT-3' (21). PCR conditions were as follows: 50ºC for 30 min and 94ºC for 2 min, followed by 35 cycles of 94ºC for 30 s, 50ºC for 30 s and 72ºC for 1 min. The final products were separated on 1.2 % agarose gel, stained with ethidium bromide and visualized under a UV lamp. Amplified DNA fragments from influenza A virus M1, TNF-α and β-actin transcripts were expected to be 684, 374 and 567 bp, respectively.

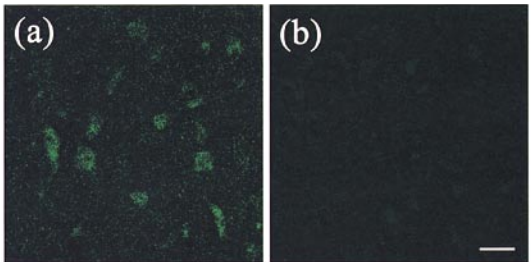

Fig. 3. Expression of JNK and p38 MAPK in the ventral tegmental area of a normal brain. JNK is occasionally detectable in a cytoplasmic staining-pattern (a), while p38 MAPK is undetectable in the normal brain parenchyma (b). The bar represents 20μm.

Results

Clinical observation.

C57BL/6 mice, who received stereotactic microinjection with the R404BP strain of influenza A virus into the right olfactory bulb, displayed decreased motor activity on day 5, manifested hunching and emaciation on day 7 and died within 10 days. This demonstrated the lethal effect of the virus infection of the CNS. The mean survival day was 7.9 ± 0.6 (averages ± SD, n=10).

Infection of the mouse brain with the R404BP strain of influenza A virus.

R404BP virus introduced into the right olfactory bulb spread over the midbrain level of the amygdala, ventral tegmental area (VTA), pyramidal layer of the hippocampus, substantia nigra zona compacta and mammillary nucleus on day 5 of infection as reported in a previous report (16). Double immunolabelling of virus antigens and nNOS, a marker for neurons, demonstrated the virus-infected neurons selectively in these brain structures (Fig. 1a-c). Neuronal morphology was retained relatively well on day 5. *In situ* dual labelling showed that 90 % of virus-infected neurons displayed TUNEL-specific signals (n=50) (Fig. 1d-f). Furthermore, 90 % of infected neurons exhibited immunoreactivity to cloven caspase-3 (n=50) (Fig. 1g-i). Collectively, these findings demonstrated

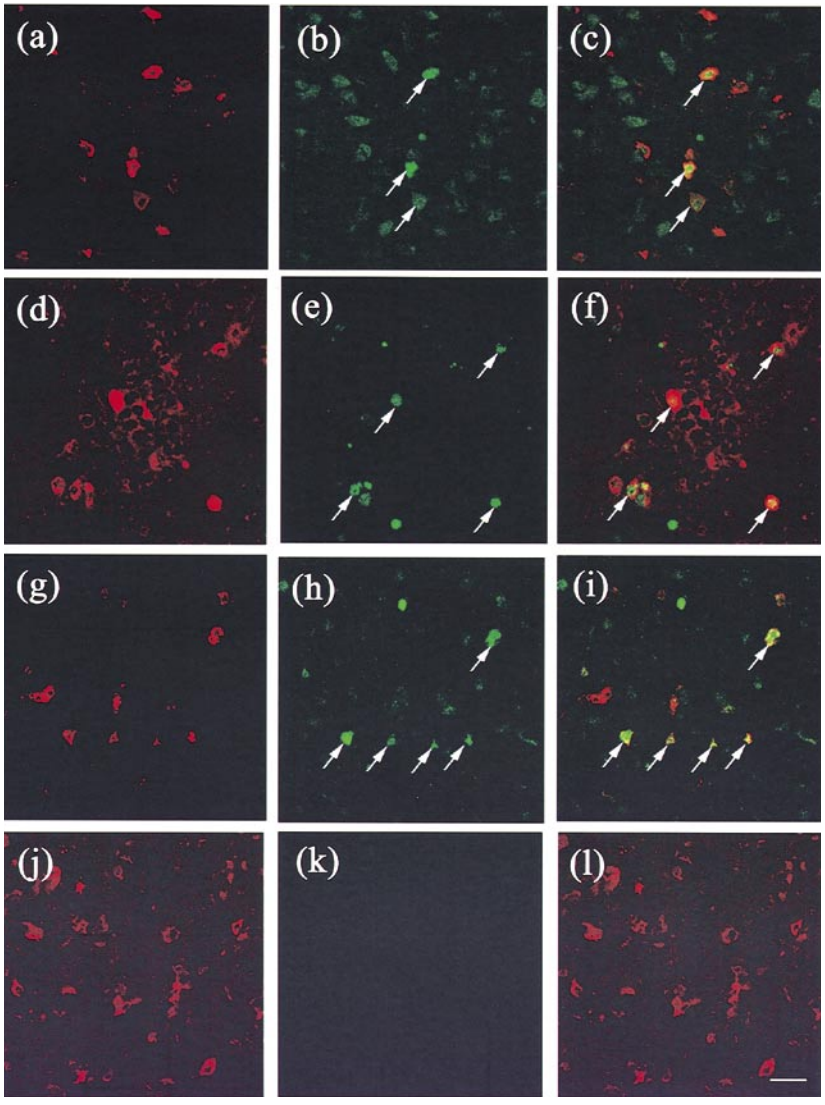

Fig. 4. Activation of the JNK signal transduction pathway in the virus-infected neurons. Amygdala on day 5 after infection. (a) Infected neurons. (b) JNK immunoreactivity. (c) Overlapped [(a) and (b)] confocal image. Note the occasional upregulation of JNK and its nuclear translocation upon infection (arrows). (d) Infected neurons. (e) Phospho-JNK immunoreactivity. (f) Overlapped [(d) and (e)] confocal image. Infected neurons display phospho-JNK immunoreactivity in a nuclear staining-pattern (arrows). (g) Infected neurons. (h) Phospho-c-Jun. (i) Overlapped [(g) and (h)] confocal image. Infected neurons display phospho-c-Jun immunoreactivity in a nuclear staining-pattern (arrows). (j) Infected neurons. (k) Phospho-p38 MAPK immunoreactivity. (l) Overlapped [(j) and (k)] confocal image. Note the undetectable level of phosho-p38 MAPK immunoreactivtiy at this time-point. The bar represents 20 μm.

the occurrence of caspase-dependent neuronal apoptosis upon virus infection. On day 7, infected neurons increased in number (Fig. 2), began to shrink and lost neurite structures, showing a process of apoptotic neurodegeneration. In the normal brain of age-matched C57BL/6 mice, the levels of both TUNEL-specific and active caspase-3-specific signals were not detectable.

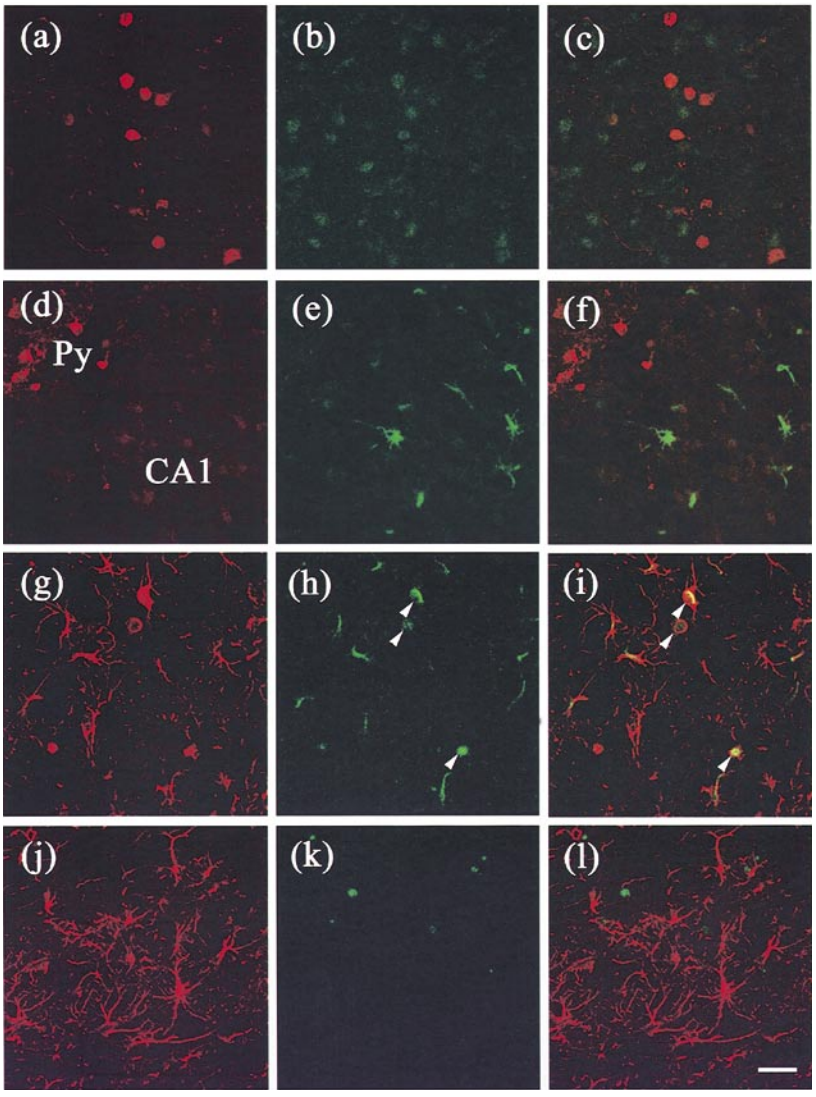

Fig. 5. Activation of p38 MAPK in the virus-infected neurons on day 7 of infection. (a) Infected neurons in the ventral tegmental area. (b) p38 MAPK immunoreactivity. (c) : (a) and (b) overlapped confocal image. Note the upregulated expression of p38 MAPK in brain cells, including virus-infected and degenerating neurons. (d) Infected neurons in the hippocampal formation where infection predominates in the pyramidal layer (Py). (e) Phospho-p38 MAPK immunoreactivity. (f) : (d) and (e) overlapped confocal image. Note the conspicuous specific signals of phosho-p38 MAPK in the CA1 region, which is not a major target of the virus. (g) GFAP-specific signals in the VTA, which is a major target of the virus. (h) Phopho-p38 MAPK immunoreactivity. (i) : (g) and (h) overlapped confocal image. Note that phospho-p38 MAPK immunoreactivity emerges inside of some GFAP-positive cells and appears occasionally in a nuclear staining-manner (arrowheads). (j) GFAP-specific signals in the VTA. (k) TUNEL-specific signals. (l) : (j) and (k) overlapped confocal image. Note the two signals do not co-localize with each other. The bar repersents 20μm.

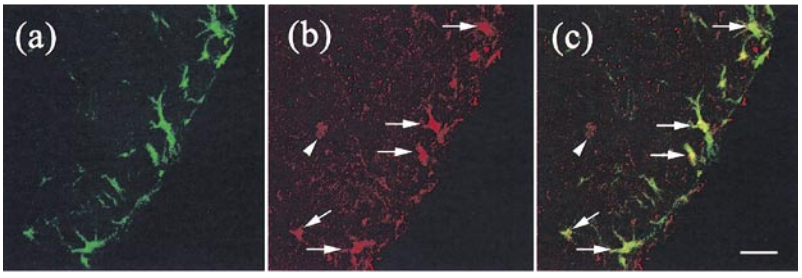

Fig. 6. Evidence of TNF-α production in phospho-p38 MAPK-immunopositive cells. Cerebral cortex. (a) Phospho-p38 MAPK immunoreactivity. (b) TNF-α immunoreactivity. (c) Overlapped [(a) and (b)] confocal image. Phospho-p38 MAPK-immunopositive cells frequently manifest TNF-α-specific signal (arrows). The arrowhead points to a TNF-α-producing cell without phospho-p38 MAPK expression. The bar represents 20μm.

Activation of the JNK/SAPK signal transduction cascade in infected mouse brain.

In the normal brain, JNK molecules were occasionally detectable in a cytoplasmic staining pattern (Fig. 3a). On day 5 of infection, signals for JNK increased in intensity and showed nuclear accumulation in some infected neurons (Fig. 4a - c). Most neurons infected with the virus displayed phospho-JNK- and phospho-c-Jun-specific signals in a nuclear staining-pattern (Fig. 4d-i). The brains of mice inoculated with UV-inactivated virus showed no activation of the pathway. These results proved unequivocally the activation of the JNK/c-Jun cascade in infected neurons. Upregulated expression of Fas ligand, a transcriptional target of c-Jun, was undetectable.

Activation of p38 MAPK.

It should be noted that p38 MAPK was undetectable in the normal brain parenchyma (Fig. 3b) (22) and that both p38 MAPK and phospho-p38 MAPK did not become detectable anywhere in the brain parenchyma, even on day 5 of virus infection (Fig. 4j-l). However, on day 7 of infection, weak p38 MAPK-specific signals appeared in brain cells (Fig. 5a-c). Cells exhibiting phospho-p38 MAPK immunoreactivity appeared widely in the brain parenchyma, notably in the cerebral cortex, the dentate gyrus and the CA1, CA2 and CA3 regions of the hippocampal formation (Fig. 5d-f). Of interest, these cells did not overlap virus-infected neurons at all but did GFAP-positive cells. This indicated that activation of p38 MAPK occurred in GFAP-positive astrocytes in the brain upon virus infection (Fig. 5g-i). Phospho-p38 MAPK-specific signals appeared occasionally in a nuclear staining-fashion. Although p38 MAPK has been implicated in induction of apoptosis, GFAP-immunopositive cells that emerged in virus-infected regions did not show any TUNEL-specific signals (Fig. 5j-l). Since p38 MAPK is involved in post-transcriptional regulation of interleukin-1β-induced TNF-α production in cultured human astrocytes (23), we examined the *in vivo* production of this cytokine in phospho-p38-immunopositive astrocytes. TNF-α immunoreactivity overlapped phospho-p38 MAPK immunoreactivity (Fig. 6). RT-PCR detected TNF-α transcripts on days 5 and 7 of infection (Fig. 7). These results raise the possibiblity that p38 MAPK may

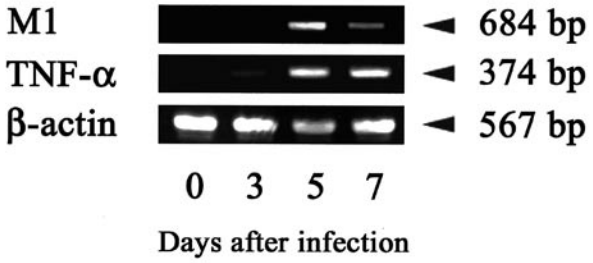

Fig. 7. Detection of TNF-α-specific mRNA by RT-PCR at the midbrain level. M1, influenza A virus membrane protein 1.

regulate synthesis of TNF-α molecules in astrosytes in response to neuronal infection with the neurovirulent influenza A virus *in vivo*.

Discussion

In this study, we have investigated activation patterns of JNK/SAPK and p38 MAPK in the mouse brain following infection with the neurovirulent influenza A virus. Our results provide the first evidence that the JNK cascade can be activated in CNS neurons upon virus infection and the p38 counterpart in astrocytes with a significant time-lag.

Recently, we have reported apoptosis of murine olfactory receptor neurons with activation of the JNK/c-Jun/Fas ligand pathway following intranasal infection with the R404BP strain of influenza A virus (24). In the present study, however, we could not detect upregulated expression of Fas ligand molecules in the mouse brain following infection with the same virus. Alternatively, JNK activation in neurons may lead to induction of BIM, a member of the BH3-only pro-apoptotic subfamily of the Bcl-2 protein family, as well as BAX-dependent cytochrome-c release from mitochondria, which induces caspase activation (7, 8). These findings underscore the importance of the JNK cascade in induction of neuronal apoptosis *in vivo*.

Neuronal apoptosis induced by influenza A virus infection in the brain is multifactorial (25). Cytotoxic lymphocytes, especially through the perforin/granzyme system-mediated mechanism, play a pivotal role in killing CNS neurons that are infected with the WSN strain of influenza A virus, as demonstrated in mice with targeted disruped *transporter associated with antigen presentation 1* and *perforin* genes (17, 18). Granzyme B released from effector lymphocytes enters the target cells and activates caspase cascades directly (26). On the other hand, subacute induction of apoptotic neurodegeneration in the brain of influenza virus-infected *perforin*$^{-/-}$ mice could be attributable to sustained activation of the JNK pathway (17, 18). Prolonged JNK activation has been demonstrated in various apoptotic paradigms (27). Thus, influenza virus-induced neuronal apoptosis in the brain involves activation of the intrinsic (i.e., apoptosome) and extrinsic (i.e., death receptors and perforin/granzyme) pathways (7).

Astrocytes with active p38 MAPK produced TNF-α molecules (Fig. 6), synchronous with the development of clinical symptoms in virus-infected mice (hunching and emaciation). Activation of p38 MAPK in astrocytes mediates interleukin (IL)-1β-signalling and results in post-transcriptional production of TNF-α (23). Interestingly, IL-1β-stimulated activation of the p38 MAPK cascade in cultured astrocytes has been reported in connection with prostaglandin E2 production, which gives another example of the relationship between the p38 MAPK and neuroinflammation (28). Global forebrain ischemia leads to neuronal death in the hippocampus, and activation of p38 takes place in microglia in the vicinity of the affected area (29). Similar to our findings, delayed induction of p38 MAPK has been noted in reactive astrocytes in the regions of the brain undergoing selective neuronal death induced by kainic acid (30). In addition, phosphorylation of p38 MAPK has been detected in glial cells within senile plaques in the brain of patients with Alzheimer's disease (31). These descriptions are consistent with the present observation that activation of p38 MAPK parallels the neuroinflammatory process during virus infection of the brain. It is expected that in combination with antiviral treatment (16), a therapeutic intervention against the MAPK pathways, using a JNK inhibitor and a p38 inhibitor (3, 15, 23), may suppress apoptotic neuronal death and neuroinflammation during acute viral encephalitis and minimize neurological sequelae.

References

(1) Bredesen, D. E. (1995). Neural apoptosis. *Ann Neurol* **38** : 839-851.

(2) Matsuzawa, A. & Ichijo, H. (2001). Molecular mechanisms of the decision between life and death: regulation of apoptosis by apoptosis signal-regulating kinase 1. *J Biochem* (Tokyo) **130** : 1-8.

(3) Mielke, K. & Herdegen, T. (2000). JNK and p38 stresskinases: degenerative effectors of signal-transduction-cascades in the nervous system. *Prog Neurobiol* **61** : 45-60.

(4) Iordanov, M. S., Paranjape, J. M., Zhou, A., Wong, J., Williams, B. R., Meurs, E. F., Silverman, R. H. & Magun, B. E. (2000). Activation of p38 mitogen-activated protein kinase and c-Jun NH_2-terminal kinase by double-stranded RNA and encephalomyocarditis virus: involvement of RNase L, protein kinase R, and alternative pathways. *Mol Cell Biol* **20** : 617-627.

(5) Morishima, Y., Gotoh, Y., Zieg, J., Barrett, T., Takano, H., Flavell, R., Davis, R. J.,Shirasaki, Y. & Greenberg, M. E. (2001). β-amyloid induces neuronal apoptosis via a mechanism that involves the c-Jun N-terminal kinase pathway and the induction of Fas ligand. *J Neurosci* **21** : 7551-7560.

(6) Luo, Y., Umegaki, H., Wang, X., Abe, R. & Roth, G. S. (1998). Dopamine induces apoptosis through an oxidation-involved SAPK/JNK activation pathway. *J Biol Chem* **273** : 3756-3764.

(7) Putcha, G. V., Moulder, K. L., Golden, J. P., Bouillet, P., Adams, J. A., Strasser, A. & Johnson, E. M., Jr. (2001). Induction of BIM, a proapoptotic BH3-only BCL-2 family member, is critical for neuronal apoptosis. *Neuron* **29** : 615-628.

(8) Whitfield, J., Neame, S. J., Paquet, L., Bernard, O. & Ham, J. (2001). Dominant-negative c-Jun promotes neuronal survival by reducing BIM expression and inhibiting mitochondrial cytochrome c release. *Neuron* **29** : 629-643.

(9) Yang, D. D., Kuan, C.-Y., Whitmarsh, A. J., Rincón, M., Zheng, T. S., Davis, R. J., Rakic, P. & Flavell, R. A. (1997). Absence of excitotoxicity-induced apoptosis in the hippocampus of mice lacking the Jnk3 gene. *Nature* **389** : 865-870.

(10) Xia, X. G., Harding, T., Weller, M., Bieneman, A., Uney, J. B. & Schulz, J. B. (2001). Gene transfer of the JNK interacting protein-1 protects dopaminergic neurons in the MPTP model of Parkinson's disease. *Proc Natl Acad Sci USA* **98** : 10433-10438.

(11) Kummer, J. L., Rao, P. K. & Heidenreich, K. A. (1997). Apoptosis induced by withdrawal of trophic factors is mediated by p38 mitogen-activated protein kinase. *J Biol Chem* **272** : 20490-20494.

(12) Horstmann, S., Kahle, P. J. & Borasio, G. D. (1998). Inhibitors of p38 mitogen-activated protein kinase promote neuronal survival *in vitro*. *J Neurosci Res* **52** : 483-490.

(13) Ghatan, S., Larner, S., Kinoshita, Y., Hetman, M., Patel, L., Xia, Z., Youle, R. J. & Morrison, R. S. (2000). p38 MAP kinase mediates BAX translocation in nitric oxide-induced apoptosis in neurons. *J Cell Biol* **150** : 335-347.

(14) Zou, W., Zeng, J., Zhuo, M., Xu, W., Sun, L., Wang, J. & Liu, X. (2002). Involvement of caspase-3 and p38 mitogen-activated protein kinase in cobalt chloride-induced apoptosis in PC12 cells. *J Neurosci Res* **67** : 837-843.

(15) Kikuchi, M., Tenneti, L. & Lipton, S. A. (2000). Role of p38 mitogen-activated protein kinase in axotomy-induced apoptosis of rat retinal ganglion cells. *J Neurosci* **20** : 5037-5044.

(16) Mori, I., Liu, B., Hossain, Md. J., Takakuwa, H., Daikoku, T., Nishiyama, Y., Naiki, H., Matsumoto, K., Yokochi, T. & Kimura, Y. (2002). Successful protection by amantadine hydrochloride against lethal encephalitis caused by a highly neurovirulent recombinant influenza A virus in mice. *Virology,* **303** : 287-296.

(17) Mori, I., Diehl, A. D., Chauhan, A., Ljunggren, H.-G. & Kristensson, K. (1999). Selective targeting of habenular, thalamic midline and monoaminergic brainstem neurons by neurotropic influenza A virus in mice. *J Neurovirol* **5** : 355-362.

(18) Mori, I. & Kimura, Y. (2000). Apoptotic neurodegeneration induced by influenza A virus infection in the mouse brain. *Microbes Infect* **2** : 1329-1334.

(19) Urabe, M., Tanaka, T., Odagiri, T., Tashiro, M. & Tobita, K. (1993). Persistence of viral genes in a variant of MDBK cell after productive replication of a mutant of influenza virus A/WSN. *Arch Virol* **128** : 97-110.

(20) Tucker, P. C. & Sack, G. H., Jr. (2001). Expression of serum amyloid A genes in mouse brain: unprecedented response to inflammatory mediators. *FASEB J* **15** : 2241-2246.

(21) Meyding-Lamadé, U., Haas, J., Lamadé, W., Stingele, K., Kehm, R., Fäth, A., Heinrich, K., Storch Hagenlocher, B. & Wildemann, B. (1998). Herpes simplex virus encephalitis: long-term comparative study of viral load and the expression of immunologic nitric oxide synthase in mouse brain tissue. *Neurosci Lett* **244** : 9-12.

(22) Maruyama, M., Sudo, T., Kasuya, Y., Shiga, T., Hu, B.-R. & Osada, H. (2000). Immunolocalization of p38 MAP kinase in mouse brain. *Brain Res* **887** : 350-358.

(23) Lee, Y. B., Schrader, J. W. & Kim, S. U. (2000). p38 MAP kinase regulates TNF-α production in human astrocytes and microglia by multiple mechanisms. *Cytokine* **12** : 874-880.

(24) Mori, I., Goshima, F., Imai, Y., Kohsaka, S., Sugiyama, T., Yoshida, T., Yokochi, T., Nishiyama, Y. & Kimura, Y. (2002). Olfactory receptor neurons prevent dissemination of neurovirulent influenza A virus into the brain by undergoing virus-induced apoptosis. *J Gen Virol* **83** : 2109-2116.

(25) Mori, I. & Kimura, Y. (2001). Neuropathogenesis of influenza virus infection in mice. *Microbes Infect* **3** : 475-479.

(26) Trapani, J. A., Davis, J., Sutton, V. R. & Smyth, M. J. (2000). Proapoptotic functions of cytotoxic lymphocyte granule constituents *in vitro* and *in vivo*. *Curr Opin Immunol* **12** : 323-329.

(27) Tobiume, K., Matsuzawa, A., Takahashi, T., Nishitoh H., Morita, K., Takeda, K., Minowa, O., Miyazono, K., Noda, T. & Ichijo, H. (2001). ASK1 is required for sustained activations of JNK/p38 MAP kinases and apoptosis. *EMBO Rep* **2** : 222-228.

(28) Molina-Holgado, E., Ortiz, S., Molina-Holgado, F. & Guaza, C. (2000). Induction of COX-2 and PGE_2 biosynthesis by IL-1β is mediated by PKC and mitogen-activated protein kinases in murine astrocytes. *Br J Pharmacol* **131** : 152-159.

(29) Walton, K. M., DiRocco, R., Bartlett, B. A., Koury, E., Marcy, V. R., Jarvis, B., Schaefer, E. M. & Bhat, R. V. (1998). Activation of p38 MAPK in microglia after ischemia. *J Neurochem* **70** : 1764-1767.

(30) Che, Y., Yu, Y.-M., Han, P.-L. & Lee, J.-K. (2001). Delayed induction of p38 MAPKs in reactive astrocytes in the brain of mice after KA-induced seizure. *Mol Brain Res* **94** : 157-165.

(31) Hensley, K., Floyd, R. A., Zheng, N.-Y., Nael, R., Robinson, K. A., Nguyen, X., Pye, Q. N., Stewart, C. A., Geddes, J., Markesbery, W. R., Patel, E, Johnson, G. V. W. & Bing, G. (1999). p38 kinase is activated in the Alzheimer's disease brain. *J Neurochem* **72** : 2053-2058.

(32) Mori, I., Goshima, F., Koshizuka, T., Koide, N., Sugiyama, T., Yoshida, T., Yokochi, T., Nishiyama, Y. & Kimura, Y. (2003). Differential activation of the c-Jun N-terminal kinase/stress-activated protein kinase and p38 mitogen-activated protein kinase signal transduction pathways in the mouse brain upon infection with neurovirulent influenza A virus. *J Gen Virol* **84** : 2401-2408.